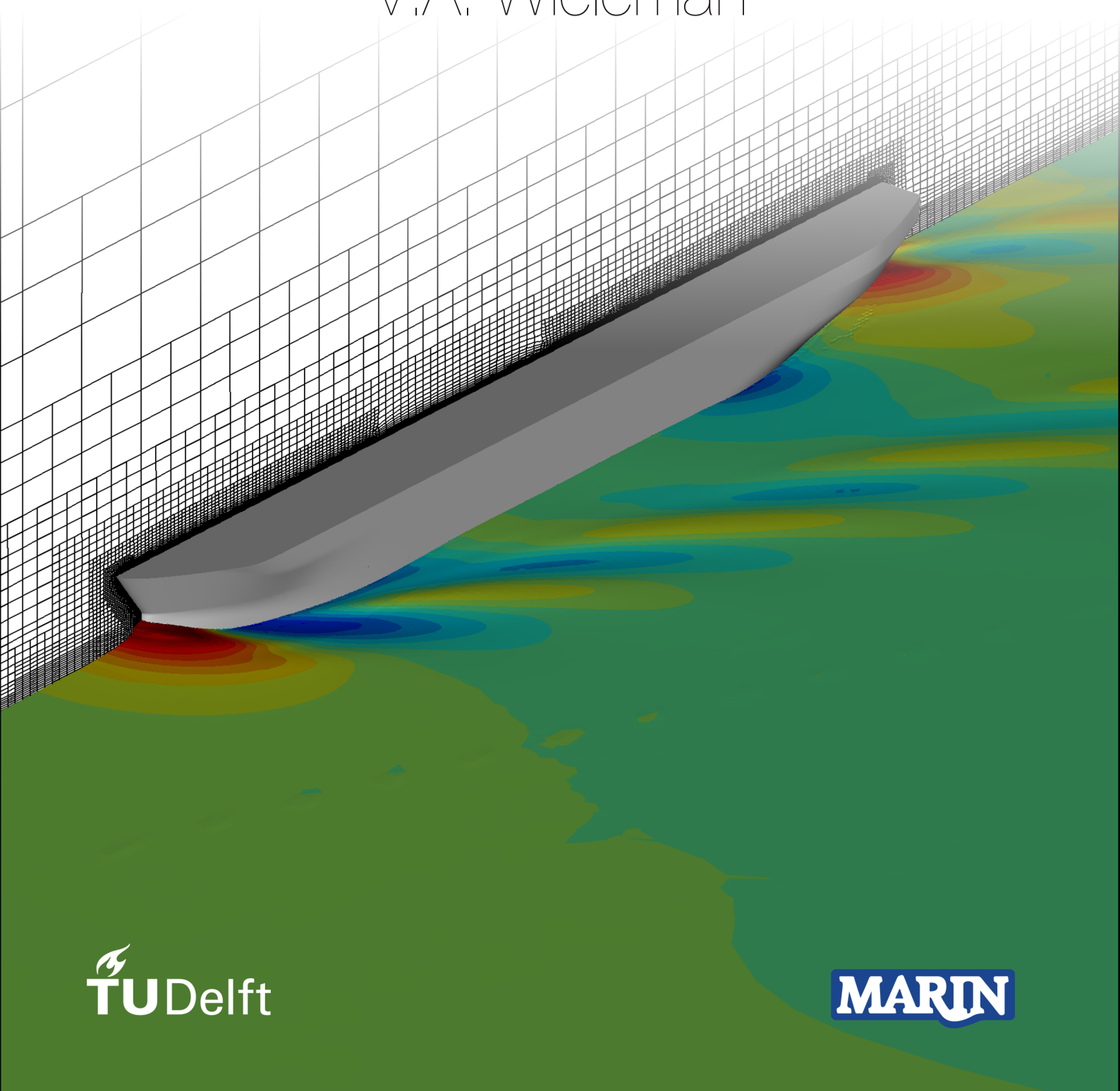


Verification and validation of full-scale propulsion analysis using CFD

Master's Thesis

V.A. Wieleman



Verification and validation of full-scale propulsion analysis using CFD

Master's Thesis

by

V.A. Wieleman

To obtain the degree of Master of Science
at the Delft University of Technology,
to be defended publicly on Friday July 6, 2018 at 14:00.

Student number:	4163702	
Thesis committee:	Prof. T. Van Terwisga,	TU Delft
	Dr. ir. M. Pourquoi,	TU Delft
	ir. S. Schenke,	TU Delft
	ir. B. Schuiling,	MARIN
	Dr. ir. G. Vaz.	MARIN

An electronic version of this thesis is available at
<http://repository.tudelft.nl/>.



Acknowledgements

This thesis has been a great opportunity to expand my knowledge of Computational Fluid Dynamics and put to the test all the knowledge I have gathered throughout the last year at university. For that I would like to thank my supervisors at MARIN, Bart en Guilherme, for their patience in guiding me and the knowledge that they shared. Resources made available by MARIN should be especially acknowledged. The hours spend on the Marclus3 cluster are large for full-scale calculations and could not have been done without them.

Secondly I want to thank the whole committee for taking the time to read and grade my work. But also for the discussion and widening of the view.

Last but not least I want to thank my friends and family for their encouragement and support during the project. I want to give special thanks to my boyfriend who created a home, so I could fully focus on my project.

Vera Wieleman,
June 2018

Abstract

An accurate prediction of propeller hull interaction is an important step in the design of a new vessel. The prediction of full-scale flow phenomena, which eliminates scale effects, is becoming available due to increasing computational power. However, the complexity of full-scale CFD calculations combined with a lack of validation data results in unknown uncertainties. This study contributes to the uncertainty estimation for full-scale calculations by answering the question *With what uncertainty can we currently numerically predict resistance and propeller power on full-scale Reynolds numbers?*

The resistance and propeller flow predictions are done for the general cargo vessel MV-regal for three cases; a double body, a free surface resistance simulation and an open water propeller simulation. The simulations are performed for the design speed of 14 knots, resulting in a full-scale Reynolds number of $Re = 1.12 \cdot 10^9$. The discretization error is determined by the grid refinement study as presented by Eça and Hoekstra for the propulsion parameters; resistance coefficients and the wake factor. For each case the flow field is analysed, an uncertainty assessment is made and the results are compared to a group of numerical results for the same simulation performed by 20 participants of a case study organised by Lloyd's register on the same vessel as is considered in this thesis.

Modelling the boundary layer of a flat plate on model and full-scale Reynolds numbers encourages the use of unstructured grids for full-scale Reynolds numbers. The uncertainties as predicted by the grid refinement study, vary between 0.6 and 24.5 percent for the friction coefficient. For the $Re = 10^7$ the values are compared to a structured grid study, which had a better trend over the grid refinement series. Comparison to theoretical friction coefficient calculations confirmed the absolute friction result.

The double body simulation, performed on the full-scale number $Re = 1.12 \cdot 10^9$, demonstrated the use of the unstructured grids on the full-scale Reynolds numbers. The iterative error had to be closely monitored in order to get a stable solution. While the iterative errors had the same order of magnitude, the uncertainties as predicted by the grid refinement study for the propulsion parameters varied between 1.5 and 140 percent. This is an unacceptable large scatter in uncertainty which calls for another method to determine the uncertainty.

The free surface simulation added complexity, by modelling the free surface resistance of the vessel. The order of convergence is lower for the free surface simulation, which creates a higher iterative error in the uncertainty assessment. The discretization uncertainty prediction varies between 2.7 and 23.5 percent.

The open water simulation, which is based on a hybrid grid of structured and unstructured grids, showed for the monitored parameters a sufficiently low iterative error and a low discretization uncertainty (between 0.1 and 3.4 percent) for the thrust and torque coefficients.

Although all different cases showed mixed results for the discretization error, the absolute values are well within the range of results from the test group of 20 participants. This is a good starting point of the repeatability of the flow parameters. It is noted that the current uncertainty estimation is larger than the difference between two grids.

Contents

Acknowledgements	iii
Abstract	v
List of symbols	xi
List of abbreviations	xiii
List of Figures	xv
List of Tables	xix
1 Introduction	1
1.1 Motivation and relevance.	1
1.2 Comparable work.	2
1.3 Objective and scope	3
1.4 Plan of Approach	4
1.5 Report structure	5
2 Theoretical framework: Computational Fluid Dynamics	7
2.1 Governing Equations	7
2.1.1 Conservation of mass: Continuity Equation.	7
2.1.2 Conservation of momentum: Navier-Stokes momentum equation.	7
2.1.3 Boundary conditions and initialisation	8
2.2 Computational Fluid Dynamics	9
2.2.1 RaNS equations	9
2.2.2 Turbulence	9
2.2.3 Grid	9
2.2.4 Time discretization	9
2.2.5 Transport equations	9
2.2.6 Numerical procedure	10
3 Method: Verification and validation	11
3.1 Verification: uncertainty and errors in numerical methods	11
3.2 Grid refinement study	12
3.2.1 Refinement Diffusion	13
3.2.2 Viscous layer	14
3.3 Validation	14
4 Method: Numerical setup	15
4.1 Grid generation: Hexpress	15
4.2 Numerical calculations: ReFresco	16
4.2.1 Spatial discretization	16
4.2.2 Temporal discretization.	17
4.2.3 Turbulence	17
4.2.4 Free surface	17
4.2.5 Convergence	17
4.3 Case 1: Double body simulations	17
4.3.1 Domain and boundary conditions	17
4.3.2 Final grid parameters.	18
4.4 Case 2: Free surface simulations	18
4.4.1 Domain and boundary conditions	19
4.4.2 Final grid parameters.	20
4.4.3 Solver	21

4.5	Case 3: Propeller open water simulations	22
4.5.1	Domain and boundary conditions	22
4.5.2	Final grid parameters and refinements	22
4.5.3	Solver	23
5	Flat plate verification study	25
5.1	Calculation setup	25
5.1.1	Domain and boundary conditions	25
5.1.2	Grid settings	26
5.1.3	Geometrical grid similarity	27
5.2	Results	28
5.2.1	Iterative error	28
5.2.2	Discretization uncertainty	30
5.2.3	Comparison with Friction line theory.	31
5.2.4	Analysis of grid similarity	32
5.3	Conclusions on initial calculations	34
6	Case 1: Double body	35
6.1	Evaluation of flow field characteristics.	35
6.2	Flow comparison for the full and half modelled ship	38
6.3	Uncertainty	40
6.3.1	Iterative error	40
6.3.2	Discretization uncertainty	41
6.4	Evaluation of the resistance	44
6.5	Conclusions.	45
7	Case 2: Free Surface	47
7.1	Evaluation of flow field characteristics.	47
7.2	Uncertainty	50
7.2.1	Iterative error	50
7.2.2	Discretization uncertainty	51
7.3	Comparison to Double body simulations	54
7.3.1	Friction coefficients	54
7.3.2	Pressure coefficients	54
7.4	Comparison to Lloyd's case	55
7.4.1	Resistance coefficients.	55
7.4.2	Dynamic trim and sink	55
7.4.3	Wave cuts.	56
7.5	Conclusion	56
8	Case 3: Open Water	59
8.1	Evaluation of flow field characteristics.	59
8.2	Uncertainty	61
8.2.1	Iterative error	61
8.2.2	Discretization uncertainty	62
8.3	Comparison to Lloyd's case	63
8.4	Conclusions.	64
9	Conclusions	65
9.1	Double body	65
9.2	Free surface	66
9.3	Open water	66
10	Recommendations	69
	Bibliography	71
A	Flat plate grid quality study	73
A.1	Hexpress-Default	73
A.2	Geometrical Similar	73

B	Grid refinement study for propeller parameters	81
C	ReFresco input	85
C.1	Flat plate	85
C.2	Case1: Double Body	92
C.3	Case2: Free Surface	101
C.4	Case3: Propeller	112

List of symbols

Latin

Symbol	Units	Description
c_f	[—]	Friction coefficient
c_p	[—]	Pressure coefficient
c_t	[—]	Total resistance coefficient
D	[m]	Propeller diameter
d_i	[—]	Diffusion depth at grid i
Fn	[—]	Froude Number
f_i	[m/s ²]	Vector containing external forces
g	[m/s ²]	Gravitational acceleration
h_i	[m]	Initial viscous layer cell size at grid i
I_{tu}	[%]	Turbulence intensity
J	[—]	Advance ratio
Kt	[—]	Thrust coefficient
KQ	[—]	Torque coefficient
L	[m]	Length
L_2	[—]	Average residuals
L_∞	[—]	Highest residuals
n	[s ⁻¹]	Propeller speed
p	[Pa]	Pressure
Re	[—]	Reynolds Number
r_i	[—]	Refinement of grid i
t	[s]	Time
U	[%]	Uncertainty
u	[m/s]	Velocity in x direction
u_i	[m/s]	Velocity vector
v	[m/s]	Velocity in y direction
v_a	[m/s]	Advance velocity
w	[m/s]	Velocity in z direction
x_i	[m/s]	Location vector
y^+	[—]	Dimensionless wall-function

Greek

Symbol	Units	Description
γ	[N/m]	Surface tension
γ_i	[—]	Cell size Growth in the viscous layer of grid i
η_0	[—]	Open water efficiency
μ	[kg/(m·s)]	Dynamic viscosity
μ_t	[kg/(m·s)]	Turbulent viscosity
ρ	[kg/m ³]	Fluid density
σ	[N/m]	Stress
Φ_0	—	Predicted value of the parameters
Φ_i	—	Parameter at grid i.

List of abbreviations

BEM	Boundary Element Method
CFD	Computational Fluid Dynamics
CFL	Courant–Friedrichs–Lewy condition
MARIN	Maritime Research Institute
NUA	Numerical Uncertainty Analysis
OWD	Open Water Diagram
QUICK	Quadratic Upwind Interpolation for Convective Kinetics
RaNS	Reynolds averaged Navier Stokes
SST	shear stress transport

List of Figures

1.1	Speed-power curve prediction, simulation (points) and measurements(ISO15016) from the Lloyd's workshop [2], which show the large scatter for individual results.	2
2.1	Schematic overview of the SIMPLE algorithm.	10
3.1	Flowcharts of the numerical errors present between the continuous mathematical model and the computed result. [20].	11
3.2	Five refined grids that are geometrically similar.	13
3.3	Geometrically similar viscous layer for a simple 1D case with the wall located at the left side.	14
4.1	Various steps in Hexpress (image source [21]).	15
4.2	View of the domain with the size of the domain expressed in the L_{pp} of the vessel. The domain is shown from the inflow and the side of the domain.	18
4.3	Overview of the grid for the full vessel for grid 0 (top) and grid 6 (bottom). The geometrical similarity of the refinement levels is visible in this figure.	19
4.4	Comparison of grid details for grid 0 to 6.	19
4.5	View of the domain with the size of the domain expressed in the L_{pp} of the vessel. The domain is shown from the inflow and the top of the domain.	20
4.6	Comparison of grid details for grid 0 to 5.	21
4.7	Various views of the open water domain for the coarsest grid (Grid 0) and the finest grid (Grid 6).	24
5.1	Sideview of the domain of the flat plate (shaded part is the plate).	25
5.2	Grid for the flat plate study for Reynolds 10^4	27
5.3	Image of the structured and unstructured (<i>Hexpress-Default</i> and <i>Geometrical Similar</i>) grid showing part of the plate and part of the wakefield (same scale) for the coarsest grid.	28
5.4	Convergence of the coarsest grids (left) and the finest grids (right).	29
5.5	Uncertainty Analysis.	30
5.6	Reynolds 10^7 with three grid types and the three friction lines.	32
5.7	Comparison of the smoothness of the transition from the Euler grid to boundary layer in grid refinement 10 (finest grid) for the <i>Geometric Similar grid</i> and the <i>Hexpress Default grid</i> . In the most right image the contour and vector plot for the <i>Geometric similar grid</i> is show with the white line indicating the $V_x/V_{tn} = 0.99$	32
5.8	Image of the normalised velocity in x direction at the end of the plate, with the grid projected on the flow field (for the <i>Hexpress-Default</i> grid). This shows the influence of the cell shape on the flow field.	33
5.9	Reynolds 10^7 for <i>Hexpress-Default</i> grid.	33
5.10	Reynolds 10^7 with three grid types.	34
6.1	Normalised velocity field at the rudder on the symmetry plane. Shown for the finest grid with and without the mesh.	36
6.2	The gradients in the boundary layer together with the grid used to model the viscous layer. The location of this image is at the bottom midship at the symmetry plane.	36
6.4	Q criteria ($Q>0$).	36
6.5	Vectors (V_t) in the Wakefield which show the bilge vortex through the wakefield.	36
6.3	Various locations with a contour plot of the pressure coefficient presenting the highest gradients and the global pressure distribution around the ship.	37
6.6	Friction coefficient on the vessel and a close-up of the friction coefficient on the rudder.	38

6.7	Contour plot of the Velocity in X-direction of the wakefield for the half body calculations for the finest and the coarsest grid.	38
6.8	Difference in X velocity normalised with the ship speed at the longitudinal through the middle of the ship. The results of the mirrored calculation is subtracted from the half ship simulation. So, negative values present a higher prediction in the full ship result.	39
6.9	Wakefield comparison for the half and full body on grid 4. Contains contours of the velocity in x direction.	39
6.10	Difference in normalised X velocity for the full and the half body.	39
6.11	Convergence graphs of the finest and coarsest grid for the double body simulation.	40
6.12	Location of the residuals in the finest grid, grid 6. The residuals are located in the complex flow coming from the stern.	41
6.13	The quality of the grid cells for the coarsest grid, grid 0. Grid 0 is presented here, because the finer grid have a better grid quality.	42
6.14	Uncertainty of the two resistance components and the total values based on the number of cells on the hull.	43
6.15	Comparison of the calculated grid refinement series compared to the frictions lines as defined by ITTC '57 [1], Katsui [18] and Grigson [15].	45
6.16	Comparison of the friction component with the Lloyd's register case for 14 knots.	45
7.1	Two velocity flow details for the free surface simulations.	48
7.2	The wakefield for grid 4, showing the axial velocities in the contour plot and the transverse velocities and directions in the contour plot.	48
7.3	Waves viewed with the Kelvin wedge in the grid projected on the contours of the waves, and a presentation of the number of cells per wave for an indication of the grid quality.	49
7.4	Visualisation of the main wave systems of the ship by presenting a 3D view of the free surface and the number of cells per wavelength.	50
7.6	Visualisation of the residuals for the turbulent variable ω	51
7.7	The results of the grid refinement study by Eça and Hoekstra for the resistance components and wake.	52
7.8	The results of the grid refinement study by Eça and Hoekstra for the trim and sink.	53
7.9	Wave cut presentation of the grids 0,1,2 and 4 in order to visualise the discretization error in the wave cut.	54
7.10	Grid refinement comparison for the double body (red) and the free surface (blue) simulations.	54
7.11	Comparison of the friction component with the Lloyd's register case for 14 knots.	55
7.12	Comparison of the pressure component with the Lloyd's register case for 14 knots.	55
7.13	Comparison of the total resistance component with the Lloyd's register case for 14 knots.	56
7.14	Wave cuts at $0.1L_{PP}$ for the coarsest (yellow) and the finest (blue) grid, plotted together with results of the Lloyd's workshop. The bow is located at 0.5 and the stern at -0.5	56
8.1	Axial velocities in the open water simulation for a low advance ratio and the advance ratio for the design point.	60
8.2	Pressure gradients on the propeller blade for a low advance ratio and the advance ratio for the design point at the location $r/R = 0.7$	60
8.3	Comparison of the open water diagram for the coarsest (grid 0) and the finest grid (grid 3).	60
8.4	Iterative Error over the complete open water simulation on grid 3.	61
8.5	Iterative Error over the complete open water simulation on grid 3 zoomed in for $J = 0.5$	61
8.6	Discretization uncertainty for the torque, thrust and open water efficiency on the design point ($J = 0.5$).	62
8.7	Comparison of the open water diagram for the finest grid (grid 3) and the resulting averaged OWD from the Lloyd's workshop.	63
8.8	Comparison with Lloyd's results for K_t and $10K_Q$ at $J = 0.5$	64
A.1	Grid Properties of the coarsest <i>Hexpress-Default</i> grid.	74
A.2	Grid Quality of the coarsest <i>Hexpress-Default</i> grid.	75
A.3	Residuals on the coarsest grid: Velocity X.	76
A.4	Residuals on the finest grid: Omega (ω).	76
A.5	Grid Properties of the coarsest <i>Geometric Similar</i> grid.	77

A.6	Grid Quality of the coarsest <i>Geometrical Similar</i> grid.	78
A.7	Residuals on the finest grid: Omega (ω).	79
A.8	Residuals on the coarsest grid: Velocity X.	79
B.1	Thrust coefficients for the total range of advance ratio's.	82
B.2	Torque coefficients for the total range of advance ratio's.	83

List of Tables

1.1	General specifications of the general cargo vessel MV-Regal.	4
3.1	Input parameters for example on refinement diffusion parameter, with parameters from table 3.1.	13
4.1	Grid refinement settings and resulting y^+ data for the double body simulation. Per case the initial cells size in the viscous layer h_0 , the growth factor γ , average $\overline{y^+}$ and maximum y_{max}^+ is given.	18
4.2	Level of refinement on the ship based on findings in [7].	19
4.3	Grid refinement settings and resulting y^+ data for the free surface simulation. Per case the initial cells size in the viscous layer h_0 , the growth factor γ , average $\overline{y^+}$ and maximum y_{max}^+ is given.	20
4.4	Level of refinement on the ship based on findings in [7].	21
4.5	Courant numbers on the finest refinement level (10) in the grid for the unsteady free surface simulation.	22
4.6	Grid refinement settings and resulting y^+ data for the open water simulation. Per case the initial cells size in the viscous layer h_0 , the growth factor γ , average $\overline{y^+}$ and maximum y_{max}^+ y^+ is given.	23
4.7	Level of refinement in the propeller domain.	23
5.1	Inflow boundary conditions, based on experience with ReFresco and the validation study of Eça et all. [14].	26
5.2	Grid refinement settings and resulting y^+ data for the flat plate case study. Per case the initial cells size in the viscous layer h_0 , the growth factor γ , average $\overline{y^+}$ and maximum y_{max}^+ y^+ is given.	27
5.3	Numerical results of the finest grids and the estimated uncertainty. Also the difference between the maximum and minimum result of the grid study are given as a percentage of the finest grid.	31
6.1	Comparison of flow parameters for full ship and half ship	40
6.2	List of the estimated values and uncertainty by the method of Eça and Hoekstra.	44
6.3	Friction line values for $Re = 1.12 \cdot 10^9$	44
7.1	List of the estimated values and uncertainty by the method of Eça and Hoekstra.	53
8.1	List of the estimated values and uncertainty by the method of Eça and Hoekstra for $J=0.5$	63

Introduction

The computation of ship resistance and flow in an early design stage provides a significant contribution in the whole process of ship design and the prediction of required installed power. Computational fluid dynamics (CFD) are rapidly gaining ground compared to experimental fluid dynamics. The main reason for this is the reduced cost of analysing a large variety of scenarios. The cost of model tests increase nearly proportional with every scenario in contrast to CFD. Next to that, CFD can give detailed insight in local flow phenomena, which can not be observed in model tests (or are quite expensive to perform). Furthermore, CFD has the possibility to perform calculations on full-scale which, if verified and validated, is of more value than results on model-scale. At this moment the lack of precision and accuracy is the weak element in the chain of full-scale calculations.

1.1. Motivation and relevance

A propulsion analysis allows for a prediction of the flow around the ship and thereby yields the power necessary to reach the design speed of the vessel. This is an important aspect in ship design, since most building contracts are based on the design speed. The flow around the ship, which exerts pressure forces and shear stresses on the ship, gives insight in the corresponding resistance components. The friction component of the resistance is based on the shear stress in the flow acting on the hull. The pressure component is based on the three dimensional body flow and the wave system [20]. With computer calculations these components (shear stress and pressure) can be analysed separately.

A propulsion analysis on full-scale Reynolds numbers results in the flow, resistance and power parameters that apply directly to the real ship. A (numerical or experimental) model size prediction should comply with all the scaling laws; geometric-, dynamic- and kinematics similarity, but this is never actually the case because of the dilemma in speed of the vessel (Froude number dictates lower speeds, Reynolds number dictates higher speeds on model-scale) [20]. The Froude scaling is usually used in this dilemma, but corrected for the Reynolds number. The corrections used are defined by, for example, the International Towing Tank Contention (ITTC) of which, because of years of experience, the error and uncertainty are known.

Increasing computational power creates possibilities to perform larger calculations. This means an increased level of detail or expanding from model-scale to full-scale calculations. A comparison is made in [16] on the difference in model- and full-scale calculations. Their findings describe a loss of detail in the model calculations mainly in the boundary layer, flow separation and the wave breaking calculations. Full-scale verification is not done regularly and full-scale experimental test are almost impossible to perform therefore more focus should be placed on verification of the numerical results.

Not much information on the uncertainty analysis is available. In the workshop for example the results are presented without uncertainty and thus is it hard to analyse the value of these results.

A clear example on the unknown uncertainty and accompanying scatter of full-scale CFD results is a case study organised by Lloyd's Register almost two years ago (June 2016). This workshop focused on full-scale calculations of the general cargo vessel MV-Regal. A group of 20 participants performed full-scale calculations, with a numerical method of their choice, for four cases; free surface, open water, self-propulsion calculations and a cavitation observation. For the third case, the self-propulsion point, three

propeller speeds are given and the resulting speed and power are plotted in Figure 1.1. In this figure a wide scatter in power and speed can be seen for all three propeller speeds and with increasing rpm the scatter for the power prediction increases. The highest speed prediction of case 3.2 is even higher than the lowest speed prediction for case 3.3. This illustrates that currently unknown uncertainties are present in CFD calculations.

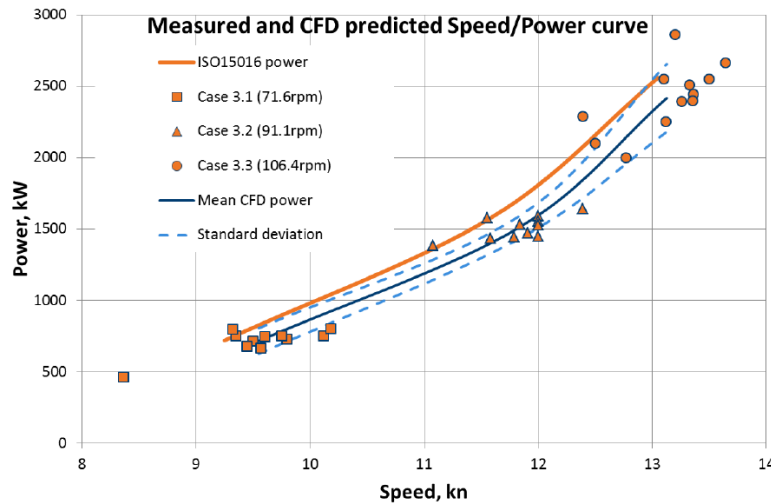


Figure 1.1: Speed-power curve prediction, simulation (points) and measurements(ISO15016) from the Lloyd's workshop [2], which show the large scatter for individual results.

Uncertainty of numerical calculations can be determined by quantifying the different types of errors that occur. In a numerical model, going from reality to a computer result, three main types of errors can occur; input errors, modelling errors and numerical errors. Input errors are a consequence of a wrong first interpretation of the problem. Modelling errors are the neglected physical effects in the solver. Various turbulence models are available such as LES, (U)RaNS and DNS. RaNS solvers (Reynolds Average Navier Stokes) are the less detailed, but are more robust and faster than the LES and DNS solvers, which solve directly Large Eddies and the Direct Navier Stokes equations. Within the RaNS model various assumptions have to be made, for example in the implementation of turbulence and the integration of the pressure in the equation. These assumptions contribute to the modelling error. Numerical errors consist of discretization, convergence and round-off errors. The discretization error is the most important one since this error can be influenced by changing your grid. For full-scale modelling there is need for unstructured grids with lesser cells compared to structured grids. Also, the construction of an unstructured grid is faster than the construction of structured grids. But an error estimation of these settings is needed.

Summarising, the infrastructure is ready for full-scale CFD calculations but the uncertainties are still unknown. This calls for a thorough verification and validation study for full-scale propulsion calculations, which is the goal for this thesis

1.2. Comparable work

The main point of reference for this thesis is the overall result of the Lloyd's workshop[2]. This dataset is chosen because it does not only give a motivation to access the uncertainty, but also provides comparable results for the flow fields of 20 participants for four cases. The necessity to model the first three cases from the Lloyd's workshop (free surface, open water and self-propulsion) are emphasised by Castro et al. [6], where also full-scale self-propulsion simulations were performed. One of the main advantages of full-scale simulations was the thinning of the boundary layer at higher Reynolds numbers. This thinning resulted in a more uniform wakefield which causes a lower hull interaction and less cavitation on the propeller. On model-scale the propeller is modelled too conservative, too much influence of the hull on the wakefield, and thus a full-scale calculation is recommended. Regarding flow properties Castro et al. [6] also found that the prediction of the viscous wave system differs a lot on model and on full-scale simulations. These conclusions are also supported by Hänninen et al.

[17] who specifically looked into the difference in boundary layer, flow separation and wave profiles between model and full-scale calculations. Based on those results, it is advised to use a turbulence model with sufficient accuracy for modelling the wakefield.

More fundamental research is done in the work by Abrue et al [3], which presents a sensitivity study for domain size, inlet and boundary conditions. According to the authors, attention must be given to make fine grid structures at locations with high gradients. They also concluded that the combination of domain size and boundary conditions (such as pressure and turbulence inflow quantities) should be implemented with caution, so no numerical effects arise at the domain boundary. Additional to that Vaz et al. [24] shows a validation study for the FRESKO code, on which ReFRESKO is based. Various problems are discussed and concluded that it is an adequate platform for free surface flows. Modelling for a self-propulsion situation is done by Bugalski et al. [5] for model-scale situations. This article yields the difficulty of modelling the interaction between the hull and the propeller.

An elaborate verification and validation study with focus on turbulence modelling for full-scale calculations is done for the KVLCC2 by Pereira et al. [22]. The calculations are done for a double body, without wall functions. For their full-scale simulation the robustness of the turbulence models is tested and confirmed, but their recommendation is to quantify the modelling errors which do require more insight in the numerical accuracy of the CFD model.

1.3. Objective and scope

As explained in the previous sections there is a global desire to increase the knowledge on the uncertainty and error in the full-scale numerical prediction of a vessel. The goal of this research is summarised in the main research question:

With what uncertainty can we currently numerically predict resistance and propeller power on full-scale Reynolds numbers?

The scope will be clarified in the next paragraphs by discussing parts of the research question. The error and uncertainty of a parameter can be estimated by systematic studies. Various quantities can be altered, such as grid cell size (grid refinement study), domain size, number of refinement levels, use/location/size of refinement boxes. A study by Crepier [7] already gives a recommendation for the location of refinement boxes and levels for the combination of unstructured grids with ReFRESKO. Therefore the focus will be on a grid refinement study. The expectation is that this will give the largest error and possible instabilities in calculations. This does provide a challenge because for full-scale it is common to use unstructured grids which is conflicting with the requirement for systematic grid refinement studies.

For the numerical prediction the open-source code ReFRESKO will be used, which is continuously under development at MARIN and accompanying universities¹. Chapter 4 will elaborate on the use of this program and how the problem will be discretized.

The focus for the parameters is based on variables that are important in propulsion analysis, but can also be used in verification and validation studies. The parameters chosen are the resistance coefficients (friction, pressure and total), wake factor, thrust, torque, and wave pattern where possible.

The test case for this study is the general cargo vessel MV Regal, as defined in the Lloyd's Register workshop (later referred to as Lloyd's Workshop). There are two reasons why this vessel is chosen. First, a lot of reference data is available from the workshop. This includes calculations done by 20 participants, sea-trial data, and a 3D scan of the underwater ship including the propeller. Additionally, the geometry is relatively simple, which makes the ship ideal for CFD calculations. It has not many appendages, no bulb, single screw, no thrusters, and no energy saving devices are present. In Table More information on the vessel and the case can be found in the proceedings of the workshop [2].

¹for a list of the contributors: <http://www.refresco.org/community/users/>

Table 1.1: General specifications of the general cargo vessel MV-Regal.

Parameter	Value	Unit
Service speed	14	[Knots]
Service speed	7.202	[Knots]
Deadweight	16 890	[Tonnes]
Displacement	12790	[m ³]
Length	138	[m]
Breadth	23	[m]
Depth	12.1	[m]
Draft aft	5.6	[m]
Draft forward	4.9	[m]
Wetted surface	3702	[m ²]

1.4. Plan of Approach

As stated before the verification will be done by a grid refinement study. Since all these cases are also performed in the Lloyd's Workshop, the solution will be compared to the solutions of the participants. The focus within this thesis lies on the uncertainty assessment.

To identify the uncertainties in the full-scale calculation, a grid refinement study is done for the design speed of the vessel (14 knots). Because of the complexity of unstructured grids with a grid refinement study, a test of the method will be performed on a flat plate on full-scale Reynolds numbers. This refinement study will be done for three simulation cases, which will be performed chronologically.

1. Double hull
2. Free surface resistance
3. Open-water propeller

Case 1: Double hull

The double hull calculations are steady turbulent calculations without a free surface. In terms of calculation time this means that these are relatively fast simulations and can therefore be used to locate high gradients in the results and improve the grid quality for these locations. This means no wave resistance is present and the remaining resistance is caused by friction and body shaped flow. No roughness will be used, but the calculations will be performed without wall functions.

The double body simulation is easier than a free surface resistance calculation, because it has no free surface modelling. This calculation will give insight in the complexity of the full-scale body flow. The lack of free surface effects creates the possibility to focus on the friction component of the hull resistance. This friction can be compared to various friction line theories like ITTC[1], Grigson[15] and Katsui[18].

The Lloyd's case did not provide double body calculations but the friction results from the free surface calculation can be used, although with caution. The wave system will not extensively influence the friction component of the resistance and thus preliminary conclusions can be drawn from this comparison.

Case 2: Free surface resistance

The next step is free surface resistance tests which provide the complete modelling of flow around the hull. This is expected to be a quasi-steady simulation which means that the unsteady simulation will result in a steady result. The free surface resistance calculation should contain free dynamic trim angle and sinkage. This will cost additional calculation time, but will save time in the final self-propulsion case.

The flow results will be compared to the double body case and the results given by the Lloyd's case. The influence of the free surface on the wakefield and resistance components will be discussed, together with the grid refinement study of this flow. Also the resistance components and the wave system can be compared to the prediction by the participants in the Lloyd's case. Finally an image of the actual wave system seen from the bridge available and can be visually compared to the simulated wave system.

Case 3: Open water

In the open water case the whole open water diagram will be calculated at a constant rpm, but varying inflow. Since the open water diagram has normalised values this should provide the results for sailing the vessel at various speeds. All four blades are modelled to take into account discrepancies on the individual blades.

Together with the free surface simulation this should already give an indication for the self-propulsion point and power necessary, although this does not include yet the propeller hull interaction. For the grid refinement study the thrust and torque components of the flow will be analysed. The pressure component is the driving force of the propeller

1.5. Report structure

The outline of the report is as follows; this chapter clarified the introduction and problem description. Chapter 2 lists the necessary theory and formulations to physically understand the case discussed. Chapter 3 discusses in detail the errors that can be made in the numerical modelling. It further elaborates on the challenges that arise with the use of unstructured grids in a grid refinement study. In Chapter 4 the usage and working principles of Hexpress (grid generation) and ReFresco (RaNS solver) are presented along with the domain and numerical setup of the 3 cases. After that the flat plate grid study is presented in Chapter 5 and the method is discussed based on the findings in this case. Next, the three cases will be discussed in Chapters 6, 7 and 8. This will contain the verification and validation for the certain cases and the details of the flow. The overall conclusions of the report are summarized in Chapter 9. The report will be finalized with the recommendations for improvement and further research in Chapter 10.

2

Theoretical framework: Computational Fluid Dynamics

This chapter provides the theoretical framework for this thesis. Starting with the governing equations in Section 2.1 which discusses the conservation laws and various types of boundary conditions necessary to describe the problem in terms of equations. The second part of this chapter, Section 2.2, gives an introduction into Computational Fluid Dynamics which includes the RaNS equations and a schematic visualisation of algorithms of numerical solvers.

2.1. Governing Equations

Almost all problems in fluid mechanics can be solved by the Navier-Stokes equations, taking into account the appropriate boundary conditions. The Navier-Stokes equations consist of conservation of mass, conservation of momentum and conservation of energy. For this thesis the conservation of mass and momentum are the most important. Below, both equations are presented and for a detailed derivation [19, 20] is recommended.

2.1.1. Conservation of mass: Continuity Equation

The conservation of mass is expressed in the continuity equation. In words, conservation of mass means the net in- and outflow in any of the directions should be equal to zero, assuming there is no mass source or sink. The differential form of the equation is shown in Equation 2.1. The velocity vector is given by u_i and the spatial vector is given by x_i .

$$\frac{\partial u_i}{\partial x_i} = 0 \quad (2.1)$$

2.1.2. Conservation of momentum: Navier-Stokes momentum equation

The Navier-Stokes momentum equations (NS-equations) describes an momentum equilibrium in the flow. The formulation of the differential form in Einstein notation for incompressible flow is shown in Equation 2.2. The following parts can be distinguished in the formula from left to right; local acceleration, transportation, pressure gradients, viscous forces and external forces.

The unknown variables in the Navier-Stokes equation are the velocities u, v, w and the pressure p , the remaining parameters in the equation are determined by the fluid and surroundings and geometry. The remaining parameters are time t , density ρ , dynamic viscosity μ , location x, y, z and external forces f_i . An example of external forces is gravity, which is important for modelling waves in the free surface. Together with the continuity equation, this is a solvable set of equations (four variables, four equations).

$$\frac{\partial u_i}{\partial t} + u_j \frac{\partial u_i}{\partial x_j} = -\frac{1}{\rho} \frac{\partial p}{\partial x_i} + \frac{\mu}{\rho} \frac{\partial^2 u_i}{\partial x_j \partial x_j} + f_i \quad (2.2)$$

2.1.3. Boundary conditions and initialisation

Boundary conditions and initialisation of the domain are necessary in order to express the problem with the governing equations. For problems in hydrodynamics, both physical and numerical boundaries can be distinguished. Primary focus is placed on solid surfaces and liquid surfaces for the physical domain. Next to that, the infinity boundary for the location where local physical effects are dampened to zero is considered as a boundary in accordance with literature [20]. These groups are discussed below.

Solid surfaces

For solid interfaces one constraint is present in the normal direction, the watertight condition. At a solid interface no net flow normal to the surface can be present.

$$u_{n_{solid}} = u_{n_{fluid}} \quad (2.3)$$

For the velocity tangential to the solid-liquid interface, various conditions are applicable depending on the problem described. Three possible boundary conditions in tangential direction are no-slip, slip and free-slip. In the no-slip condition the tangential velocity of the fluid flow is the same as the tangential velocity of the solid. Down to a molecular level of flow description this is a valid boundary condition. If the solid velocity in the reference frame is zero, then the fluid velocity at the solid interface is also zero.

$$u_{t_{solid}} = u_{t_{fluid}} \quad (2.4)$$

In the slip condition a velocity difference between the solid and the fluid is possible. This can be visualised in the equation by adding a constant (Equation 2.5). The free-slip condition states that the tangential fluid velocity is not influenced by the presence of a solid. It can move freely along the solid interface and only the watertight condition is applied. The slip and free-slip conditions are rarities in physical problems, but could help to simplify the numerical problem.

$$u_{t_{solid}} = c \cdot u_{t_{fluid}} \quad (2.5)$$

Liquid interfaces

After the solid-liquid interface the liquid-liquid interface is discussed by the kinematic and dynamic boundary conditions. First, based on the kinematic boundary condition, there is no flow present through the interface. This is the same definition as the watertight conditions for the solid surface (Equation 2.3). Secondly, the dynamic forces on the interface should be in equilibrium. Both tangential and normal forces should comply with this equilibrium. In terms of shear stresses (σ) (for fluid 1 and 2) this boundary condition is shown in Equations 2.6 and 2.6. For normal stresses the force equilibrium is shown in Equation 2.8. This shows the relation between the normal stresses(σ), pressure(p) and surface tension(γ).

$$\sigma_{(ns)1} = \sigma_{(ns)2} \quad (2.6)$$

$$\sigma_{(nt)1} = \sigma_{(nt)2} \quad (2.7)$$

$$(\sigma_{(nn)} - p)_1 = (\sigma_{(nn)} - p)_2 + \Delta p_\gamma \quad (2.8)$$

Domain boundaries

The domain boundaries also have three possible boundary conditions; solid-fluid interface, represent infinity or a symmetry boundary. The properties of a solid-fluid interface have been discussed in the corresponding subsection above. The representation at infinity states that no disturbances for a parameter (such as pressure or velocity) are present at that boundary. For most cases this means that the flow is in initial state, and that this boundary is suitable for initialisation of the flow. The symmetry conditions represent a mirror in the domain. The flow properties, like velocity, are symmetrical. In most cases this has the same result as the free-slip condition. To avoid numerical reflection an outflow condition should be applied at the outflow location of the domain.

2.2. Computational Fluid Dynamics

Nowadays various ways to numerically calculate the flow round a ship are available. A couple of methods are stated from high calculation time to short; Direct Numerical Simulation (DNS), Large Eddy Simulation (LES), Reynolds-average Navier-Stokes (RaNS). On one end, DNS will simulate all the details in the flow and on the other RaNS equations will give a time averaged solution and thus the average flow. In this thesis RaNS equations will be used, since a large number of calculations will be done and the level of detail present in DNS or LES, as clarified in the introduction, is not required.

2.2.1. RaNS equations

The RaNS equations are the result of time averaging the NS-equations and substituting the variables (velocity and pressure) by an average term and a fluctuation term. These are notated with \bar{u} and u' respectively (example for velocity u). The time scale used for averaging should be the largest time scale present in the problem.

$$\frac{\partial \bar{u}_i}{\partial t} + \frac{\partial}{\partial x_i} (\bar{u}_j \bar{u}_i) + \frac{\partial}{\partial x_j} (\bar{u}'_j \bar{u}'_i) = -\frac{1}{\rho} \frac{\partial \bar{p}}{\partial x_i} + F_i + \frac{1}{\rho} \frac{\partial \sigma_{ji}}{\partial x_j} \quad (2.9)$$

The averaged RaNS equation (Equation 2.9) contains an extra term compared to Equation 2.2. This extra term is a non-linear term which represents the so-called Reynolds-stresses (defined as R_{ji} in the equations below).

$$\frac{\partial \bar{u}_i}{\partial t} + \frac{\partial}{\partial x_j} (\bar{u}_j \bar{u}_i) = -\frac{1}{\rho} \frac{\partial \bar{p}}{\partial x_i} + F_i + \frac{1}{\rho} \left(\frac{\partial \sigma_{ji}}{\partial x_j} + R_{ji} \right) \quad (2.10)$$

$$R_{ji} = R_{ij} = -\rho \frac{\partial}{\partial x_j} (\bar{u}'_i \bar{u}'_j) \quad (2.11)$$

2.2.2. Turbulence

Physically, turbulence energy is generated in the largest vortex scales and transferred to medium scale vortices and dissipated in micro scale vortices. Turbulent vortices are complex and time intensive to model, but mostly only the average influence of the turbulence on the flow is desired. This turbulence model determines the time averaged Reynolds stresses in the flow (R_{ji} part) and complete the RaNS equations.

The most turbulence models are based on the Boussinesq hypothesis, which determines the turbulent viscosity to complete the RaNS equations. The model used in this thesis is the $k - \omega$ SST model. The $k - \omega$ SST model consists of two equations, one for the turbulence kinetic energy (k) and a second for the specific rate of dissipation (ω). This model is widely used in the industry because of its stability.

2.2.3. Grid

To perform the spatial discretization a grid is generated. Two main types of grids can be distinguished in the discretization of the domain, structured and unstructured grids. Structured grids contain significantly more cells than unstructured grids, which results in a significant calculation time. Also, unstructured grids can be adapted to relatively complex geometries, like the hull of a ship. Therefore, the unstructured grid is favourable for the planned full-scale calculations.

2.2.4. Time discretization

Two schemes can be distinguished concerning the time discretization, explicit and implicit solvers. Explicit solvers solve the equations with the values of the previous time steps and implicit solvers solve the equations with the current time step. In general the implicit solvers need more calculation power per time step, but are more stable than the explicit solvers.

2.2.5. Transport equations

The grid gives the main framework for the spatial discretization of the problem, but the choice of numerical solver also determines the accuracy of the calculated value. Multiple schemes are available for calculation of the transport terms: convection and diffusion. The main trade-off in numerical schemes is the stability versus the accuracy. Low order schemes are mostly very stable, but have a less accurate

solution. Higher order schemes are more accurate, but are less stable and need more care to implement. A few spatial solvers are listed below from low order accurate to high order accurate.

- First-order upwind scheme
- Central differences
- Powers-law scheme
- Second-order upwind scheme
- QUICK (Quadratic Upwind Interpolation for Convective Kinetics)

A combination of the schemes can be used to optimise the properties, for example, a more stable, but inaccurate solver to start the solution, which will be followed up by a more accurate unstable solver.

2.2.6. Numerical procedure

The model used is based on the SIMPLE (Semi-Implicit Method for Pressure Linked Equations) algorithm. The procedure is based on various loops; the innerloop, the outerloop and the time steps. This is visualised in Figure 2.1.

The momentum equations and pressure equation are solved in chronological order within the software as a linear set of equations called the innerloop. This is completed by calculating scalars, such as turbulence, mass flows and a free-surface. The influence between two outerloops or between innerloops can be changed by using relaxation factors. On most equations under-relaxation is applied, which means that the influence of the new values is lowered. This will create a more stable simulation because it limits the changes. Nevertheless, the relaxation factors should be high as possible to ensure a fast solution method.

Two types of relaxation factors can be distinguished; explicit and implicit. Explicit relaxation factors regard the relation between outerloops and can be used freely to control the simulation. The implicit relaxation factors concern the relations in the set of equations in the innerloop and actually change the matrix to be solved. Therefore they should be closed to the original equation, which means a relaxation factor close to one.

Next in the outerloop is the redefining of the properties of the fluid, in for example a thermodynamic problem. At the end of the outerloop the convergence is checked with the norm set. If the solution converged completely, the next time step can be calculated (for an unsteady problem) or the simulation can be terminated (steady problem).

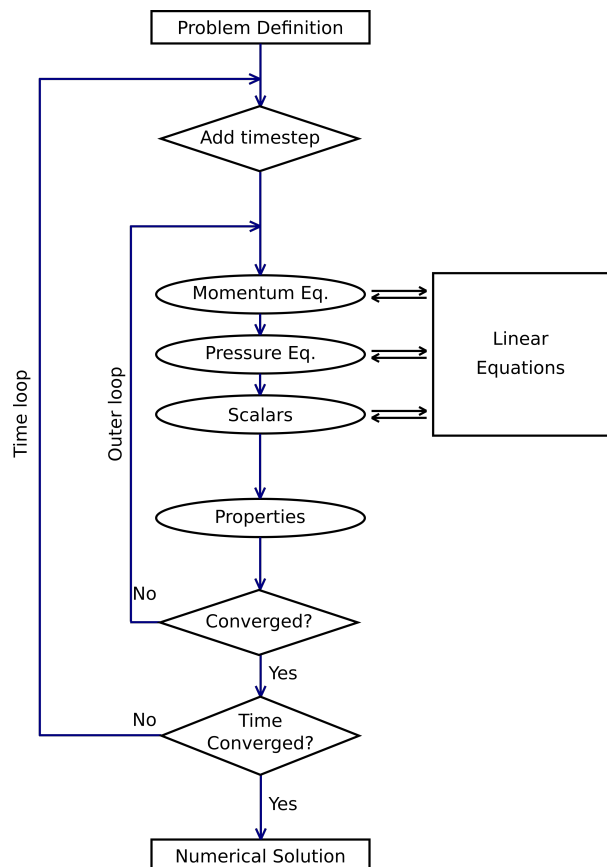


Figure 2.1: Schematic overview of the SIMPLE algorithm.

Method: Verification and validation

The goal of this chapter is to present the method for verification and validation. The verification is done by estimating the discretization error through a grid refinement study. The validation will be based on a data set of numerical results. The first section, Section 3.1 lists the numerical errors. Section 3.2 focuses on the grid refinement study and the assumptions made for the use with an unstructured grid. The last section (Section 3.3) will elaborate on the numerical data set used for comparison.

3.1. Verification: uncertainty and errors in numerical methods

Verification consists of two parts: code verification and solution verification. The code used in this thesis is ReFRESKO and the reader can find more information on the code verification in [12, 24] and in [13] which gives a more general approach on code verification.

The solution verification is accomplished by assessment of the numerical error. The numerical error in a calculation consists of four errors: discretization errors, programming errors, convergence errors and round-off errors [11, 20]. Figure 3.1 shows schematically the origin of the errors in the transformation from a mathematical model to a computed result. In the following paragraphs these errors will be discussed more in-depth.

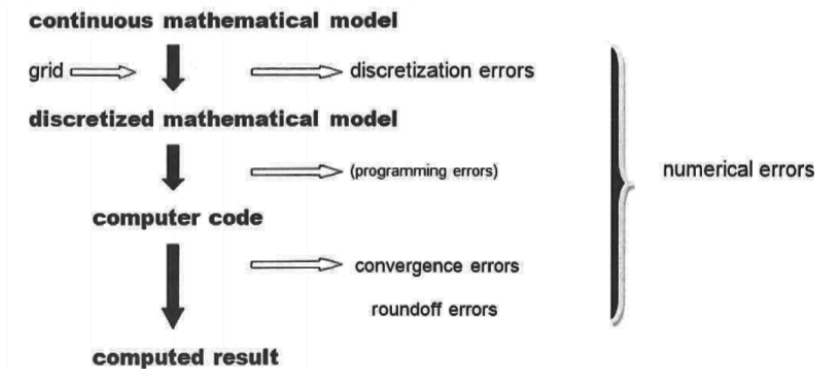


Figure 3.1: Flowcharts of the numerical errors present between the continuous mathematical model and the computed result. [20].

The discretization error is a consequence of the discretization of the RANS-equations, the solver and the grid used to do the calculation. The importance of the error decreases with a finer grid, as a finer grid would look more like a continuous field than a very coarse grid. The discretization error made in the numerical solver is discussed in Chapter 4. The error that occurs based on the construction of the grid can be estimated with a grid refinement study, as described by Eça and Hoekstra [11]. This method and the application for unstructured grids will be discussed in Section 3.2.

The process from the discretized mathematical model towards a computer code introduces programming errors. The programming error is caused by wrong implementation of the equations. Since the software used (ReFRESKO) is commonly known and currently being developed and monitored, the programming errors will be negligible.

The last step going from a computer code towards a computed result results in convergence errors and round-off errors. The convergence error (or iterative error) is the residual between the left and right hand side of the implemented equations. A convergence criteria will be set on the residuals in the simulations. When the solution reaches this convergence criteria, the calculation is finished. In theory, this error should be at the same order of magnitude as the round-off error [11]. To reach that level, the convergence criteria should be sufficiently low, in the order of 10^{-12} for an 64-bit computer.

The monitoring of the residuals is done by a L_2 and L_∞ norm which are respectively the average residual and the largest residual of the domain. The average, L_2 norm, indicates the convergence of the total model. But the average alone will not show the highest peaks which are guiding in the accuracy of the total model. The mathematical description of the L_2 and the L_∞ (for the parameter x_i) are given below.

$$L_2 = \sqrt{\sum_{i=1}^n x_i^2} \quad (3.1)$$

$$L_\infty = \max_{i=1}^n x_i \quad (3.2)$$

Round-off errors are caused by the finiteness of the computer decimals. The calculations will be performed on the marclus3 cluster located at MARIN. The calculation capacity of this system is high enough to ensure that the round-off errors are sufficiently low.

3.2. Grid refinement study

A grid refinement study will estimate the discretization error in the calculation. Eça and Hoekstra [11] described a method for such a grid refinement study. In short, calculations will be done for a grid series with decreasing cell size then a power function is fitted to the results in a least squares sense. The fitting of this function can be done for different power functions and also a weight factor can be added to the least squared method in this calculation. The general equation for the fit function is given in Equation 3.3 in which the parameter considered (ϕ) is estimated by a function based on the typical cell size with a power p . Depending on the scatter in the data a safety factor of 1.25 or 3 is applied in the uncertainty estimation. A tool is developed at MARIN to estimate the uncertainty in this way: Numerical Uncertainty Analysis (NUA). This program is based on the method described by Eça and Hoekstra [11].

$$\epsilon_\phi \simeq \phi_i - \phi_0 = \alpha \cdot h_i^p \quad (3.3)$$

The method is based on a couple of assumptions. First, the grids should have a typical (non-dimensional) cell-size assigned to a grid. In other words, the grids should be geometrically similar. Second, the other errors (round-off and convergence errors) should have no significant influence on the solution. The round-off error will be low enough, but for the convergence error to be in the order of magnitude of the round-off error is more difficult, because of the complexity of the flow. However, it turned out to be sufficient if the convergence error is two or three orders of magnitude lower than the discretization error [10]. Thirdly, the trend of the result should be monotonic with the order of grid. If too much scatter is present in the data the estimation will give a very large uncertainty. This is mostly present in somewhat coarser grids series.

With the above written conditions the first challenge arises. In this work an unstructured grid will be used, which means that it will be more difficult to create a grid serie that is geometrical similar. Two properties of the grid and grid creating process can be controlled that will create a more geometrical similar grid serie. This is the location of hanging nodes, which is controlled by the refinement diffusion, and size of the viscous layer, which is controlled by the initial cell size (h_0) and the growth of the cells (γ).

3.2.1. Refinement Diffusion

The refinement diffusion is the number of cells that is inserted between two levels of refinement and thereby influences the location of the hanging nodes. The changing of cell sizes causes that this number has to change with finer grids. Based on the findings in Vink [25] and Crepier [7] a new formulation for the refinement diffusion is stated which is valid for all initial diffusion numbers. This formulation is shown in Equation 3.4 in which the diffusion refinement d_i is given at grid i . Further in this equation the refinement level r_i is used together with the diffusion refinement used at the coarsest grid d_1 .

$$d_i = r_i \cdot (d_1 + 1) - 1 \quad (3.4)$$

To visualise the geometrical similarity of grid with these equations a square field with three refinement levels is refined 4 times, creating a series of 5 grids. The starting refinement diffusion is $d_1 = 1$. The resulting calculated grid parameters are given in Table 3.1 and the resulting grids are shown in Figure 3.2, at the same location with the same length scales. It can be seen from this figure that with the changing diffusion refinements the grids are geometrical similar.

Table 3.1: Input parameters for example on refinement diffusion parameter, with parameters from table 3.1.

Grid No.	1	2	3	4	5
N_x	8	16	24	32	40
N_y	8	16	24	32	40
r_i	1	2	3	4	5
d_i	3	7	11	15	19

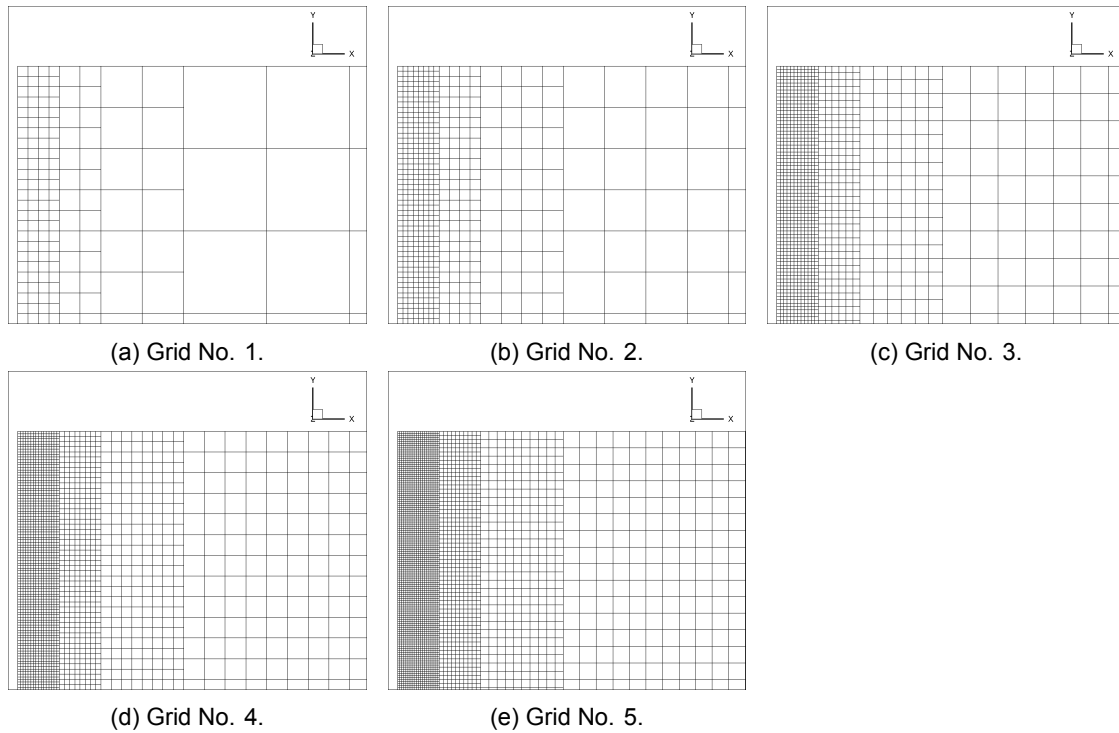


Figure 3.2: Five refined grids that are geometrical similar.

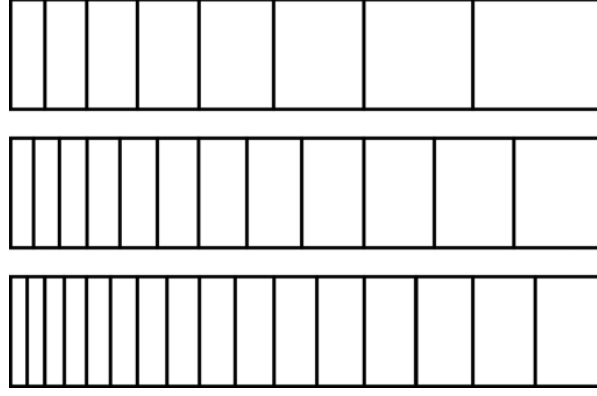


Figure 3.3: Geometrically similar viscous layer for a simple 1D case with the wall located at the left side.

3.2.2. Viscous layer

The viscous layer also needs to comply with the geometrical similarity condition. The viscous layer can be controlled by the growth (γ) and the initial cell size (h). The findings by Vink [25] and Crepier [7] gave the following formulations for the viscous layer on the refined grids (subscript i), depending on the coarsest grid (subscript 1).

$$h_i = h_1 \cdot \frac{\gamma_i - 1}{\gamma^{r_i} - 1} \quad (3.5)$$

$$\gamma_i = \gamma_1^{\frac{1}{r_i}} \quad (3.6)$$

Figure 3.3 shows the geometrical similar viscous layers created by implementing the initial cells size and growth from Equation 3.5 and 3.6. In Hexpress, the grid generating program, the height of the total viscous layer is determined by the Euler grid size at the surface. because of exponential growth of the number of cells in the viscous layer the program is limited to maximum viscous layer size of 2.5 Euler cells. The consequence for the grid series is that the height of the boundary layer gets smaller with finer grids, which does not comply with the grid similarity. Therefore, the generation of the viscous layer is analysed in Chapter 5, the test case for the method.

3.3. Validation

Validation of the model is defining the modelling error between reality and the model. Some experimental data, propeller torque, speed and power, are given in the Lloyd's workshop. This data can be used for the validation of the (future) self-propulsion case. Additionally, results and numerical setups from the 18 participants of the workshop are available and can be used for validation. Despite the fact that these are not experimental values they can be of grate value because of the size of the group and the diversity of used codes.

Method: Numerical setup

This chapter describes the tools used to execute the numerical calculations and presents the numerical settings used in the cases. The grid generation is performed with Hexpress (Section 4.1) and ReFRESCO (Section 4.2) is the numerical solver used. Section 4.3 up to 4.5 give in chronological order the numerical setup of the double body, free surface and open water simulations. This will include a short recap of the expected analysis, a schematic overview of the domain, general grid settings and the numerical input.

4.1. Grid generation: Hexpress

The program Hexpress by NUMECA will be used for the generation of unstructured grids. A geometry and domain has to be supplied to the program (which in this case is available from the Lloyd's workshop). Hexpress will then, in a couple of steps, create a mesh. These steps are visualised in Figure 4.1 and listed below.

1. Creating an initial mesh
2. Adapting to the geometry
3. Snapping and optimising to the shape
4. Adding a viscous layer

In the first step the coarsest part of the grid is generated in the total domain. This is based on the initial number of cells required. In the second part the grid is refined in order to create the right amount of detail in the domain. Refinements can be placed on surfaces or in boxes. Thereafter the grid is snapped to the hull and further optimised to get the highest grid quality in a maximum number of iterations. The last step is inserting the viscous layer in the grid. Here the cells at the geometry are inflated and filled with boundary layers cells based on a initial cell size and growth ratio. The inflation is maximum 2.5 times Euler cell size [21].

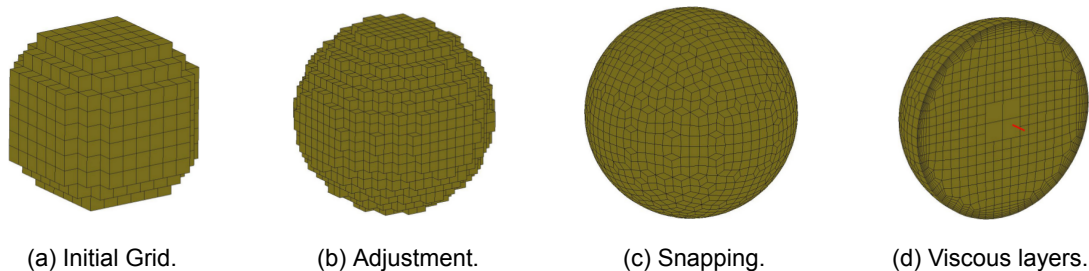


Figure 4.1: Various steps in Hexpress (image source [21]).

The main advantages of unstructured grids are the reduction in the amount of cells and the possibility to capture complex geometries. Because the cells do not have to be equally shaped and there is a possibility for hanging nodes in the grid, the grid can adapt to various shapes. A simple ship is already quite a complex shape when used in CFD analysis, so an unstructured grid gives freedom of the shape and thus a faster generation of grids. Both the hanging nodes and the non uniformity of cell shapes reduces the amount of cells used in a complex shape compared to a structured grid.

However, due to the freedom in form and sizes of the cells a geometrical similar grid is harder to generate and thus undesirable for a grid refinement study. As discussed in Chapter 3 the grid refinement study is based on the geometric similarity of the grid. So, for the analysis of the discretization error the grid refinement study, the grid should comply with the guidelines given in Chapter 3 and by [7].

The grid generation is an iterative process towards a high quality grid. The grid properties which define the quality are the skewness, aspect ratio and the smoothness of changes in cell sizes. To avoid losses in the computation and minimise corrections in the calculation the skewness should be minimised, the aspect ratio of the cells should be close to 1 and the transition between cells should be smooth. These quality properties can be optimised by altering the diffusion, location and level of refinement and viscous layers.

The diffusion is the amount of cells that is inserted before the next refinement level is started. A small diffusion number results in a quicker transformation from fine to coarser grids, but this does sometimes conflict with the grid smoothness. Depending on the complexity of the flow and the level of detail required, the trade-off between calculation time and smoothness is made.

Refinement levels should be placed on surfaces with a viscous layer to reduce the number of cells necessary to model the flow. High refinement levels should be location at high gradients in the geometry (this reduces the skewness of cells) and high gradients in the flow. Furthermore, the number of refinements should be in balance over the geometry, to ensure the same amount of details that can be calculated in the flow. For example, the bow and the stern of the ship should be discretized with the same refinement level to avoid unnecessary imbalances in the flow prediction due to difference in flow details.

The viscous layer is based on the initial cell size and the growth. The initial cell size is determined by the use of wall functions. The boundary layer will be modelled completely (from $v_x = 0$ to $v_x = v_s$) in this study and therefore requires a dimensionless wall distance around 0.1. A growth factor of 1.2 is known to be sufficient for most ship hull flow problems and will ensure a smooth transfer of the viscous layer to the Euler grid.

4.2. Numerical calculations: ReFRESHCO

ReFRESHCO is the program used to perform the numerical calculations. ReFRESHCO [23] is a community based code currently developed by MARIN and other institutions. This solver is based on the free surface code FRESHCO. ReFRESHCO can solve the multiphase unsteady incompressible RaNS equations with and without turbulence models. The finite volume approach is used in this software, which is relatively robust and cheap [9]. The current version of ReFRESHCO which is used in this thesis is 2.4.0.

4.2.1. Spatial discretization

For this thesis the Quadratic Upwind Interpolation for Convective Kinetics (QUICK) scheme will be used for discretization of the spatial discretization terms in the RaNS equations. In this scheme a quadratic curve is fitted through two upstream nodes and one downstream and interpolates for the value on the surface. It takes into account the second derivative and is therefore third order accurate. The main advantage of this scheme is the accuracy it provides. Since the aim in this thesis is to say more about the accuracy, or inaccuracy, a more accurate scheme is desirable.

The main disadvantage is the stability in regions with strong gradients. Because of the strong gradients an under- and/or over- shoot can occur and cause stability problems. In order to deal with these stability problems limiters are applied in the software, when the flux exceeds a certain limit the scheme will change to a first order scheme for that iteration.

4.2.2. Temporal discretization

In the temporal discretization the same trade-off for higher and lower order schemes needs to be done. A higher order scheme (like three level implicit) will result in smaller time steps. In the thesis by Vink [25] the same type of calculations is done (on model-scale). He found that the influence of the higher order scheme is insignificant. This is in accordance with the assumption that the calculations are unsteady but converging to a steady solution.

4.2.3. Turbulence

In this thesis the $k-\omega$ SST (shear stress turbulence) is used. This model is determined to be sufficiently accurate in the Lloyd's workshop. In short, the $k-\omega$ SST model is a two equation model. It solves the instantaneous kinetic energy (k) and the transport equation (ω). These parameters together define the turbulent viscosity but solves the turbulent equation.

4.2.4. Free surface

The free surface will be modelled with the ReFRICS scheme for the volume fraction equation. This equation has little numerical diffusion and is therefore an efficient model for the free surface. It is suited for modelling steady wave patterns.

4.2.5. Convergence

When using a numerical solver the convergence of the model determines the iterative error. As explained in the previous chapter the iterative/convergence error should be small enough, in such way that the discretization error is the only significant error. Settings like relaxation factors and convergence tolerance should be altered in order to get sufficient convergence.

Relaxation factors can be applied in several ways for the different parts of the model as described above. Relaxation factors influence the way the new calculated time step is implemented in the model. A lower relaxation factor means the influence of the next time step is lower. The convergence tolerance gives a limit to which the innerloop should be converged before going to the outerloop. A lower convergence tolerance will give a slower convergence, but a more stable one.

To make sure the iterative error is in the model and not in the grid the residuals can be visualised and the location can be checked. High residuals in the grid can be caused by low grid quality or a complex flow, like a separation area, which is hard to solve in a RANS model. If the residuals accumulate in a location away from the structure analysed, the problems are probably in the grid and not in the model.

4.3. Case 1: Double body simulations

In accordance with the introduction the double body simulations will be performed on the design speed and will qualitatively focus on the flow details and analysis of the friction coefficient. Quantitatively, the discretization error for the resistance components and the wake factor will be analysed. The numerical setup in ReFresco as determined in the control files for all the simulations can be found in Appendix C.

4.3.1. Domain and boundary conditions

The domain is schematically given in Figure 4.2 which shows the inflow view of the domain and the top view of the domain. The total size of the domain is seven times the L_{pp} in the length and four times L_{pp} in the width of the domain. This is assumed sufficiently large for the boundaries to have no influence on the flow, in both the double body as the free surface simulation, based on [2, 7]. The depth and trim of the vessel is taken the same as instructed for the calculation from the Lloyd's workshop, average depth is 5.25 meter and trim is The boundary conditions as applied in the domain are listed below.

- At the hull of the ship the velocities are set to zero because of the no-slip condition. The dimensionless wall distance (y^+) is always lower than 1 to avoid extra modelling errors.
- The the location of the water surface ($z = 5.2485m$) and the symmetry plane along the length of the vessel ($y = 0m$) the symmetry condition is applied, assuming zero flux for all quantities.
- At the inflow plane ($x = +4L_{pp}$) the velocity profile is uniform and constant in the -x direction. The turbulence inflow conditions are defined by the turbulence intensity ($I_T = 0.1$) and the turbulence

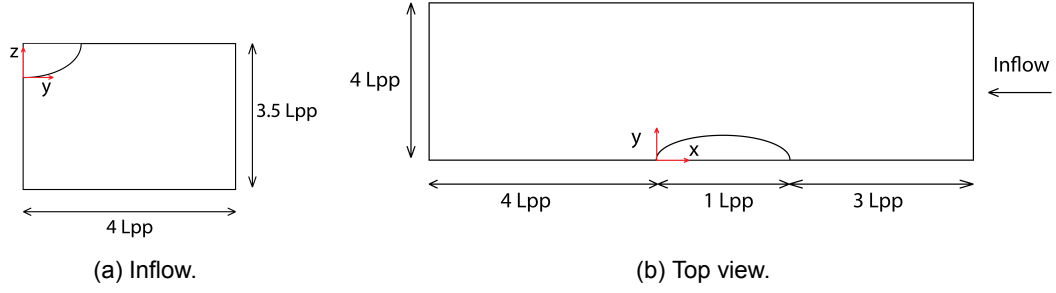


Figure 4.2: View of the domain with the size of the domain expressed in the L_{pp} of the vessel. The domain is shown from the inflow and the side of the domain.

viscosity ($\mu_T = 10$).

- At the outflow plane ($x = -3L_{pp}$), the derivatives of the velocities with respect to x are equal to zero.
- The left exterior ($y = 4L_{pp}$) has the symmetry condition, to avoid influence if any is present. The domain is assumed to be wide enough for these calculations.
- The bottom plane will represent infinity and is therefore a good location for the constant pressure boundary condition ($p = 0$) imposed.

4.3.2. Final grid parameters

The final grid parameters are given in Table 4.1 in which the initial grid, the total number of cells, the diffusion and values of the viscous layer with the corresponding dimensionless wall function values. These values are obtained with the formula's given in Chapter 3 for geometrical similar grids. The initial cells are aimed to be squared, aspect ratio is equal to one, but are adjusted a bit for the sequence of the next grids. The diffusion of three is chosen to obtain the required amount of smoothness in the grid.

Table 4.1: Grid refinement settings and resulting y^+ data for the double body simulation. Per case the initial cells size in the viscous layer h_0 , the growth factory, average y^+ and maximum y_{max}^+ is given.

Grid	0	1	2	3	4	5	6
$r_i[-]$	1	1.25	1.5	1.75	2	2.25	2.5
Nx Cells [-]	12	15	18	21	24	27	30
Ny Cells [-]	8	10	12	14	16	18	20
Nz Cells [-]	8	10	12	14	16	18	20
Ntotal Cells [-]	3063723	5155428	7796634	11269428	15484660	20829575	26850308
Diffusion [-]	3	4	5	6	7	8	9
$h_0 [\cdot 10^{-6}m]$	4.57	3.57	2.91	2.43	2.08	1.80	1.58
$\gamma[-]$	1.2	1.2	1.2	1.2	1.2	1.2	1.2
$y^+[-]$	0.474	0.373	0.306	0.257	0.220	0.193	0.170
y_{max}^+	1.092	0.836	0.728	0.609	0.535	0.485	0.429

On the hull various refinement levels are placed based on [7]. The location of these refinements and their depth are based on the initial cell size. The main motivation for the relatively high refinement levels is the aspect ratio in the grid. Especially the cells in the viscous layer, full boundary layer is modelled, high refinements are necessary in order to keep the aspect ratio within reasonable levels. The values of the refinements are listed in Table 4.2. An impression of the grid, a couple of details of the grid and the refinements are given in Figures 4.3 and 4.4.

4.4. Case 2: Free surface simulations

In the free surface simulation the wave systems will be analysed, and the velocity field and resistance components are compared to the Lloyd's case and the double body calculations. The aim for the grid and the domain therefore is that mainly the same grid settings will be used.

Table 4.2: Level of refinement on the ship based on findings in [7].

	Bow	Foreship	Midship	Afstship	Stern	Rudder& Hub	Rudder & Hub Edges
Refinement	9	8	7	8	9	10	11

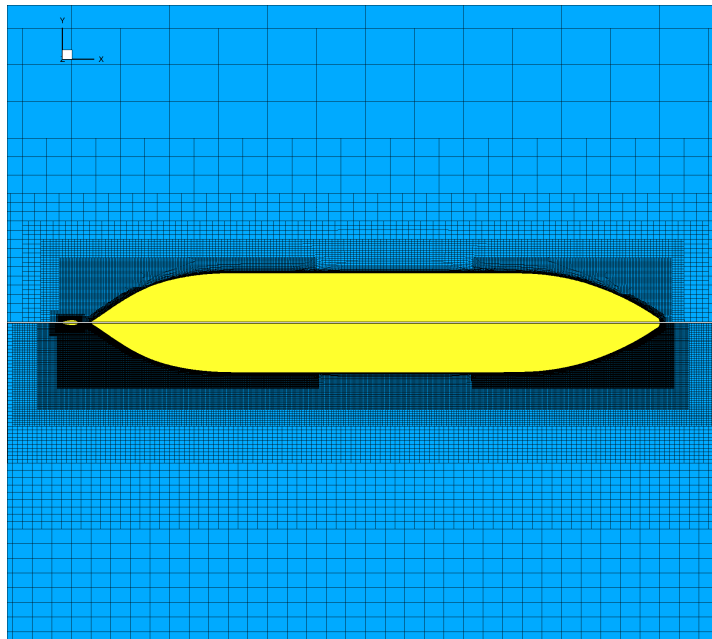


Figure 4.3: Overview of the grid for the full vessel for grid 0 (top) and grid 6 (bottom). The geometrical similarity of the refinement levels is visible in this figure.

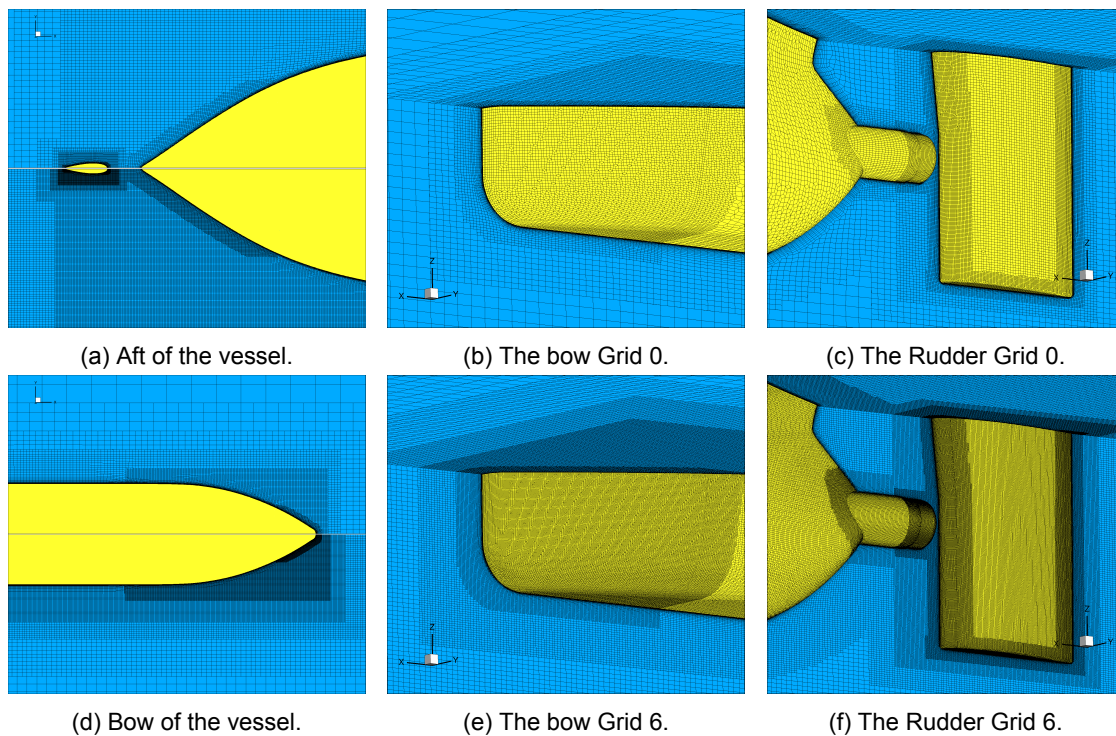


Figure 4.4: Comparison of grid details for grid 0 to 6.

4.4.1. Domain and boundary conditions

The domain for the free surface calculations is basically the same as for the double body simulations. The part of the ship above the water line is modelled as an extra domain part for the air. Additional

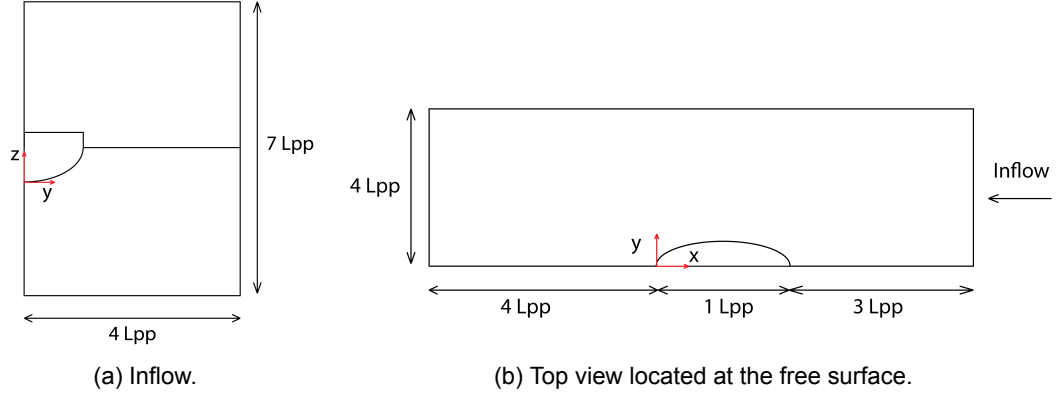


Figure 4.5: View of the domain with the size of the domain expressed in the L_{pp} of the vessel. The domain is shown from the inflow and the top of the domain.

refinements are placed for the wave system in the shape of the Kelvin Wedge and the free surface through the domain. The refinement on the Kelvin wedge and the free surface are mainly focused in the Z direction to make sure enough resolution is available to correctly model the free surface. In Figure 4.5 the domain for the free surface calculations are shown from the inflow side and from the top view at the free surface. The boundary conditions for the free surface simulation are the same as for the double body simulations. Except, on the deck free-slip is applied, because the focus is on the underwater forces.

4.4.2. Final grid parameters

The final grid parameters for the free surface simulation are given in Table 4.3. One of the aims in the free surface grid was to make a similar grid as the double body simulations. The domain in x and y direction has the same dimensions but the number of initial cells is twice as high. The reasoning is that the grid optimisation for the free surface calculation and the refinement depth is lower, so to create about the same cell size at the full the number of initial cells is doubled to counter this effect. In the viscous layer no adaptations have been made compared to the double body simulation.

Table 4.3: Grid refinement settings and resulting y^+ data for the free surface simulation. Per case the initial cells size in the viscous layer h_0 , the growth factory, average y^+ and maximum y^+_{max} is given.

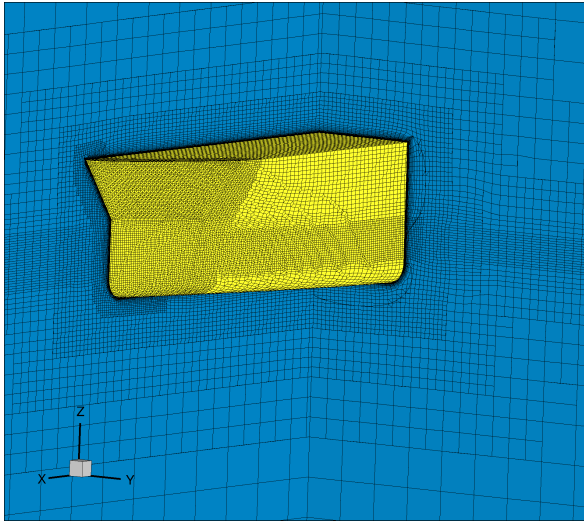
Grid	0	1	2	3	4	5
$r_i[-]$	1	1.25	1.5	1.75	2	2.25
Nx Cells [-]	24	30	36	42	48	54
Ny Cells [-]	16	20	24	28	32	36
Nz Cells [-]	28	35	42	49	56	63
Ntotal Cells [-]	3941664	6652466	10387517	15170341	21051142	28500041
Diffusion [-]	3	4	5	6	7	8
h_0 [$\cdot 10^{-6}m$]	4.57	3.57	2.91	2.43	2.08	1.80
$\gamma[-]$	1.2	1.2	1.2	1.2	1.2	1.2
$y^+[-]$	0.301	0.232	0.188	0.159	0.136	0.115
y^+_{max}	1.15	0.872	0.731	0.643	0.572	0.491

Also for the refinement levels placed on the ship the same distribution is taken into account. In Table 4.4 the location and depth refinements in the domain are given. It can be noticed that the refinement depths for the free surface and the double body differ. The calculations are quite unstable, therefore more optimisation needed to be done on the grid for the free surface. This actually resulted in a less coarse grid at the hull.

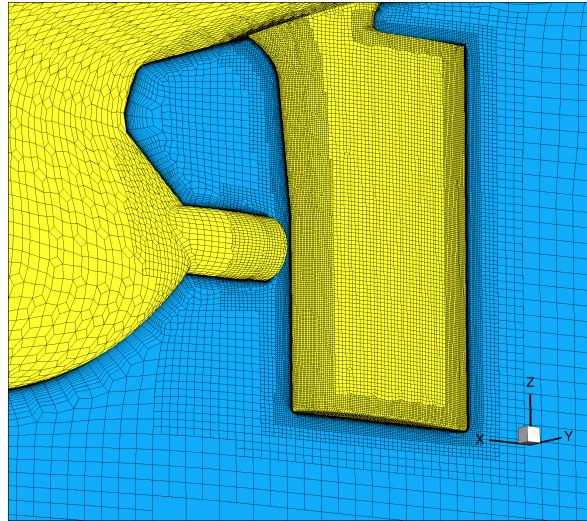
Some grid details are given in Figure 4.6. This shows details of the bow and aft, but also the refinement around the free surface. To solve the free surface layer, a refinement of at least 10 cells high is constructed throughout the domain. Additional refinement is located in the shape of a Kelvin wedge, with should cover the wave system around the ship.

Table 4.4: Level of refinement on the ship based on findings in [7].

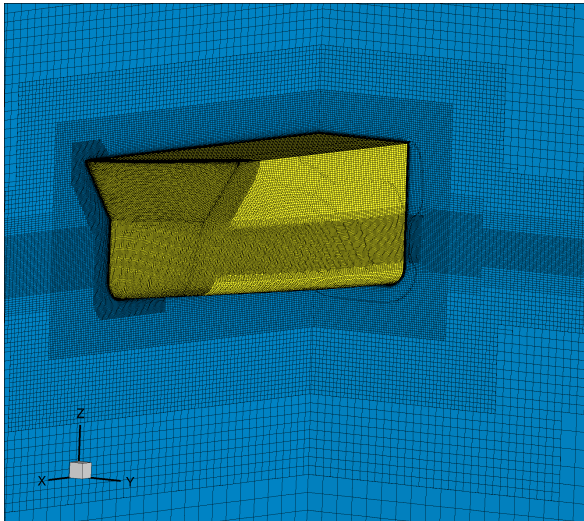
	Bow	Foreship	Midship	Aftship	Stern	Rudder & Hub	Rudder & Hub Edges	Deck	Kelvin Wedge	FS
Refinement	7	6	5	6	7	9	10	5	7	7



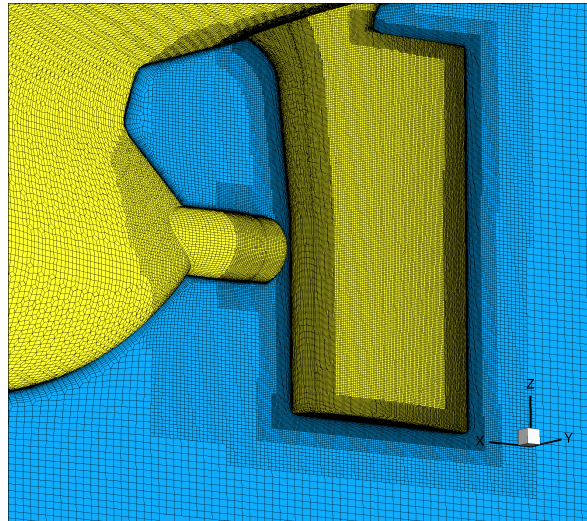
(a) The bow Grid 0.



(b) The Rudder Grid 0.



(c) The bow Grid 5.



(d) The Rudder Grid 5.

Figure 4.6: Comparison of grid details for grid 0 to 5.

4.4.3. Solver

Additionally to the steady double body simulation two things change when performing a free surface simulation; it is an unsteady simulation and contains a free surface. For the unsteady solver, the first order Euler implicit is chosen because it is assumed that the unsteady simulation will result in a steady result. To ensure a good start up of the simulation a start-up time of 30 seconds is inserted. Which means, the flow vessel interaction is slowly accelerated up to the 14 knots. The acceleration of the simulation is done with a time step of 0.1 seconds, in order to speed up the simulation time. After the force oscillations a smaller time step of 0.001 will be applied which will comply with the Courant number. The time step value of 0.001 is sufficient for complete grid series and is therefore not adjusted per grid. The resulting CFL numbers for the finest refinement level are listed in Table 4.5.

Table 4.5: Courant numbers on the finest refinement level (10) in the grid for the unsteady free surface simulation.

Grid	CFL
0	0.16
1	0.20
2	0.24
3	0.28
4	0.32
5	0.36

The free surface is solved with a REFRICS scheme, in which the free surface remains a relatively sharp line between water and air. Additionally, the gravity in the simulation needs to be activated. The ship will have dynamic trim and sinkage, which is adjusted within certain tolerances over a 50 time steps. The application of the trim and sink in the simulation is done by deforming the grid.

4.5. Case 3: Propeller open water simulations

The propeller open water simulation will perform a grid study for a range of inflow speeds, such that for every grid refinement a open water diagram can be constructed. The combination of the open water simulation with the free surface simulation will give a prediction for the self propulsion point. The verification of the results will be done by comparing the points available to the Lloyd's workshop CFD results.

4.5.1. Domain and boundary conditions

The open water simulation has a circular domain and consist of a structured grid around the propeller and an unstructured grid in the domain around it. The shaft is not modelled throughout the domain, because open water experiments in the towing tank are also finite. The shaft is considered long enough to not significantly influence the flow around the propeller. The boundary conditions that are applied are listed below.

- At the inflow plane the velocity profile is uniform and constant in the x direction.
- At the outflow plane the derivatives of the velocities with respect to x are equal to zero.
- At the blades, hub, shaft and streamcap the velocities are set to zero because of the no-slip condition. The dimensionless wall distance (y^+) is always lower than 1 to avoid extra modelling errors.
- At the outfield of the outerdomain the pressure condition is imposed.

4.5.2. Final grid parameters and refinements

The final grid parameters are given in Table 4.6. This lists the total number of cells for the inner and the outer domain. The viscous layer parameters are listed for the outer domain, but are aimed to be the same for both domains.

The grids are connected via the nearest cell method. For the quality of the grid it is important that the cell size of the two grids is the same at the transition of the grids. Also the viscous layer needs to have the same size to minimise the extra discretization errors due to the two grid types.

And overview of the coarsest and the finest grid are given in Figure 4.7. Details that are shown here are the connection between the inner and the outer domain, the structured grid on the blades and the refinements applied in the domain. The depth of the refinements placed in the domain are listed in Table 4.7. The refinement on the shaft and the inner domain is chosen in such way that the cells have approximately the same size in both domains. The refinement on the inner domain will have a non-uniform shape, therefore a refinement cylinder is placed throughout the domain. This both simplifies the generation of a geometrical similar grid and the stability of the calculation, because of the reduction of hanging nodes in the inflow area.

Table 4.6: Grid refinement settings and resulting y^+ data for the open water simulation. Per case the initial cells size in the viscous layer h_0 , the growth factory, average y^+ and maximum y_{max}^+ y^+ is given.

Grid	0	1	2	3	4
$r_i [-]$	1	1.25	1.5	1.75	2
Nx Cells [-]	32	40	48	56	64
Ny Cells [-]	32	40	48	56	64
Nz Cells [-]	32	40	48	56	64
Ntotal Cells inner [-]	1242216	1605096	5405400	9839232	21906432
Ntotal Cells outer [-]	2738172	5232636	8930492	14027776	20793274
Diffusion [-]	3	4	5	6	7
$h_0 [-10^{-6}m]$	4.80	3.75	3.05	2.55	2.18
$\gamma [-]$	1.2	1.2	1.2	1.2	1.2
$y^+ [-]$	0.347	0.264	0.212	0.166	0.133
y_{max}^+	1.28	1.00	0.777	0.617	0.500

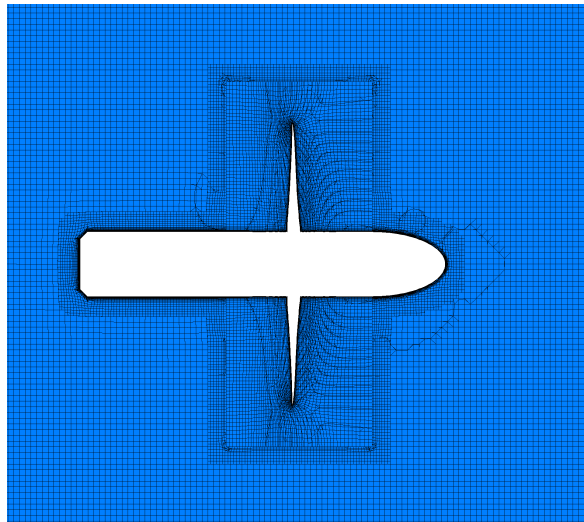
Table 4.7: Level of refinement in the propeller domain.

	Inner domain	Shaft	Inner cylinder
Refinement	4	5	3

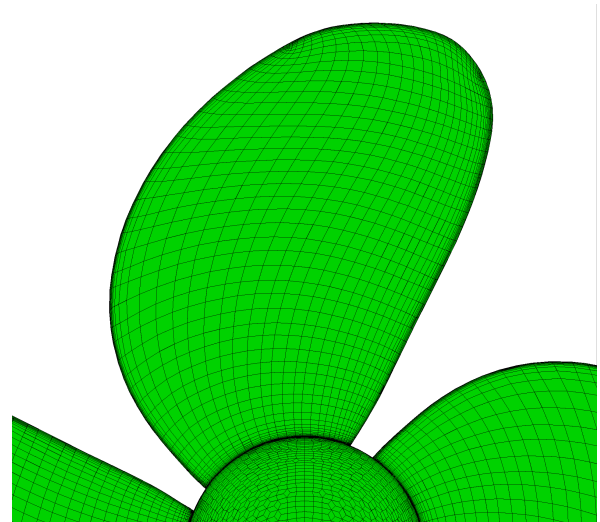
4.5.3. Solver

The setup is done with the absolute formation method (AFM). This means the propeller is modelled as a steady object in a steady flow while the rotation is added to the flow. The rotation in the flow corresponds to the speed of the propeller.

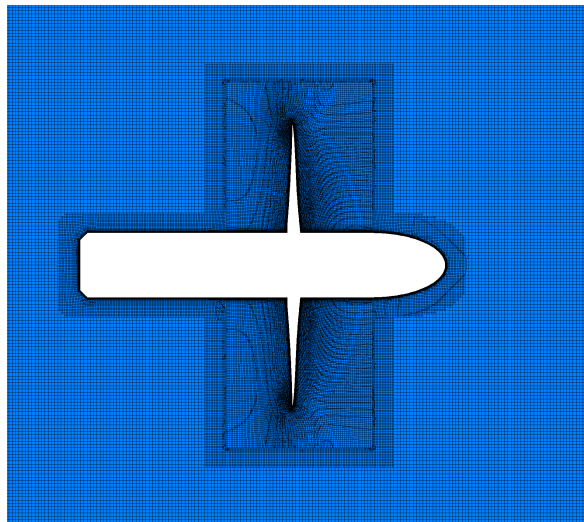
Per grid the advanced ratios(J) 0.1 to 0.6 are calculated with steps of 0.5. This gives per grid a open water diagram and the possibility to analyse the discretization error for low advanced ratios as for advanced ratios around the design point of the propeller ($J = 0.5$)



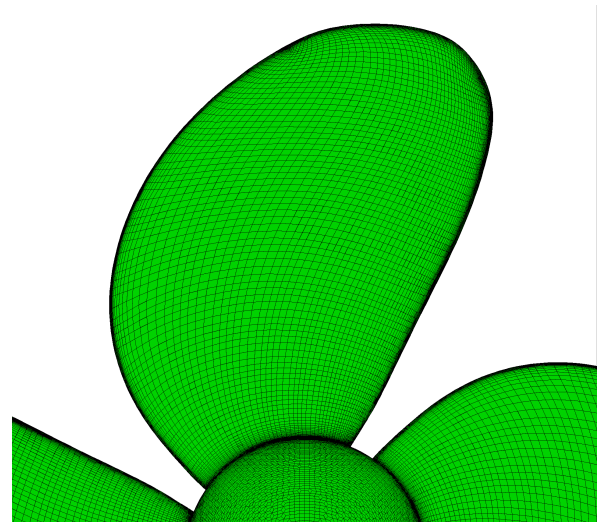
(a) Side view in Grid 0.



(b) Top blade in Grid 0.



(c) Side view in Grid 3.



(d) Top blade in Grid 3.

Figure 4.7: Various views of the open water domain for the coarsest grid (Grid 0) and the finest grid (Grid 6).

5

Flat plate verification study

This chapter presents three grid refinement studies for a flat plate model using unstructured grids. The goal is to determine an adequate verification procedure for unstructured grids. Additionally, the computations are compared for the same condition using structured grids and a different approach for the viscous layer grid generation. The objectives of this chapter are summed below.

- Confirmation of the method
- Uncertainty estimation
- Validation with theoretical drag coefficients

Section 5.1 describes the geometry and boundary conditions, the grid and the numerical setup. Section 5.2 discusses the results and the corresponding uncertainty analysis as discussed in Chapter 3.

5.1. Calculation setup

The grid refinement studies, in order to determine the discretization uncertainty) are done for three Reynolds numbers: 10^4 (laminar), 10^7 (transitional) and 10^9 (turbulent) with the corresponding flow velocities of 0.01, 10 and 1000 m/s. The simulations are considered steady and 2D, but has some cells in width due to the method used by ReFresco.

5.1.1. Domain and boundary conditions

The geometry consists of a square plate of one by one meter. The computational domain has the length of 4 times the plate length with one meter in front and two meters aft of the plate. The height of the domain is one meter and is assumed to be far enough such that it does not influence the solution. The width of the domain is 1 meter, but it still considered a two dimensional problem, due to the symmetry over the width of the plate. The domain is visualised in Figure 5.1 and the boundary conditions are listed below.

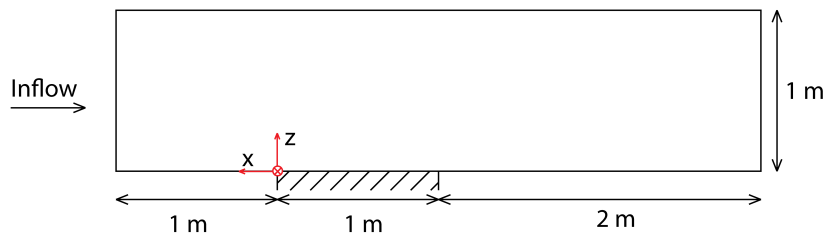


Figure 5.1: Sideview of the domain of the flat plate (shaded part is the plate).

- On the plate surface the velocities are set to zero because of the no-slip condition. The dimensionless wall distance (y^+) is always lower than 1 to avoid extra modelling errors.
- The planes front and aft of the plate ($z = 0$) have symmetry conditions, assuming zero flux for all quantities.
- At the inflow plane ($x = +L$) the velocity profile is uniform and constant in the -x direction. The turbulence inflow conditions for the higher Reynolds numbers, are defined by the turbulence intensity and the turbulence viscosity. An overview of the inflow quantities can be found in Table 5.1.
- At the outflow plane ($x = -2L$), the derivatives of the velocities with respect to x are equal to zero.
- The left and right exterior planes have symmetry boundary conditions, which supports the assumption that this 3D model will give a 2D result.
- The top plane ($z = L$) has the constant pressure boundary condition ($p = 0$) imposed.

Table 5.1: Inflow boundary conditions, based on experience with ReFresco and the validation study of Eça et al. [14].

Re	$V_x [m/s]$	$I_{tu} [\%]$	$\frac{\mu_t}{\mu} [-]$
Re 10^4	0.01	—	—
Re 10^7	10	5	0.1
Re 10^9	1000	10	10

5.1.2. Grid settings

Three main parameters of the grid quality are the aspect ratio of the cells, smoothness between cell-size variation and orthogonality of the cell. The geometry is relatively simple, which reduces the chance of cells with a low orthogonality. The Euler grid is created such that the aspect ratio will be close to one in the xz-plane. However, the flow is assumed to behave 2D which allows the cells in y direction to be larger and reduce the total amount of cells.

Refinements in the grid are located at places where the highest gradients are to be expected: the plate itself and the leading and trailing edge of the plate. The initial cell size is refined three times towards the plate and around the edges of the plate a refinement box is placed with a refinement level seven. To increase the smoothness of the grid, the symmetry planes before and aft of the plate also have a refinement level of 3. The initial grid for Re 10^4 is shown in Figure 5.2 (the grids for the higher Reynolds numbers only vary in initial cell size for the viscous layer).

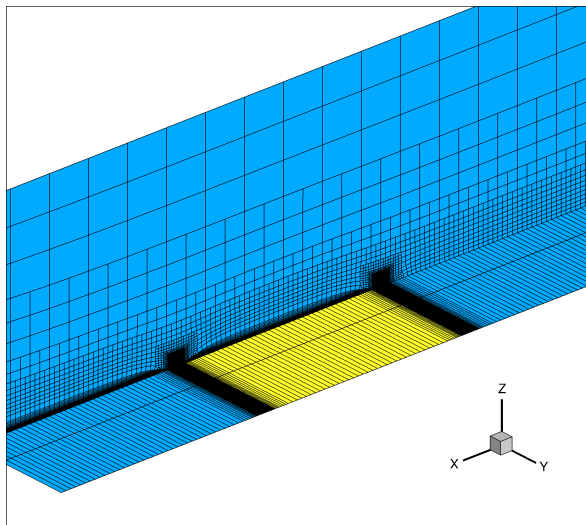
A viscous layer is needed on the plate to be able to calculate the boundary layer accurately. To achieve this high accuracy a low y^+ value is required and sufficient layers to capture the high gradients in the boundary layer. The initial estimation of the y^+ should be below 1 to avoid additional modelling errors. The viscous layer is also applied in front of the plate to improve the smoothness of the grid. The cells have to be larger in the wakefield for a more stable calculation, therefore no viscous layer is inserted aft of the plate.

A few remarks can be made for the grid shown in Figure 5.2. First, it can be seen that the grid is curved at the in- and outflow. This is caused by the optimisation in Hexpress and reduces in finer grids as cells become smaller. Furthermore, also a curvature can be seen in the viscous layer around the refinements at the end of the plates. This is also caused by optimisation in Hexpress, however in retrospect this could have been minimised by applying higher diffusion. To quantify the impact of these curvatures in the grid a grid quality study is done. This showed that indeed around these edges the grid has a low quality, but the average quality of the grid is sufficient. The results can be found in Appendix A.

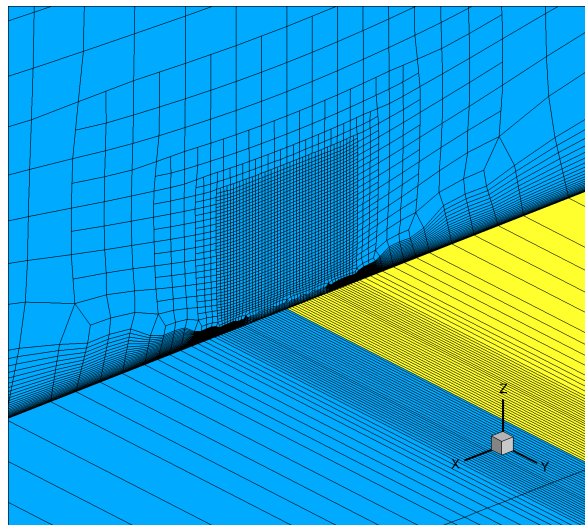
The final settings for the grid refinements can be found in Table 5.2. This includes the refinement of the grid (r_i), the number of initial cells (Nx, Ny, Nz) and per grid the initial cell size (h_0), growth factor (γ) and dimensionless wall distance (y^+). The values of the dimensionless wall distance (y^+) are determined after the calculation, but are here included for completeness.

Table 5.2: Grid refinement settings and resulting y^+ data for the flat plate case study. Per case the initial cells size in the viscous layer h_0 , the growth factory, average y^+ and maximum y^+_{max} y^+ is given.

Grid	0	1	2	3	4	5	6	7	8	9	10
$r_i[-]$	1	$1\frac{1}{3}$	$1\frac{2}{3}$	2	$2\frac{1}{3}$	$2\frac{2}{3}$	3	$3\frac{1}{3}$	$3\frac{2}{3}$	4	$4\frac{1}{3}$
Nx Cells [-]	21	28	35	42	49	56	63	70	77	84	91
Ny Cells [-]	3	4	5	6	7	8	9	10	11	12	13
Nz Cells [-]	6	8	10	12	14	16	18	20	22	24	26
Diffusion [-]	1	2	3	4	5	6	7	8	9	10	11
Re = 10^4											
h_0 [$10^{-4}m$]	2.14	1.58	1.25	1.03	0.881	0.768	0.680	0.611	0.554	0.507	0.468
$\gamma[-]$	1.150	1.111	1.087	1.072	1.062	1.053	1.047	1.042	1.039	1.036	1.033
$y^+[-]$	0.105	0.0744	0.0570	0.0457	0.0380	0.0325	0.0278	0.0250	0.0221	0.0203	0.0185
$y^+_{max}[-]$	0.458	0.360	0.302	0.263	0.232	0.208	0.189	0.174	0.162	0.151	0.142
Re = 10^7											
h_0 [$10^{-6}m$]	1.047	0.771	0.611	0.505	0.431	0.376	0.333	0.299	0.271	0.248	0.229
$\gamma[-]$	1.150	1.111	1.087	1.072	1.062	1.053	1.047	1.042	1.039	1.036	1.033
$y^+[-]$	0.207	0.153	0.122	0.102	0.0864	0.0752	0.0665	0.0598	0.0542	0.0495	0.0456
$y^+_{max}[-]$	0.426	0.336	0.281	0.246	0.219	0.197	0.180	0.166	0.155	0.145	0.136
Re = 10^9											
h_0 [$10^{-9}m$]	9.060	6.671	5.280	4.369	3.726	3.248	2.879	2.585	2.345	2.147	1.979
$\gamma[-]$	1.150	1.111	1.087	1.072	1.062	1.053	1.047	1.042	1.039	1.036	1.033
$y^+[-]$	0.129	0.0956	0.0759	0.0634	0.0541	0.0472	0.0417	0.0374	0.0334	0.0315	0.0290
$y^+_{max}[-]$	0.204	0.153	0.124	0.104	0.0919	0.0795	0.0715	0.0668	0.0612	0.0570	0.0533
Re = 10^7 HD											
h_0 [$10^{-6}m$]	1.047	0.767	0.599	0.487	0.407	0.348	0.302	0.265	0.235	0.210	0.189
$\gamma[-]$	1.150	1.150	1.150	1.150	1.150	1.150	1.150	1.150	1.150	1.150	1.150
$y^+[-]$	0.206	0.152	0.120	0.0974	0.0814	0.0696	0.0602	0.0528	0.0467	0.0417	0.0374
$y^+_{max}[-]$	0.426	0.334	0.275	0.237	0.207	0.183	0.164	0.148	0.134	0.123	0.113



(a) Overview of the grid structure of the flat plate.



(b) Close up on the refinement on the edge of the flat plate.

Figure 5.2: Grid for the flat plate study for Reynolds 10^4 .

5.1.3. Geometrical grid similarity

A requirement for determining the numerical uncertainty is the geometrical similarity of the grid (Chapter 3). Due to limitation of the inflation factor in the Hexpress software, the absolute thickness of the boundary layer is smaller as the boundary layer is not allowed to be larger then twice the Euler cell size. The consequence is that the boundary layer does not have a smooth transition any more from viscous layer to the Euler grid for the denser grid. Therefore, a second grid refinement is done for Reynolds 10^7 for which the growth factor is not scaled, but kept constant. The initial cell size is still scaled with the original formulation. The viscous layer is therefore smaller, but the transition to the Euler grid will be smoother, which could result in more numerical stability of the calculations. For convenience, this grid

serie will be called the "*Hexpress-Default*" and the original supposedly best one is called "*Geometric Similar*".

In addition, the results of the two types of viscous layer construction are compared to the results on a structured grid. For the structured grid it is possible to make an exact geometrical grid refinement. This will give more insight the accuracy of the unstructured calculations on $Re = 10^7$. The setup of this analysis is done in cooperation with B. Schuiling. The difference of the grid structure is globally given in Figure 5.3.

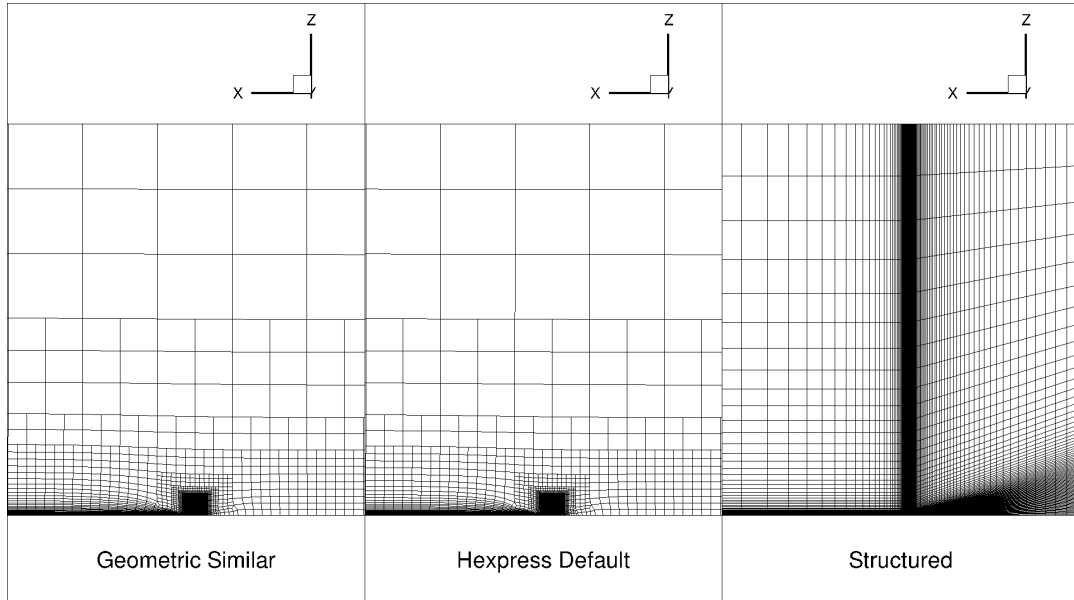


Figure 5.3: Image of the structured and unstructured (*Hexpress-Default* and *Geometrical Similar*) grid showing part of the plate and part of the wakefield (same scale) for the coarsest grid.

5.2. Results

This section includes four different verification exercises:

- Influence of iterative errors
- Assessment of discretization errors and uncertainties
- Friction line values
- Analysis of geometrical grid similarity

5.2.1. Iterative error

The convergence of the coarsest grids are shown in Figure 5.4 and the convergence of the finest grid is shown in Figure 5.4. All the grids do converge towards and L_{inf} value of 10^{-10} , except for the last grids of the $Re 10^9$. As stated by Eça and Hoekstra [11] the influence of the iterative error increases with grid refinement. However, the L_{inf} value of 10^{-10} will lead to results sufficiently accurate. For the last grids of $Re 10^9$ the convergence has a L_{inf} of 10^{-3} . It is common that for these high Reynolds numbers the iterative error is higher then for model-scale values. These values are nevertheless low enough to ensure convergence of the force; the parameter of interest.

The location of the residuals is as important as the value of the residuals. For all scenarios, the residuals are located in same region; the trailing edge of the plate. The flow at that location is relatively more complex. Also the grid has some diamond shaped cells (visible in Figure 5.2b) which makes it more challenging for the solver to solve the complex flow. Concluding, taking into account that the larger Reynolds numbers correspond with full-scale computations without wall-functions, the iterative error is adequately small ($L_{\infty} = 1E - 3$, $L_2 = 1E - 6$) and judged not to be of influence on the discretization error to continue the analysis on the flat plate.

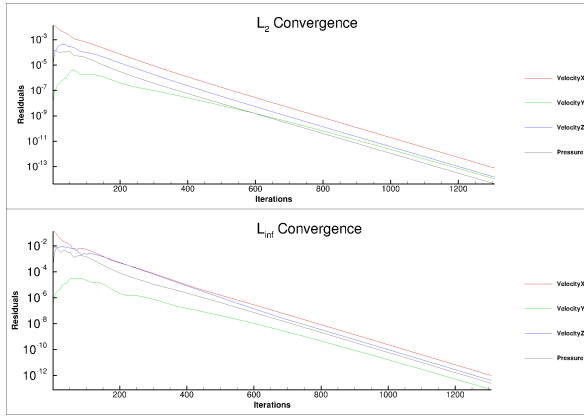
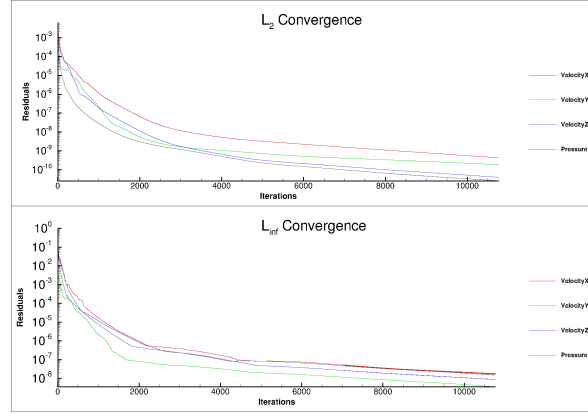
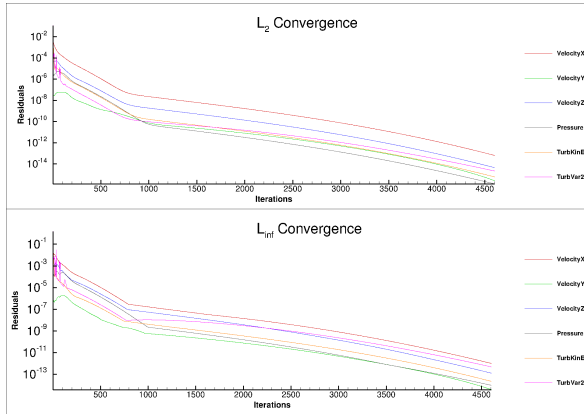
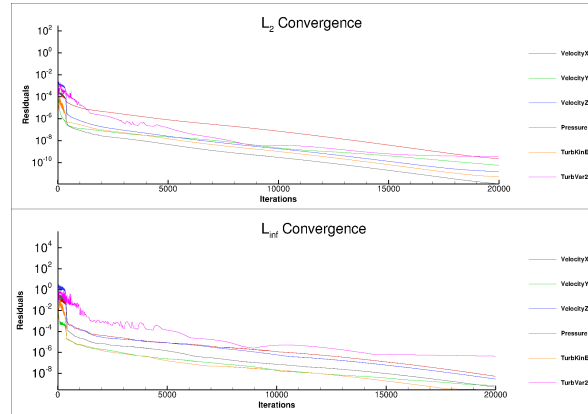
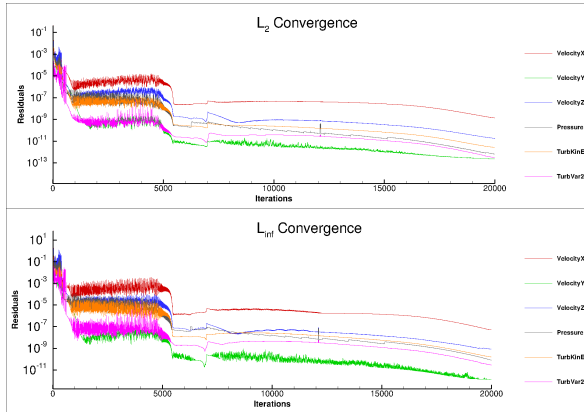
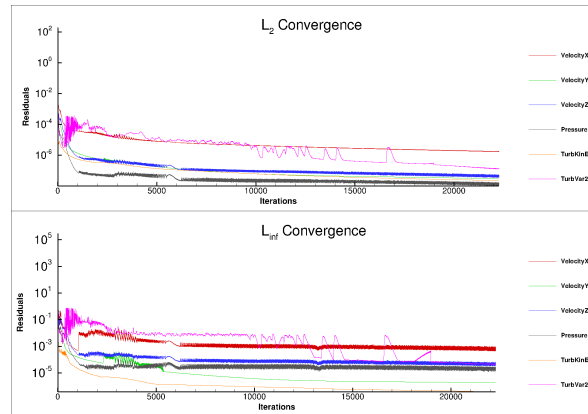
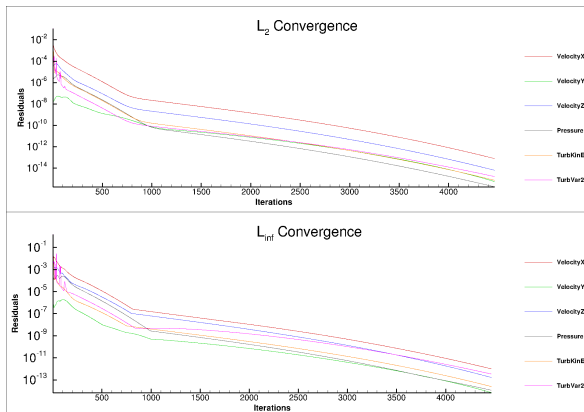
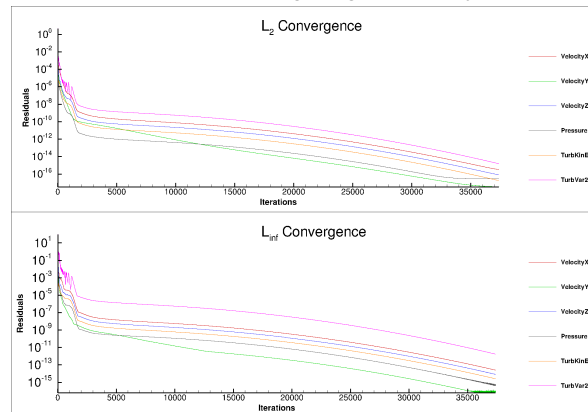
(a) Residuals of the coarsest grid (g0) for Reynolds 10^4 .(b) Residuals of the finest grid (g10) for Reynolds 10^4 .(c) Residuals of the coarsest grid (g0) for Reynolds 10^7 "Geometric Similar".(d) Residuals of the finest grid (g10) for Reynolds 10^7 "Geometric Similar".(e) Residuals of the coarsest grid (g0) for Reynolds 10^9 .(f) Residuals of the finest grid (g10) for Reynolds 10^9 .(g) Residuals of the coarsest grid (g0) for Reynolds 10^7 "Hexpress-Default".(h) Residuals of the finest grid (g10) for Reynolds 10^7 "Hexpress-Default".

Figure 5.4: Convergence of the coarsest grids (left) and the finest grids (right).

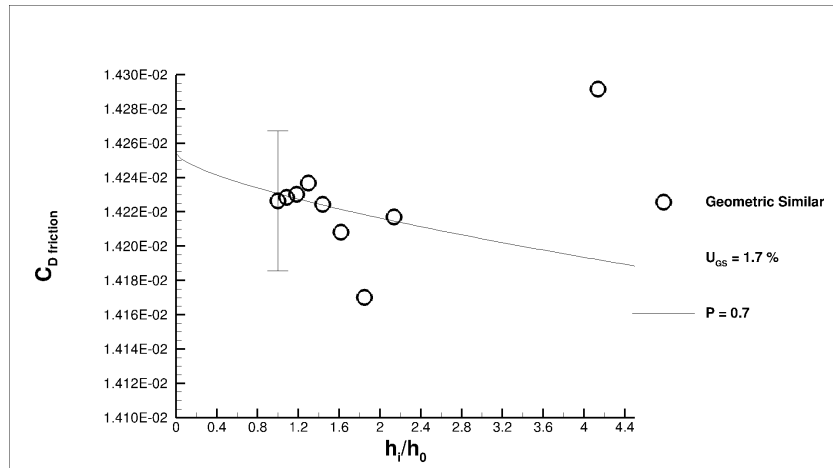
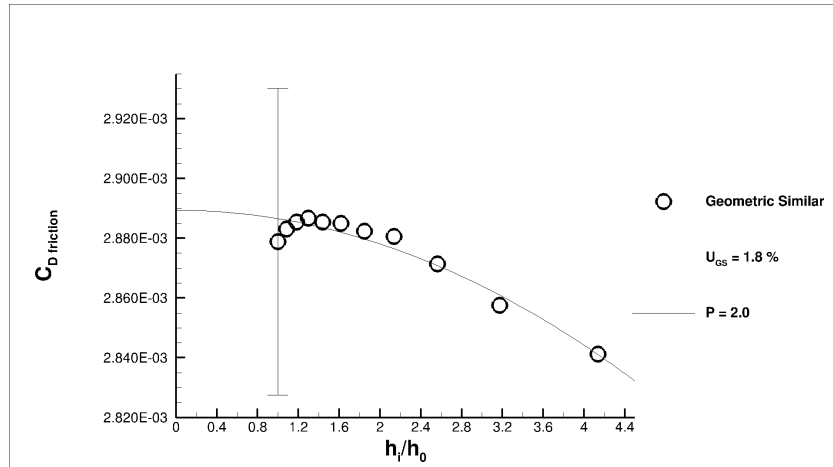
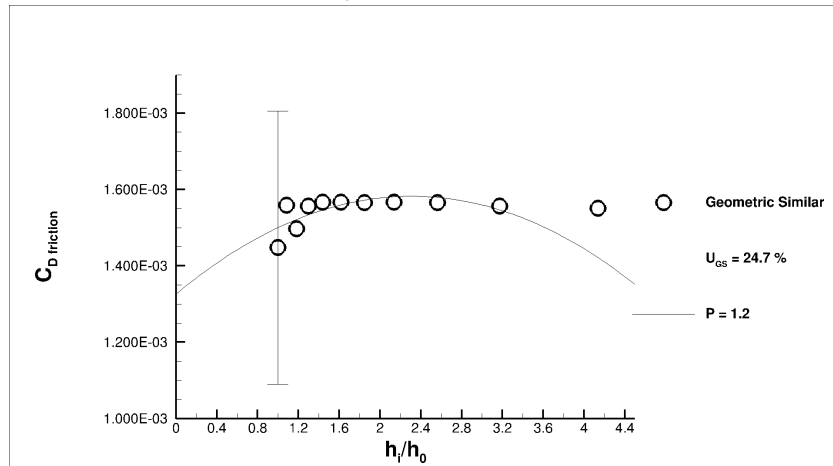
(a) Reynolds 10^4 : Close up.(b) Reynolds 10^7 : Close up.(c) Reynolds 10^9 : Close up.

Figure 5.5: Uncertainty Analysis.

5.2.2. Discretization uncertainty

Next, an assessment for the spatial discretization uncertainty and error estimation is performed for the three cases, the resulting graphs are shown in Figure 5.5. The accompanying power in the least square fit and the uncertainty are given in the figure. The results will be discussed case by case. An overview of the results and predicted drag coefficients is listed in Table 5.3

Case 1: Reynolds 10^4

The curve fitted through the results for case 1 has the power 0.6 and the finest grid has an uncertainty of 0.3%. It looks like the results are oscillating around the final answer. This is not desirable for this method, but the absolute difference between two subsequent grids is decreasing with a grid refinement.

Case 2: Reynolds 10^7

Case 2 has a more smooth convergence towards a solution compared to case 1. The computed drag coefficients are almost on a horizontal line; the absolute difference is small between the coarsest and the finest computation. However, in the close up it can be observed that the drag coefficients of the last three results do not follow the trend of the first eight results. The results look like they did not converge yet, but the residuals sufficiently low, as discussed in the previous section.

Case 3: Reynolds 10^9

The first six points are on a straight line, just like case 2. The close up of the points do show the same trend as the first six points of Reynolds 10^7 . The last grid refinements do not converge, but also do not have the same trend as Re 10^7 . This makes the uncertainty very large. Since the iterative error is small enough no reason can be found to not take these points into account.

5.2.3. Comparison with Friction line theory

Three friction line theories can be distinguished which are mainly used in naval architecture; ITTC, Grigson and Katsui. All are empirical formula and are thus dependent on the set used to make these equations. This is also the main difference between the three friction line theories, the ITTC is a very general equation which is applicable in all flows. However the Grigson and Katsui are based on physics. The equations are given in Equations, 5.1 5.2 and 5.3. Figure 5.6 shows the resulting drag coefficient together with the predicted values of Katsui, Grigson and ITTC. The values comply best with the drag coefficient prediction of Katsui.

$$\text{ITTC}[1] : c_f = \frac{0.075}{(\log_{10}(Re) - 2)^2} \quad (5.1)$$

$$\text{Grigson}[15] : c_f = [1.032 + 0.02816(\log_{10}(Re) - 8) - 0.006273(\log_{10}(Re) - 8)^2] \cdot \frac{0.075}{(\log_{10}(Re) - 2)^2} \quad (5.2)$$

$$\text{Katsui}[18] : c_f = \frac{0.0066577}{(\log(Re) - 4.3762)^{0.042612 \cdot \log(Re) + 0.56725}} \quad (5.3)$$

Table 5.3: Numerical results of the finest grids and the estimated uncertainty. Also the difference between the maximum and minimum result of the grid study are given as a percentage of the finest grid.

		Geo. sim.	Hexpress def.	Structured	ITTC	Grigson	Katsui
Re 10^4	c_f [-]	0.01422	-	-	0.01875		0.001448
	P [-]	0.6	-	-			
	U = [%]	0.3	-	-			
	$\Delta_{max-min}$ [%]	1.22	-	-			
Re 10^7	c_f [-]	0.002879	0.002871	0.002861	0.00300	0.002802	0.002851
	P [-]	2	2.0	1.5			
	U = [%]	1.7	0.9	0.2			
	$\Delta_{max-min}$ [%]	1.58	1.21	-			
Re 10^9	c_f [-]	0.001448	-	-	0.001531	0.001613	0.001532
	P [-]	1.2	-	-			
	U = [%]	24.7	-	-			
	$\Delta_{max-min}$ [%]	8.24	-	-			

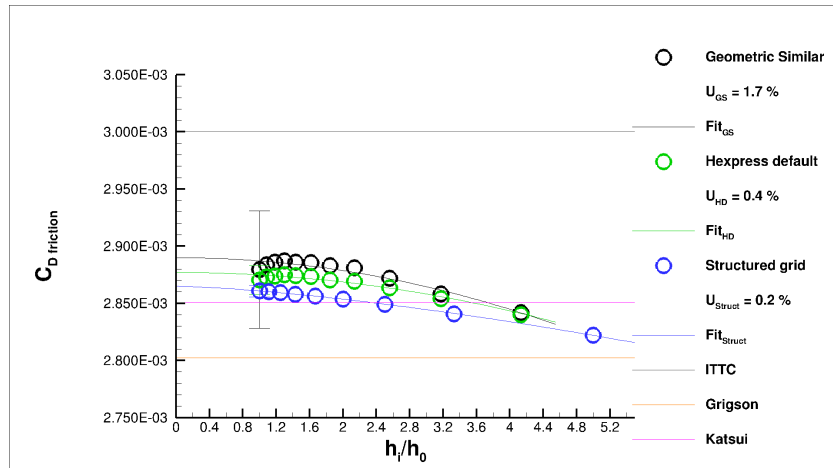


Figure 5.6: Reynolds 10^7 with three grid types and the three friction lines.

5.2.4. Analysis of grid similarity

A comparison on grid similarity is only done for Reynolds 10^7 . The iterative error for all three grid types (*Geometric similar*, *Hexpress-Default* and *structured* grid) is sufficiently small to analyse the discretization error. Starting with the grid refinement study of the *Hexpress-Default* grid, Figure 5.9, it can be seen that the behaviour of the uncertainty curve is the same as for the original geometrical similar grids. The uncertainty is lower (0.9% compared to 1.7%), which indicates that the influence of the grid is minimised in the finest grid. The difference in the grids is shown in Figure 5.7. The *Hexpress-Default* grid has a smoother transition between the boundary layer and the Euler grid and contains less cells to describe this boundary layer. As a reference, the profile of the velocity in x-direction is also given in this figure. This shows that the largest velocity gradients are fully covered by both viscous layer construction.

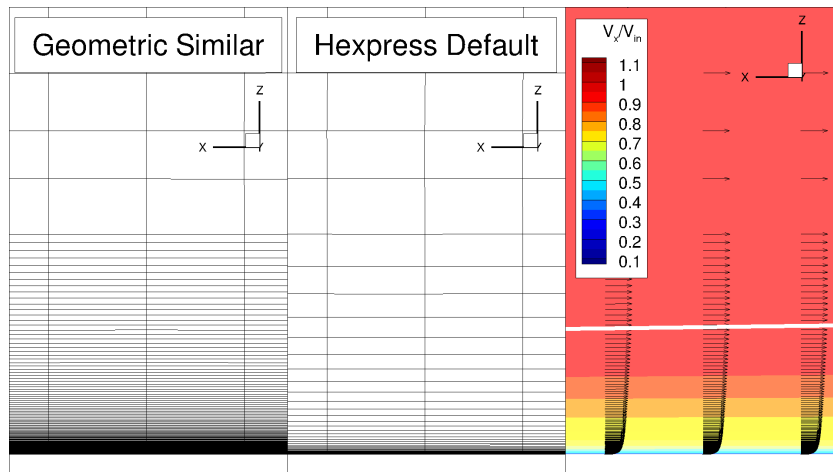


Figure 5.7: Comparison of the smoothness of the transition from the Euler grid to boundary layer in grid refinement 10 (finest grid) for the *Geometric Similar* grid and the *Hexpress Default* grid. In the most right image the contour and vector plot for the *Geometric similar* grid is shown with the white line indicating the $V_x/V_{in} = 0.99$.

For the *Hexpress-Default* the normalised flow velocity field at the end of the plate, including the refinement on the end of the plate, is shown in Figure 5.8 with the grid projected in grey. The influence of the deformed cells on the flow pattern is clearly visible. These deformed cells are a result of the optimisation in Hexpress around the end plate and could not be avoided.

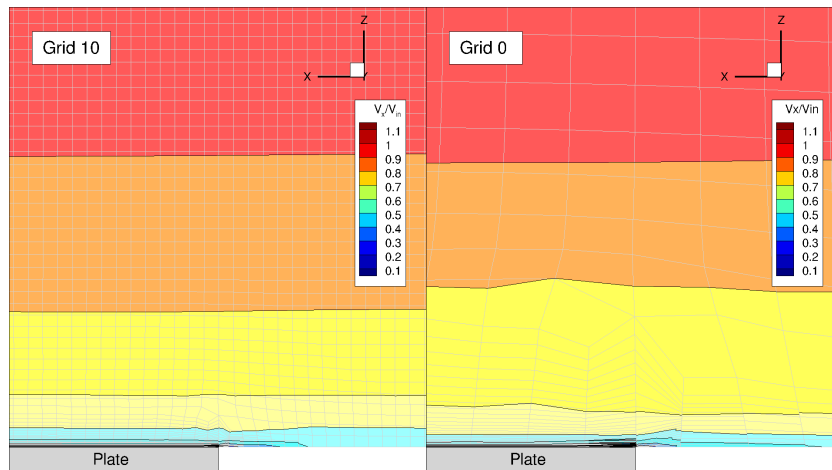


Figure 5.8: Image of the normalised velocity in x direction at the end of the plate, with the grid projected on the flow field (for the *Hexpress-Default* grid). This shows the influence of the cell shape on the flow field.

The uncertainty curve for the structured grid is fitting all the points and smoothly the difference of inbetween results decays to a final answer. Figure 5.3 shows a part of the grid containing the plate and the wakefield on the same scale for the structured grid and the original geometrical similar grid. It can be seen that the viscous layer covers the same height, so approximately the same level of resolution is reached. The study for the structured grid contains less grid refinements, but these are geometrical similar, which could not be achieved for the unstructured grids. This results in a lower uncertainty of 0.2%, which is the lowest value of the three grid types.

The results of the three grid studies for Reynolds 10^7 are presented together in one graph in Figure 5.10 and a couple of observations can be made. The value for the *Hexpress-Default* grid is closer to the value of the *structured* grid then the *geometric similar* grid. The uncertainty range of the *Hexpress-Default* grid lies within the range of the *geometric similar* grid and covers the total uncertainty range of the *structured* grid. For this flat plate analysis it can be concluded that the *Hexpress-Default* grid would give a solution with low influence of the grid and a more stable one.

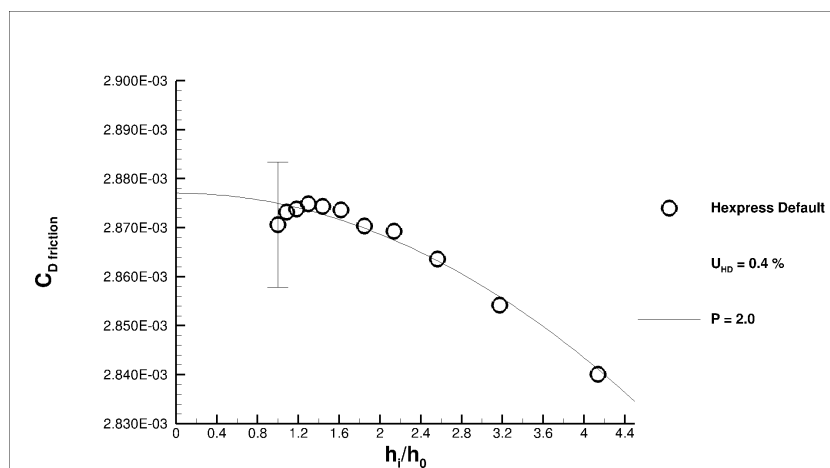


Figure 5.9: Reynolds 10^7 for *Hexpress-Default* grid.

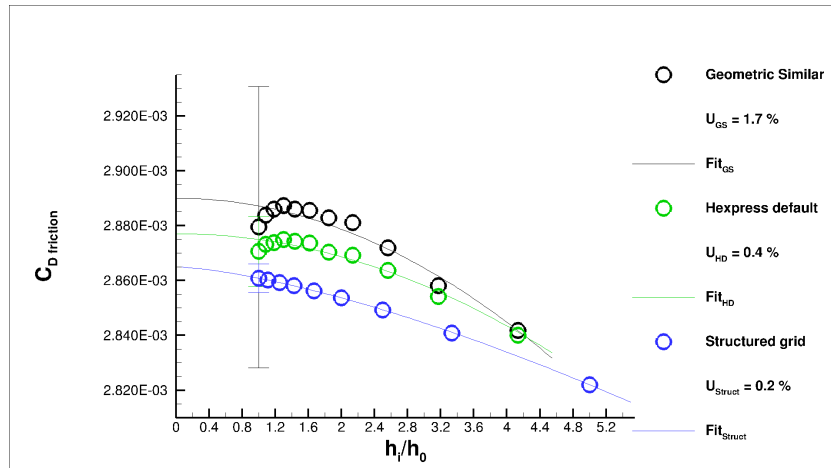


Figure 5.10: Reynolds 10^7 with three grid types.

5.3. Conclusions on initial calculations

Conclusions on the initial calculations are based on the objectives given in the introduction of the chapter.

Confirmation of the method - Although the unstructured grids do not have a perfectly geometrical similar grid, it is possible to have converging results. However, at very fine grids some strange behaviour in the uncertainty trend can be seen.

Uncertainty estimation - The generation of the viscous layer without scaling the growth factor seems to give a more accurate and precise result than with scaling of the growth factor. Based on the flat plate test-case, it is decided to use the *Hexpress-Default* as the preferred method to perform a verification study for the other cases in this thesis.

Validation with theoretical friction line theories - The values are within the empirical and theoretical values as prediction by Grigson and Katsui. This gives confidence in the result of the calculations.

6

Case 1: Double body

This chapter presents the results of the double body simulations. The RaNS equations used are described in Chapter 2 and the numerical setup, such as grids, discretization schemes and ReFresco settings, is described in Chapter 4.3. The double body simulation is performed on the design speed of 14 knots. The elimination of waves, and their added resistance, gives insight in the friction component of the resistance. The main objectives of this simulation case can thus be written as:

- Confirmation of the grid quality
- Uncertainty estimation for resistance components and wake factors
- Comparison of the friction results with theoretical values and numerical results from the Lloyd's workshop

In the first part of this chapter, Section 6.1, gives an evaluation of the flow field. The main parameters discussed are the velocity, pressure, friction and the wakefield. Continuing on the flow field characteristics, the differences in modelling half and full ship are discussed in Section 6.2. In Section 6.3, this is followed by the uncertainty analysis of the double body calculation for the resistance components and the wake factor. Finally, Section 6.4, presents a detailed evaluation of the resistance in the double body calculation, focusing on the frictional resistance. This analysis is based on comparison with both theoretical drag coefficients and friction components presented in the Lloyd's workshop.

6.1. Evaluation of flow field characteristics

In this section the flow characteristics are presented by discussing the velocity field, the pressure field, the friction on the hull and the resulting wakefield will be discussed. The results will be based on the finest grid, number 6, which contains roughly 26.8 million cells. For the pressure and the velocity fields, the gradients are compared with the refinement level applied to confirm the grid quality.

Velocity

The velocity is made dimensionless with the ship speed ($V_s = 14kn$). The velocity field around the rudder in the symmetry plane is shown in Figure 6.1, with and without the grid. At the location of hanging nodes we can see a small discrepancies in the contour plot, which are errors due to discretization. This error is assessed in the next section.

With higher refinements the differences get smaller and an more equal plot is obtained. It can be seen that the area in between the rudder and the vessel contains the highest gradients and is covered with the highest grid refinement, Figure 6.1b. From this velocity flow field it can also be seen that a bilge vortex separates from the hull and flows along the rudder. The vortex outline is shown by plotting the parameter Q (representing a turbulent area), Figure 6.4. This image shows the bilge vortex which starts just before the stern, around the shoulder.

Figure 6.2 shows the velocity in x-direction in the boundary layer at the symmetry plane midship. The white line is the $V_x = 0.99 \cdot V_s$ line, which indicates the end of the viscous layer. For both the coarse and the fine grid the grid viscous layer seem to capture the actual viscous layer. Also the visual differences between the coarse and the fine grid are minimal for the viscous layer.

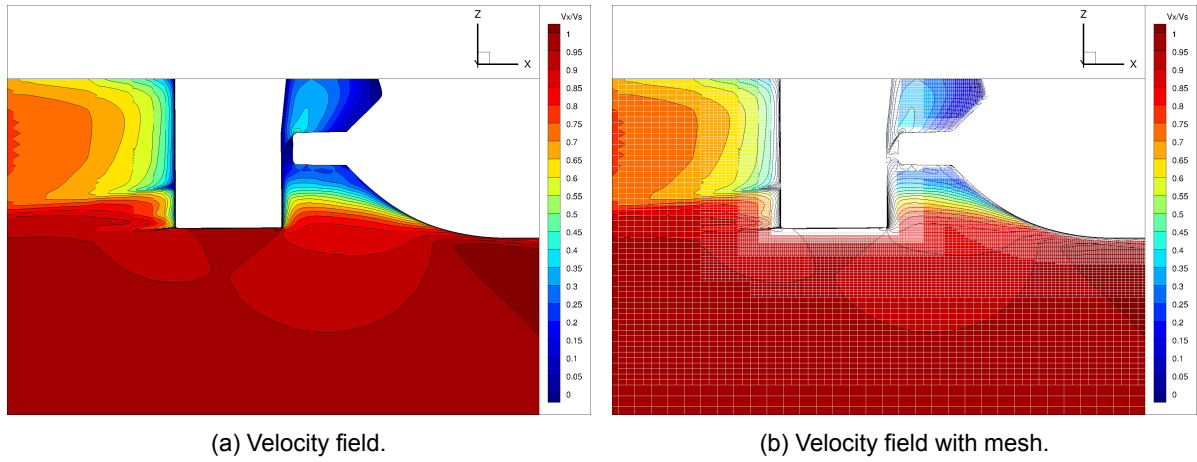


Figure 6.1: Normalised velocity field at the rudder on the symmetry plane. Shown for the finest grid with and without the mesh.

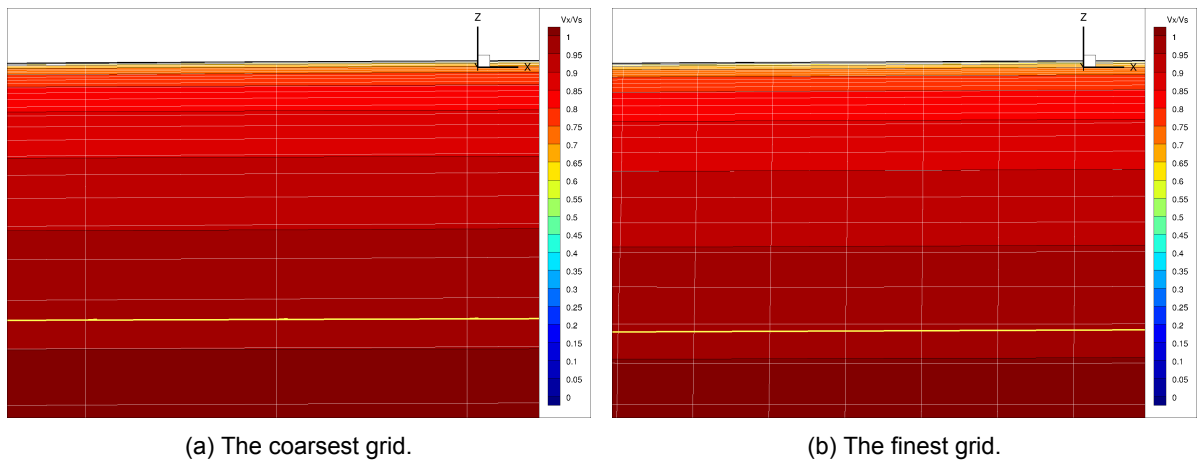


Figure 6.2: The gradients in the boundary layer together with the grid used to model the viscous layer. The location of this image is at the bottom midship at the symmetry plane.

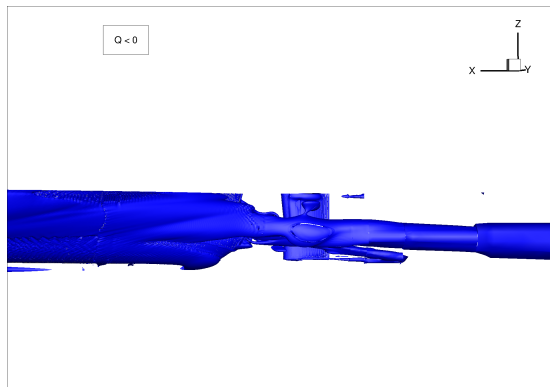


Figure 6.4: Q criteria (Q>0).

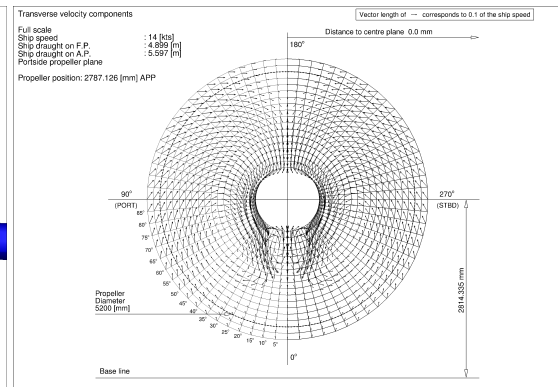


Figure 6.5: Vectors (V_t) in the Wakefield which show the bilge vortex through the wakefield.

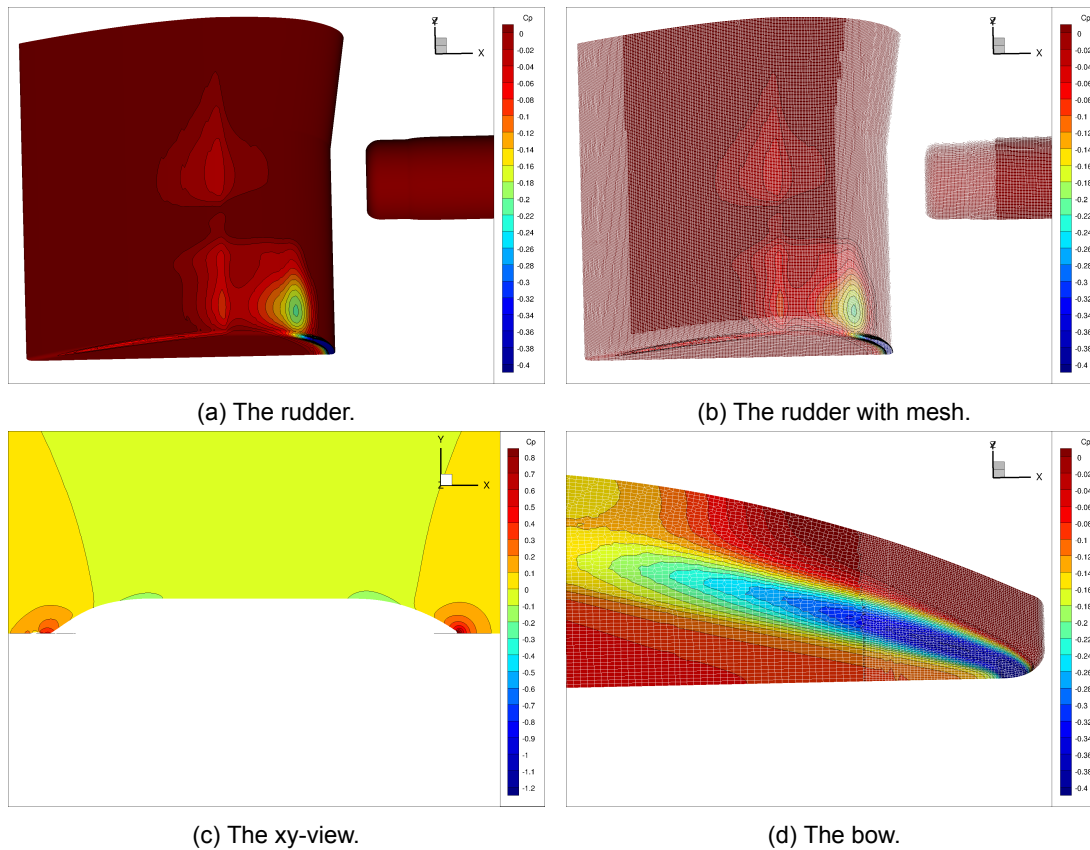


Figure 6.3: Various locations with a contour plot of the pressure coefficient presenting the highest gradients and the global pressure distribution around the ship.

Pressure field

The result of the pressure field is normalised and presented by the pressure coefficient c_p . This is done by the dividing the pressure by the dynamic pressure of the inflow field: $c_p = \frac{pressure}{1/2\rho v_0^2}$. In a global image of the ship in the XY view, a clear view is given of the stagnation points and the influence of the shoulders in the vessel, see Figure 6.3c. More interesting are the locations with high pressure gradients, these are at the bottom of the rudder (Figures 6.3a and 6.3b) and the bilge of the bow (Figure 6.3d). Also here the fineness of the grid seem to capture all the high pressure gradients.

Friction on the hull

As expected the friction on the hull increases with higher velocities and decreases at locations of flow separation or the pressure stagnation points. In the friction field on the rudder the bilge vortex is also visible, see Figure 6.6. At midship the friction coefficient reaches values that correspond to the friction line theory.

Wakefield

The propeller hull interaction is important for resistance predictions and propeller performance. In Figure 6.7 the wakefields (normalised velocity X, contour plot) for the coarsest (Grid 0) and the finest grid (Grid 6) is given. No significant changes can be found in the flow characteristics of the two grids. In both wakefields the influence of the vessel can be seen: a large decrease of velocity due to the boundary layer at the symmetry axis in the top and a hook shaped separation area with low velocities in x-direction. The circular flow trough the wakefield is visualised in Figure 6.5. In this figure the circular flow coming from the bilge vortex is clearly visible.

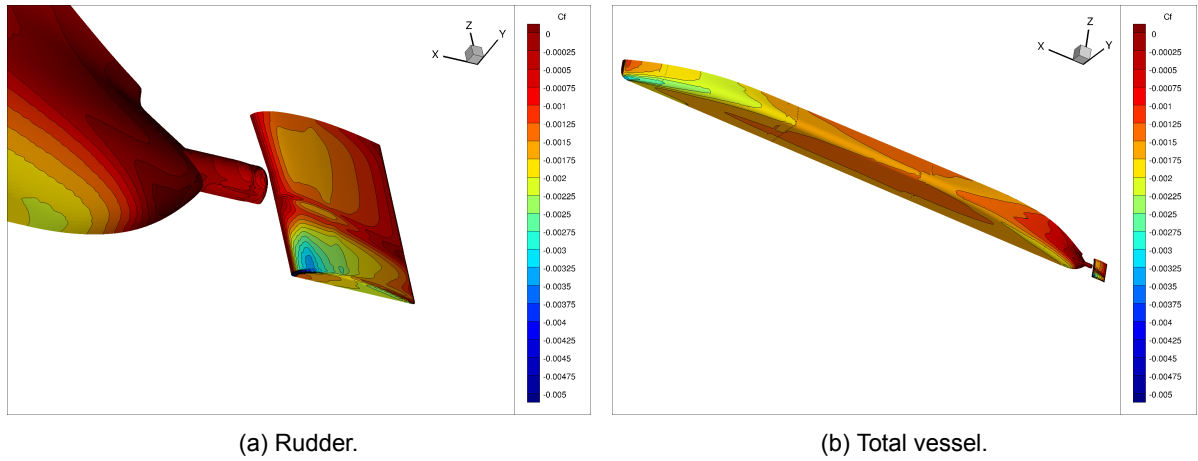


Figure 6.6: Friction coefficient on the vessel and a close-up of the friction coefficient on the rudder.

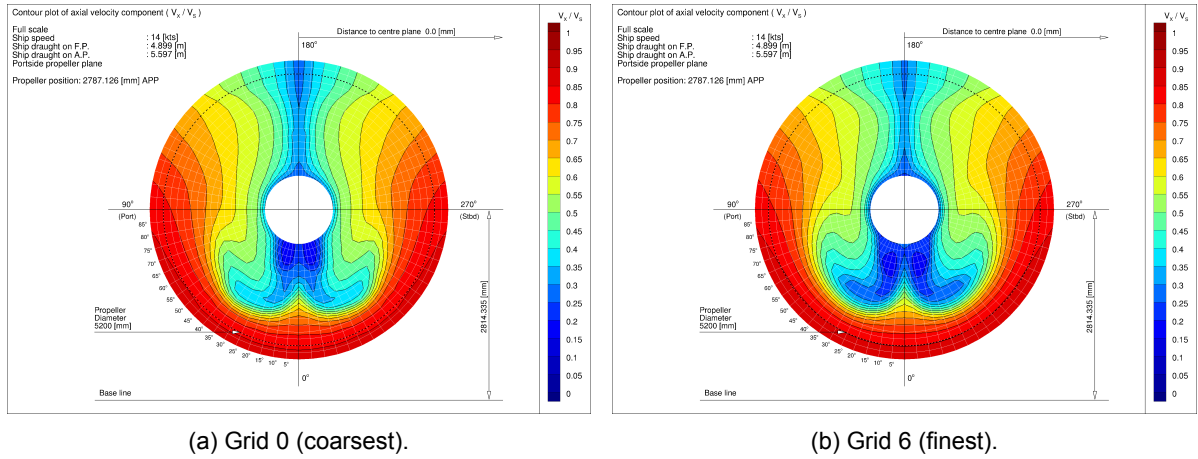


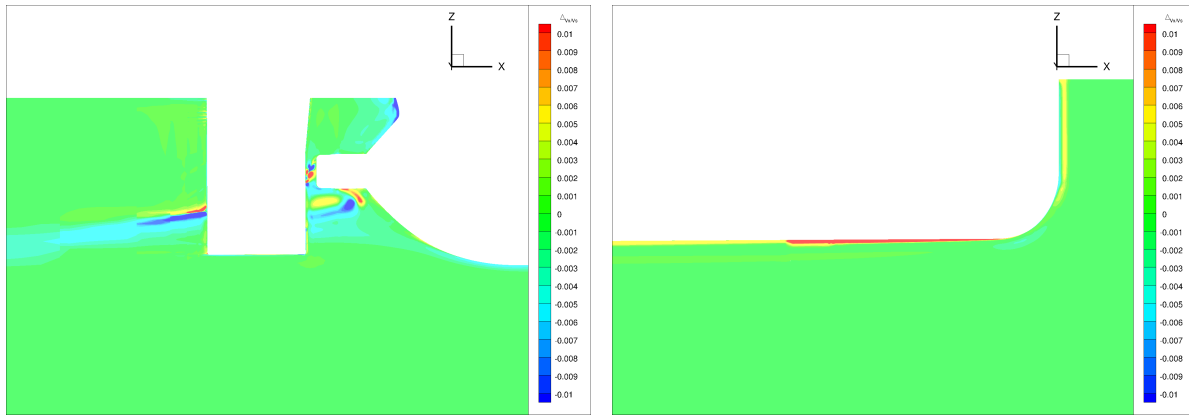
Figure 6.7: Contour plot of the Velocity in X-direction of the wakefield for the half body calculations for the finest and the coarsest grid.

6.2. Flow comparison for the full and half modelled ship

To make sure the boundary conditions implemented at the symmetry plane for half a vessel do not have significant influences on the flow, a full vessel is also modelled for grid 4. Grid 4 is expected to contain enough detailed information, but has less computing time compared to the finest grid. The expectation is that the RaNS calculations since it is time averaged, the only differences will be numerical.

In Figure 6.8 the difference in X velocity normalised with the ship speed is shown for the bow and aft body at the symmetry plane of the domain. The order of magnitude of the differences is a maximum around 0.01 for the normalised velocity. The largest differences can be found in the wakefield of the vessel, which is in accordance with expectation, because of the complexity of the flow.

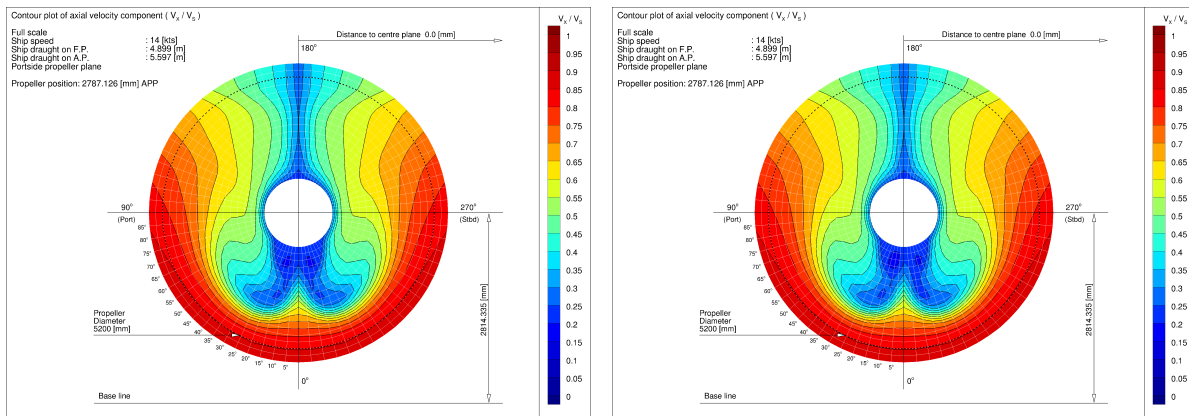
The resulting wakefields are given in Figure 6.9. A bit of numerical asymmetry can be seen in the fully modelled vessel, which is the consequence of absence of the symmetry condition. Figure 6.10 shows the differences in the wakefield at the location of the propeller. The main differences are located below the hub, the location with the most complex flow; cross-flow, vortex and the separation area. The absence of the boundary condition has the highest influence at this location.



(a) Difference in X velocity normalised with the ship speed for the aft.

(b) Difference in X velocity normalised with the ship speed for the bow.

Figure 6.8: Difference in X velocity normalised with the ship speed at the longitudinal through the middle of the ship. The results of the mirrored calculation is subtracted from the half ship simulation. So, negative values present a higher prediction in the full ship result.



(a) Half body.

(b) Full body.

Figure 6.9: Wakefield comparison for the half and full body on grid 4. Contains contours of the velocity in x direction.

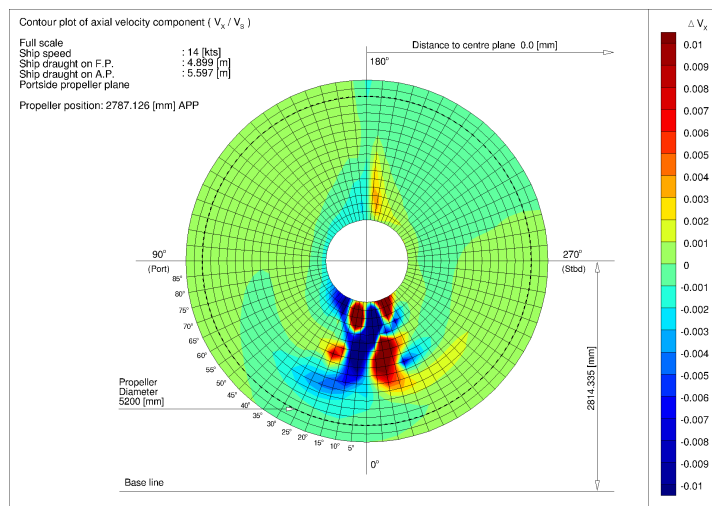


Figure 6.10: Difference in normalised X velocity for the full and the half body.

The quantification of those difference gave a highest absolute difference of 1% in the normalised velocity field. This is significantly lower than the total uncertainty of the discretization, which will be discussed into more detail in Section 6.3. In Table 6.1 the main parameters (wake factor and resistance components) of both the half and the full modelled vessel can be found. The differences between the full and the half modelled ship are less then the differences of two different grid types. Therefore the modelling of the half vessel is a sufficient representation of the flow around a full modelled vessel.

Table 6.1: Comparison of flow parameters for full ship and half ship

		Half	Mirrored	Delta [%]
Hull	$C_{D_{tot}}$	$1.884E-3$	$1.884E-3$	$2.077E-5$
	$C_{D_{Fric}}$	$1.573E-3$	$1.574E-3$	$8.384E-5$
	$C_{D_{press}}$	$3.104E-4$	$-3.103E-4$	$-2.987E-4$
	$Wakefactor$	0.4016	0.4015	$-2.294E-4$
Rudder	$C_{D_{tot}}$	$2.467E-3$	$2.473E-3$	$2.418E-3$
	$C_{D_{Fric}}$	$1.980E-2$	$1.985E-2$	$2.240E-3$
	$C_{D_{press}}$	$-2.227E-2$	$2.232E-2$	$2.260E-3$

6.3. Uncertainty

The grid refinement study is done for the 4 main parameters (friction, pressure, total resistance and the wake factor) and performed for the hull and the rudder separately. The rudder will be greatly influenced by the presence of the propeller in the later stage of the thesis. First, the iterative error is discussed and afterwards the discretization uncertainty.

6.3.1. Iterative error

The L_∞ and L_2 norms are shown for the coarsest grid (Figure 6.11a) and the finest grid (Figure 6.11b). The difference in convergence for the finest and the coarsest grid is quite significant. The iterative error for the coarsest grid drops down to machine accuracy, however the finest grid, with more equations resulting in a more complex system of equations, is harder to solve and therefore converges less. Nevertheless the convergence for the finest grid is considered sufficient, because the L_2 norm for the finest grid is three orders lower then the L_∞ norm. So, the high residuals are probably local and expected to be at location with complex flow.

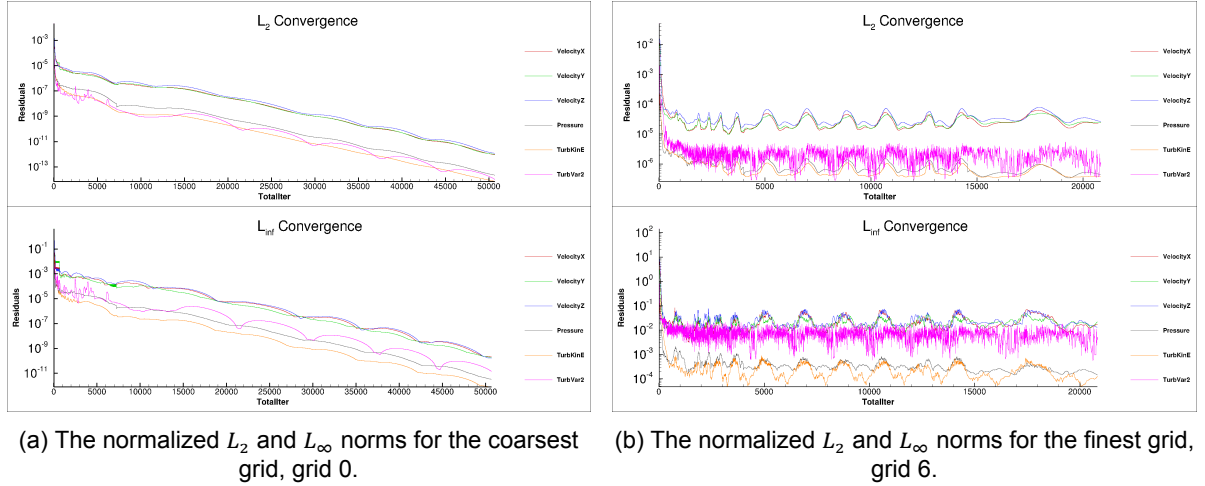


Figure 6.11: Convergence graphs of the finest and coarsest grid for the double body simulation.

From Figure 6.11b it can be seen that the velocity calculation in x,y,z has the highest residuals of the parameters, for both the coarse and the finer grid. Additionally, the behaviour of the ω is quite different for the finer grid. In this situation it is difficult for the ω to converge, because the aspect ratio of the cells is high and the cell sizes are small. This is a unavoidable consequence of simulations without wall functions.

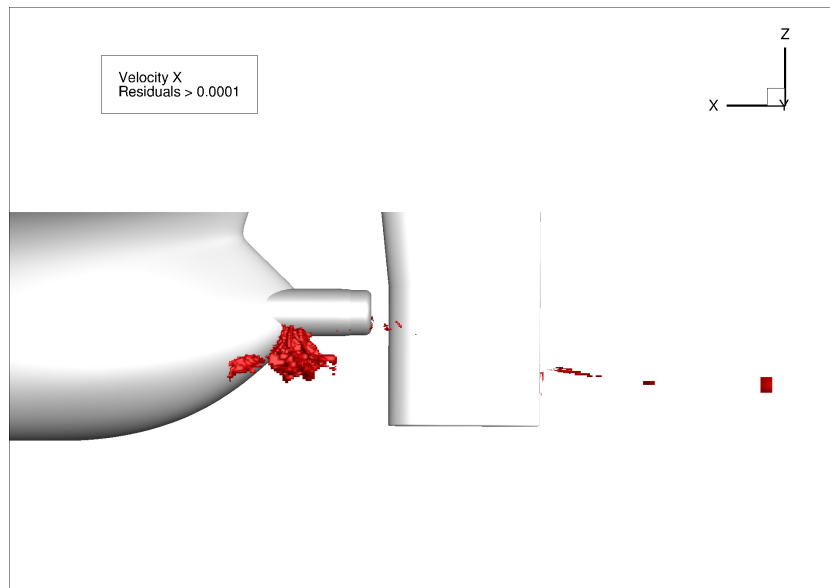


Figure 6.12: Location of the residuals in the finest grid, grid 6. The residuals are located in the complex flow coming from the stern.

The location of the highest residuals for the velocity in x direction is shown in Figure 6.12. The location of these residuals is in the wake of the vessel which has the most complex flow to solve. In Figure 6.4 the bilge vortex is visualised and it can be noticed that the location of the residuals are located in this separation area.

An interesting note is that the main location of the highest residuals is in the wake of the ship, which is not necessarily the location with the lowest grid quality. The grid quality of the coarsest grid is presented in Figure 6.13, because it has the lowest grid quality. This grid quality is based on the quality of cells, such as orthogonality, aspect ratio and skewness. The cells with the lowest quality are located close to the vessel, the location with the highest gradients in the geometry. The curvature in the vessel will cause non-orthogonality in the grid and especially the coarser grid is not able to capture this. But in general, all the cells have a quality of higher than 0.10, with an average of 0.88, and that is a sufficient grid quality.

6.3.2. Discretization uncertainty

The discretization uncertainty is calculated by the grid refinement study as proposed by Eça and Hoekstra. The analysis is done for the resistance components, pressure and friction, and for the wake factor. Note, only half of the vessel is modelled, therefore in the post-processing the values of the forces in x direction have been doubled. The doubled values are presented in this section. An overview of the resulting uncertainty is listed in Table 6.2.

Figure 6.14 presents the uncertainty graphs of the friction coefficient, pressure coefficient and the complete resistance coefficient. In this figure it can be seen that the uncertainty of the friction component is relatively low and the trend in the grid refinement study seems asymptotically towards one solution without much scatter. This almost looks like a trend as expected for a fully geometrical similar grid.

For the results of the pressure coefficient a different trend is found for the grid refinement study. The value of the finest grid does not make a trend towards one final solution. It has been seen in various studies (for example the work by Vink [25]) that the use of unstructured grids is not a perfect method to predict the uncertainty.

The total resistance consists of the friction and the pressure component together. The differences over the grid series in the pressure coefficient are larger than the differences of the series for the friction component. Therefore the total resistance coefficient has the same behaviour as the pressure coefficient.

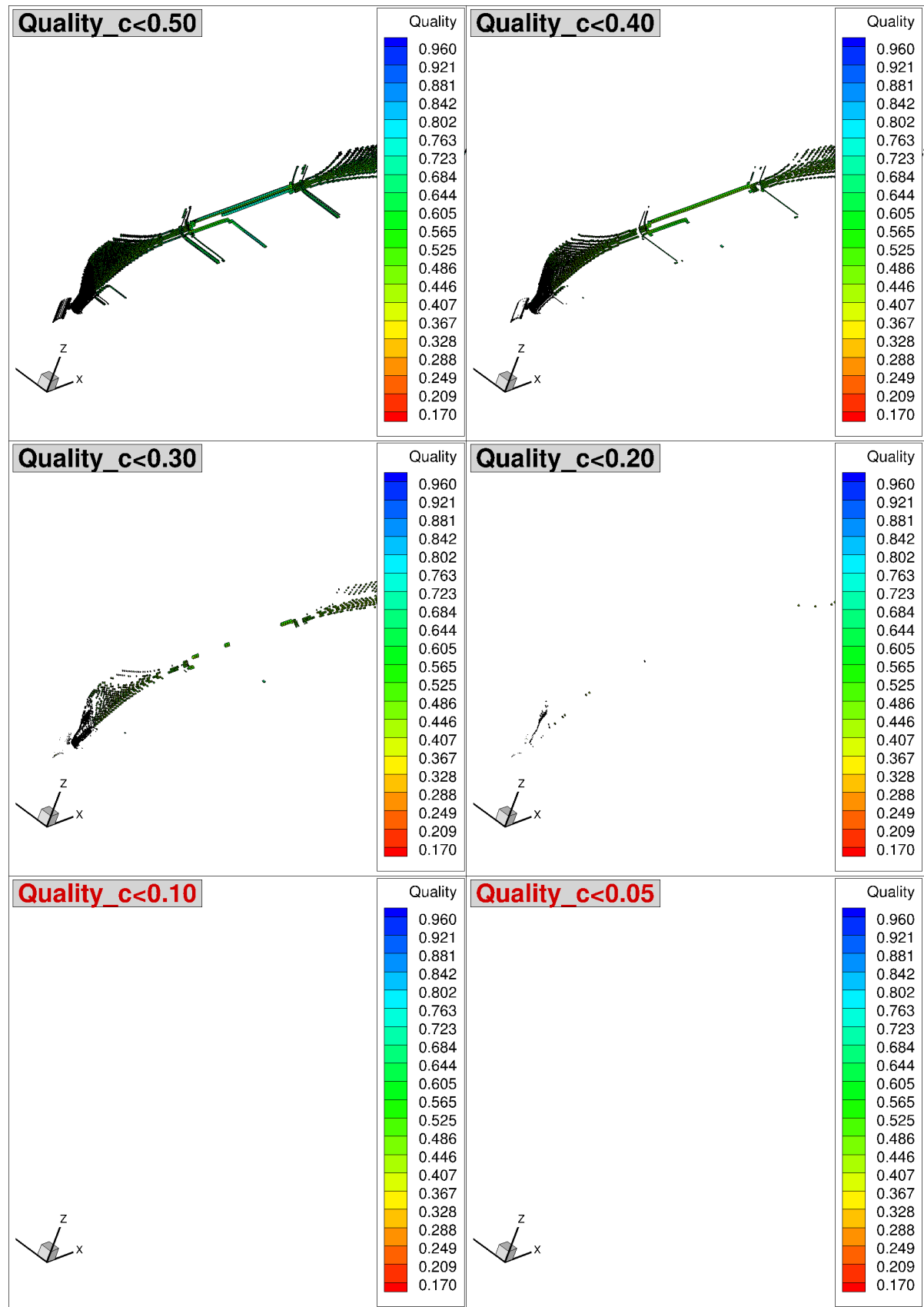
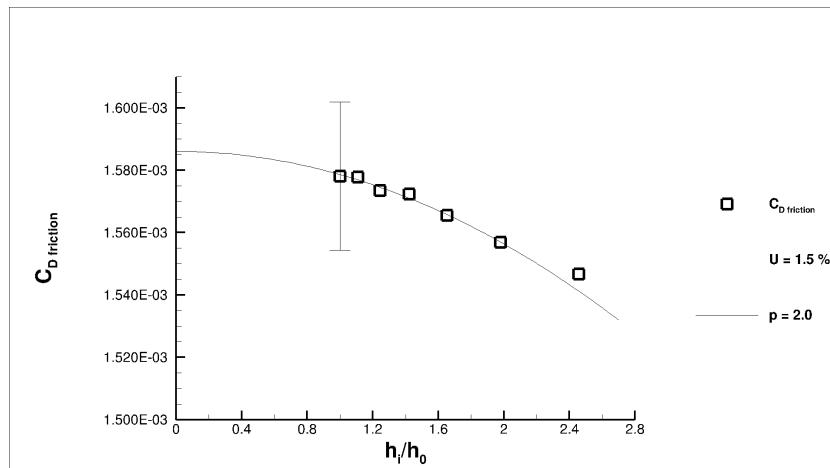
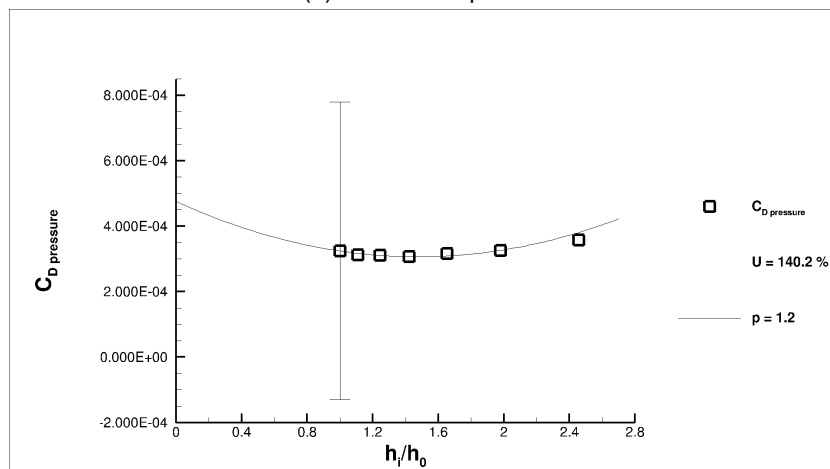


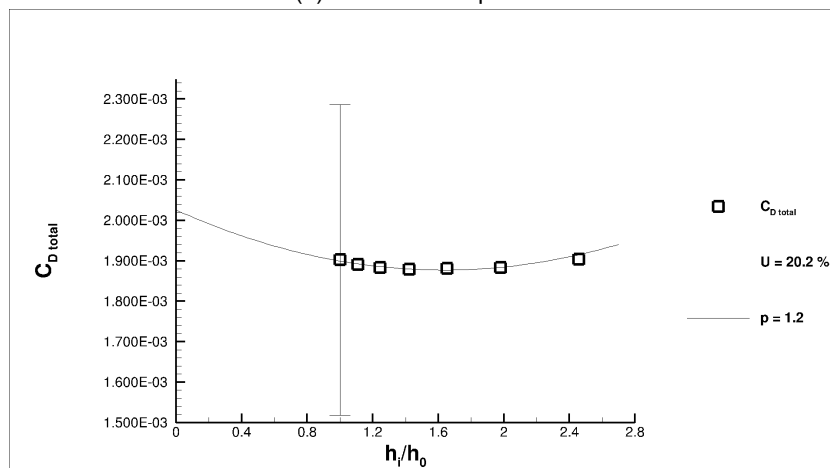
Figure 6.13: The quality of the grid cells for the coarsest grid, grid 0. Grid 0 is presented here, because the finer grid have a better grid quality.



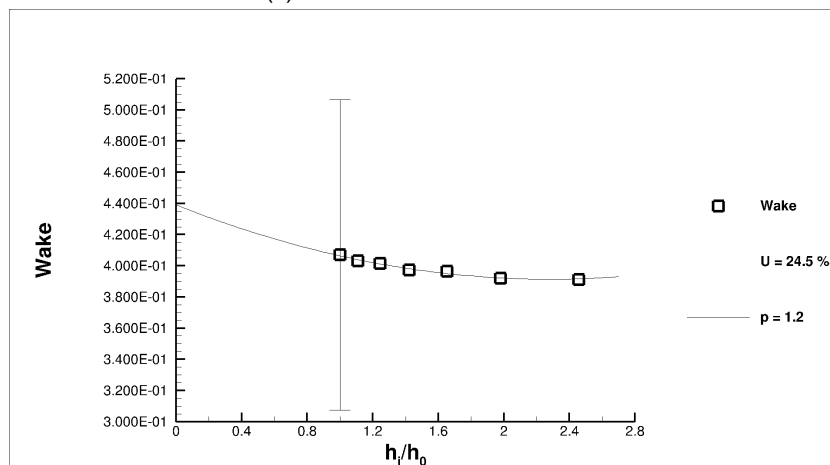
(a) Friction component.



(b) Pressure component.



(c) Total resistance coefficient.



(d) Uncertainty of the wake factor.

Next to the resistance components the uncertainty of the wake factor is analysed and the result is shown in Figure 6.14d. The wake factor w is a dimensionless factor that describes the resulting mean velocity in the wakefield, see Equation 6.1 in which V_s is the ship speed and V_a the averaged velocity in the wakefield.

$$w = \frac{V_s - V_a}{V_s} \quad (6.1)$$

The relative changes in the wake factor are increasing as the grid series goes to finer grids. This is not in accordance with the method, but can be explained by the location in the complex flow (highest residuals), and also by the fact that these factors are created by a standard method which interpolates the computed results to a standard grid for the wakefield, used in the post processing. This means this graph does not only includes discretization errors, but also interpolation errors on the grid.

Table 6.2: List of the estimated values and uncertainty by the method of Eça and Hoekstra.

	$\Phi_0[-]$	$U[\%]$	$\Delta_{max-min}[\%]$
$C_{friction}$	$1.578E-03$	1.5	1.99
$C_{pressure}$	$3.243E-04$	140.2	15.4
C_{total}	$1.902E-03$	20.2	1.28
$Wakefactor$	$4.3904E-01$	24.5	3.88

6.4. Evaluation of the resistance

The resistance consists of two components; a friction coefficient and a pressure coefficient. The pressure component in this double body calculation is expected to be low, since the only significant pressure forces are those of the dynamic pressure due to the three dimensional shape. This is in accordance with the expected value for the friction coefficient ($c_f = 1.5861E-03$) and the pressure coefficient ($c_p = 4.7555E-04$), which is one order of magnitude lower.

The second part of the verification is the comparison to friction line formulas and the friction component in the Lloyd's case. The friction lines commonly used are the ITTC '57 [1], Katsui [18] and Grigson [15] and the corresponding equations are 5.1, 5.3 and 5.2. The results are written in Table 6.3 for this situation ($Re = 1.12 \cdot 10^9$).

Table 6.3: Friction line values for $Re = 1.12 \cdot 10^9$.

	$c_f[-]$
ITTC	1.51E-3
Katsui	1.59E-3
Grigson	1.53E-3

Figure 6.15 shows that in this case the calculated values are close to the friction coefficient as predicted by Grigson, the other two lines give an under-prediction of the friction component. Although the Lloyd's case did not have a double body calculation the friction component of the free surface calculation can be compared to the calculations of this chapter. Since the pressure component is mainly affected by the presence of a free surface. Figure 6.16 shows all the friction results from the Lloyd's case with the result from this calculation. The results calculated fit within the cloud of measurements presented by this case study. The first three points from the Lloyd's case give a higher prediction of the friction force, this is because they did also model roughness on the hull, which will create additional resistance.

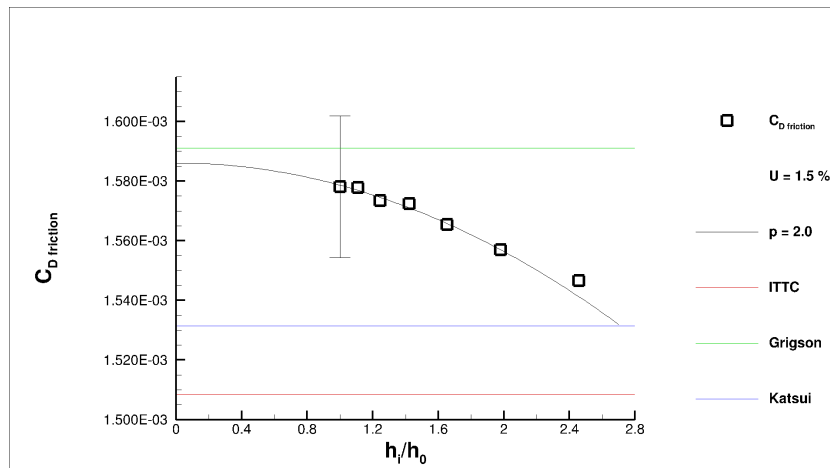


Figure 6.15: Comparison of the calculated grid refinement series compared to the frictions lines as defined by ITTC '57 [1], Katsui [18] and Grigson [15].

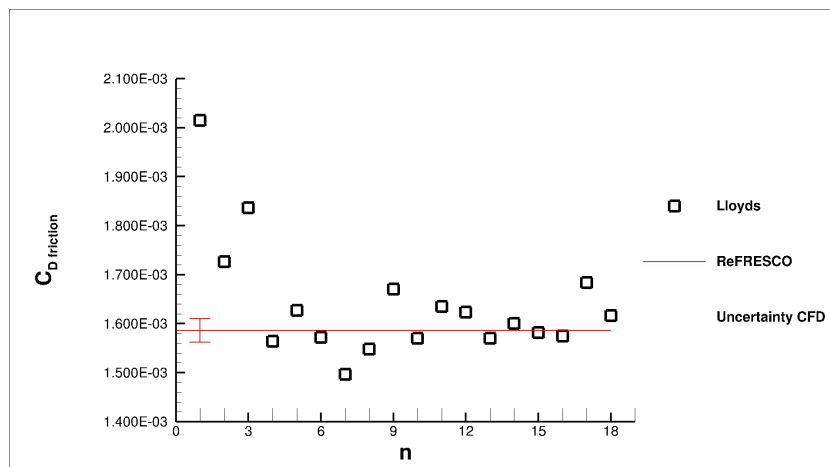


Figure 6.16: Comparison of the friction component with the Lloyd's register case for 14 knots.

6.5. Conclusions

On the double body case study the following conclusions can be drawn:

Confirmation of the grid quality - The grid quality for the currently available reference was sufficient based on the height and location of the residuals.

Uncertainty estimation for the resistance components and wake factors - Various order of uncertainty for the different parameters. From statistical analysis it seemed that the aftship had especially a large contribution for the pressure coefficient, but is also (due to separation) the location with the highest residuals in the field.

Comparison of the friction results - Within the Lloyd's group the results of the friction components are with the calculated uncertainty within the group of the numerical results. The results are actually in between of the theoretical friction lines, which is assumed to be above the lines.

Case 2: Free Surface

The goal of this chapter is to discuss the free surface simulation performed with the numerical setup described in Chapter 4. The goal of this analysis can be summed in the following objectives:

- Presentation of the properties on full-scale free surface flow
- Uncertainty estimation for resistance components and wake factors
- Comparison of the friction results with the double body calculations theoretical values and numerical results from the Lloyd's workshop

This first section, Section 7.1, discusses the flow field of the simulation. In this evaluation the velocity distribution, viscous layer, wakefield and the resulting wave pattern are discussed. The uncertainty in Section 7.2 is presented by analysing the iterative error and estimating the discretization uncertainty for ship hull and rudder. A comparison is made with the double body calculations including the of the resistance components and the flow field in Section 7.3. The last section, Section 7.4 will present the validation with Lloyd's, comparing the free surface simulation result with the numerical results of the 20 participants.

7.1. Evaluation of flow field characteristics

This section describes the flow characteristics of the free surface simulation. Flow phenomena will be discussed for the velocity, pressure, wakefield and the wave system, with more focus on details that are caused by the free surface. The results are based on the current finest grid available, grid 5, which contains roughly 28.5 million cells.

Velocity

The flow velocities are normalised in with the speed of 14 knots (V_x/V_s). In Figure 7.1 the velocity profile around the rudder is shown and next to that the viscous layer with the 99% boundary layer line is given. Flow at the aft ship is influenced by the wave systems and shows both velocities under and above water. The velocity profile has some small visualisation errors at the location of the hanging nodes, which was also seen in the double body case. The viscous layer is taken at midship around the symmetry plane. The modelling of the viscous layer seems, also in this case, to comply with the gradients in the boundary layer.

Pressure

Additionally to the dynamic pressure of the three dimensional shape, the vessel is also subjected to pressure fluctuations due to the waves. Along the side of the vessel the wave system is visible. This also increases the resistance component due to pressure.

Wakefield

The nominal wakefield of the free surface calculation is shown for grid 5 in Figure 7.2. The contour plot shows the boundary layer form the ship extending into the wake. This has roughly the same shape

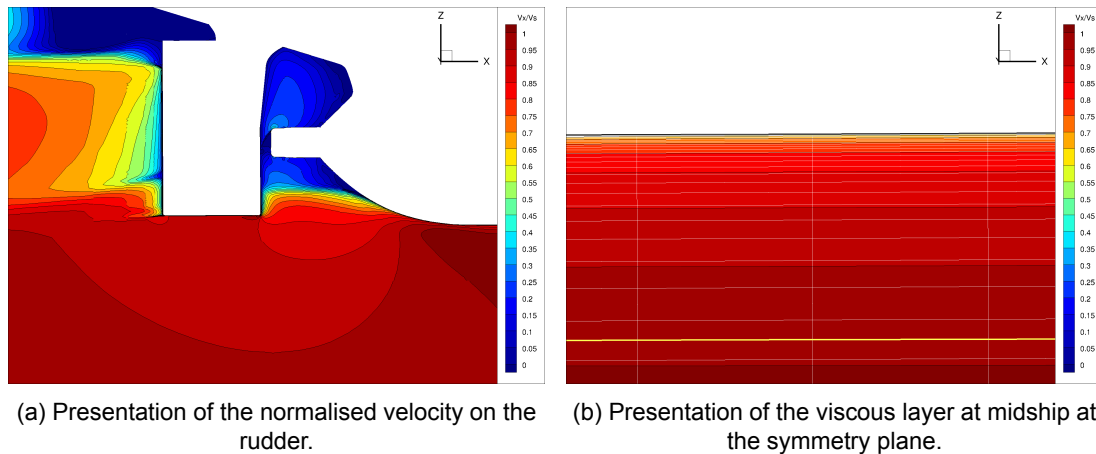


Figure 7.1: Two velocity flow details for the free surface simulations.

as the nominal wakefield as presented for the double body case. In the vectorplot for the transverse velocities (Figure 7.2b) the bilge vortex is visible in the wakefield. The wakefield grid that is used for determination of the wake factor did not change with the trim and sink of the vessel. This means that the values cannot be used for comparison to the double body calculations, but still give insight in the flow field at the location of the propeller.

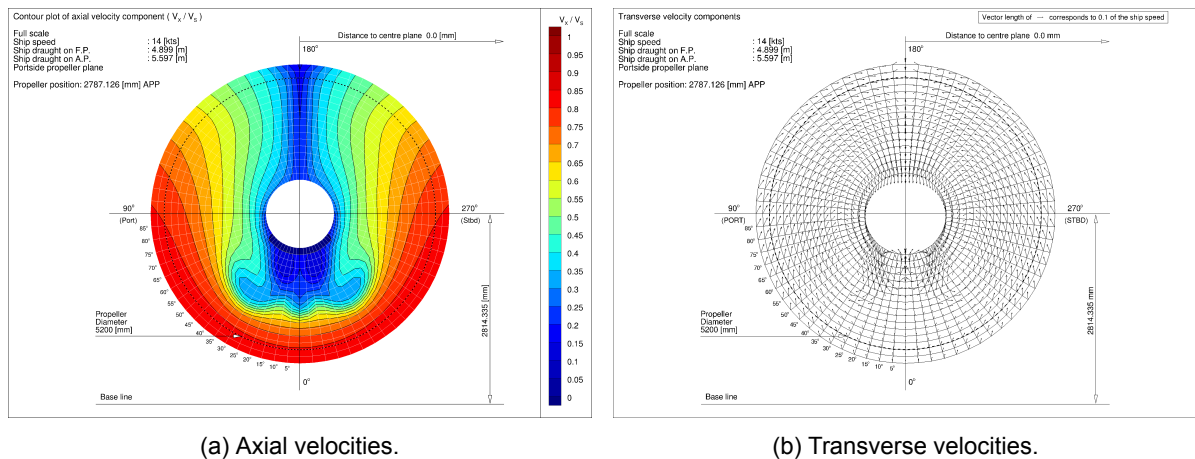


Figure 7.2: The wakefield for grid 4, showing the axial velocities in the contour plot and the transverse velocities and directions in the contour plot.

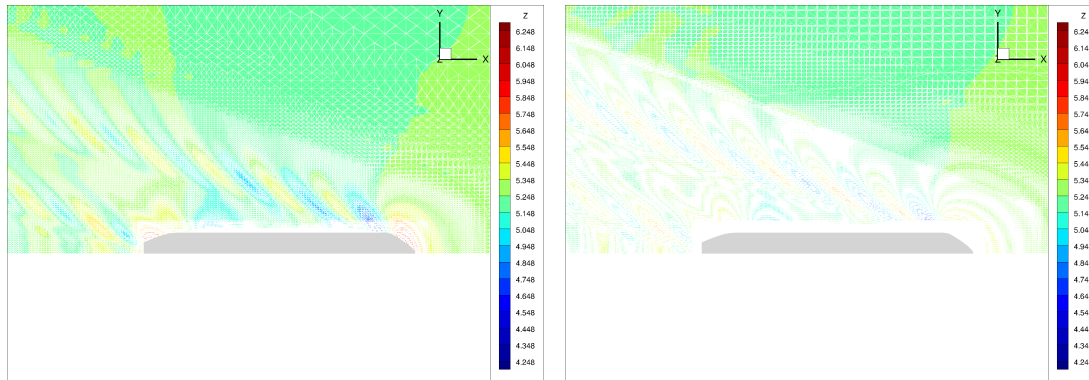
Waves

The free surface with the waves generated needed extra refinement in order to model the waves right. In Figures 7.3a and 7.3b the wavesystem and the kelvin wedge in grid are given for grid 0 and grid 4. The kelvin wedge is implemented according to guidelines and this full-scale simulation seems to be in accordance with these guidelines and captures the wave system.

The grid quality of the grid can also be reviewed in number of cells per wave length, which is shown for grid 0 and grid 4 in Figure 7.3c and 7.3d respectively. The red lines indicate the guidelines and are presented as a reference to the actual cell size. For the grid 4 the cell size is around the guideline and for grid 0 at some locations along the free surface the cell size is not in accordance with the guidelines. The differences are maximum half of the guidelines and for the cell sizes in x direction, the cells below the guidelines are mainly in the farfield. This means that the cell size will have little influence on the wave system.

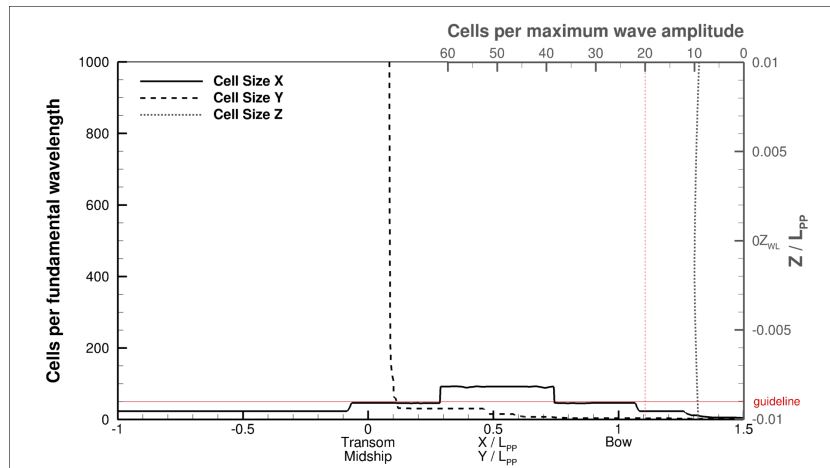
In order to visualise the wave system a general 3D view of the ship and its wave system is given in Figure 7.4a. The free surface is an iso-surface at the air-fraction = 0.5 and on this surface a contour

plot of the height is given. This gives an indication of the wave system at the bow, the shoulders and the stern waves. When looking into this figure in more detail a breaking wave at the bow can be seen. This can be of influence on the stability of the calculations and makes it harder to create a steady solution from the unsteady calculation. Therefore the parameter study is done for the same time step in the simulation, $t = 2000$ s. For validation purpose a wave cut is made from a slice of this free surface at $y = 0.1 \cdot L_{PP} = 13.8m$, this is shown in Figure 7.4b. The wave height is taken relative to the original water line ($z = 5.248$), normalised with the length of the ship.

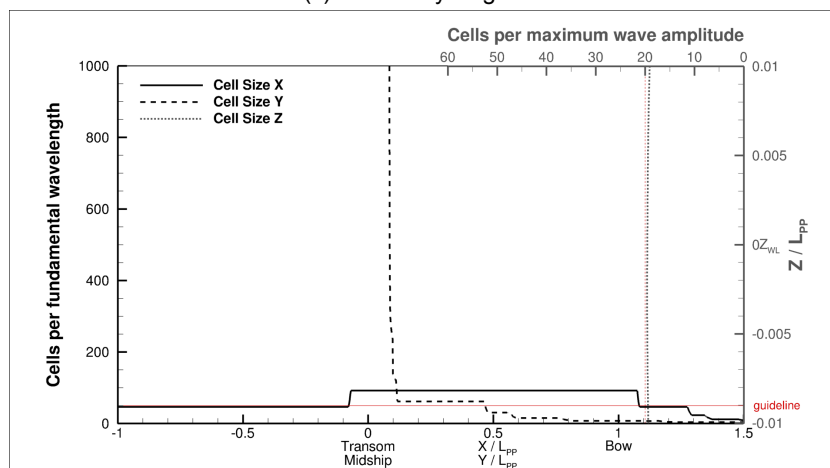


(a) Grid 0.

(b) Grid 4.

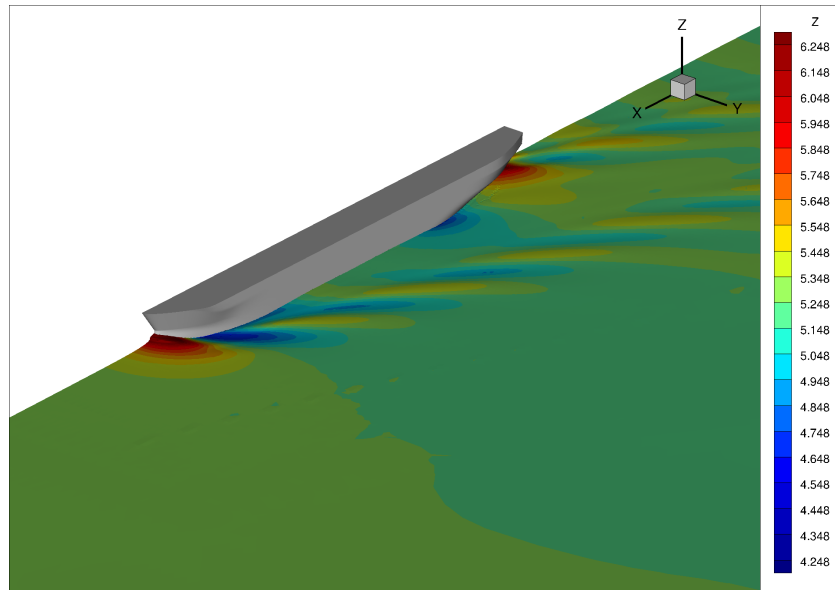


(c) Grid analysis grid 0.

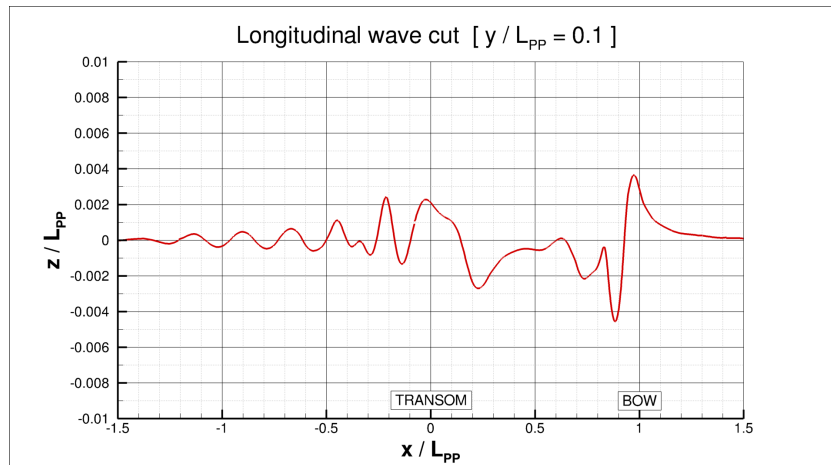


(d) Grid analysis grid 4.

Figure 7.3: Waves viewed with the Kelvin wedge in the grid projected on the contours of the waves, and a presentation of the number of cells per wave for an indication of the grid quality.



(a) 3D view of the wave system around the vessel, presented as the isosurface for airfraction = 0.5 with a contourplot of the wave elevation.



(b) Longitudinal wave cut at $0.1L_{PP}$.

Figure 7.4: Visualisation of the main wave systems of the ship by presenting a 3D view of the free surface and the number of cells per wavelength.

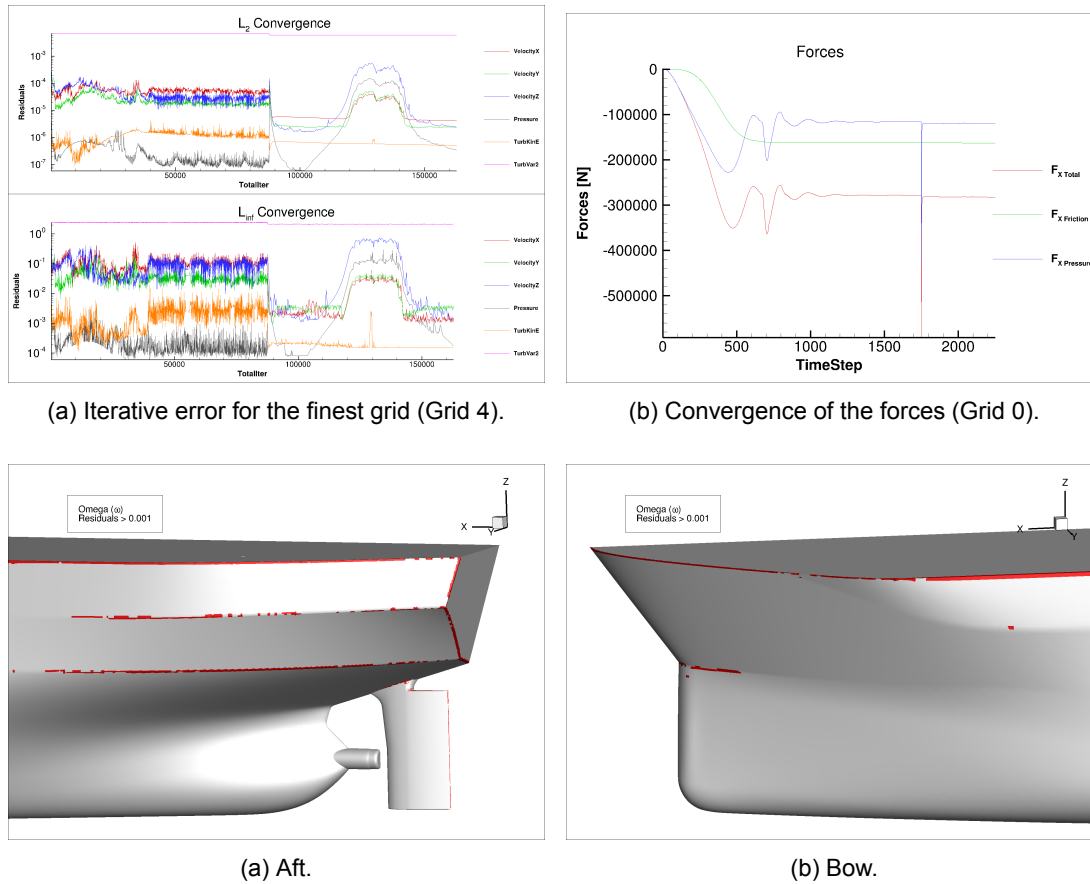
7.2. Uncertainty

The uncertainty will be determined based on the iterative error and the discretization uncertainty.

7.2.1. Iterative error

All simulations converged with the same trend, but the convergence of the finest grid had the least quality and is therefore shown in Figure 7.5a. After 8800 iterations a new control file is loaded with a smaller time step and smaller relaxation factors. It can be seen that the residuals of all parameters drop one order of magnitude. The residuals are stagnating around these values, so the forces should be monitored, to be sure the solution is not only numerical converged, but also the forces are balanced. The trend of the forces over the iterations is given in Figure 7.5b. At the end of the simulation the forces show little variation and the simulation is assumed steady and converged.

In Figure 7.5a it can be seen that the parameter with the highest residuals is the turbulence parameter ω . A small trial has been done with other turbulence models, like $k - k\sqrt{L}$, ϵ and SST-TNT, but

Figure 7.6: Visualisation of the residuals for the turbulent variable ω .

the residuals of the non-turbulent parameters were the lowest in the $k - \omega$ case. The location of the residuals, see Figure 7.6, shows that the highest residuals are located at the connection between the ship hull and deck. It is likely that the difference in boundary conditions (slip on the deck and no slip on the hull), might cause numerical difficulties of the turbulence model.

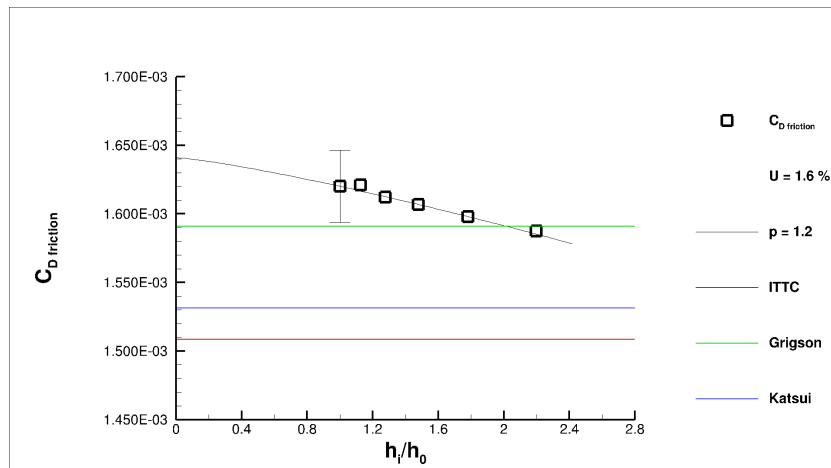
7.2.2. Discretization uncertainty

In the double body case it was already seen that the grid refinement method from Eça and Hoekstra should be used with care for unstructured grids. The current grid refinement study is based on six grids instead of seven. The discretization uncertainty will be presented for the friction, pressure and total resistance for both the rudder and the ship. Due to trim and sink in the model the wetted surface increased from 3700 to $3800 \pm 1m^2$. The variance between the wetted surface prediction of the simulation is low and the coefficients are calculated with the new wetted surface. The final uncertainty values are listed in Table 7.1.

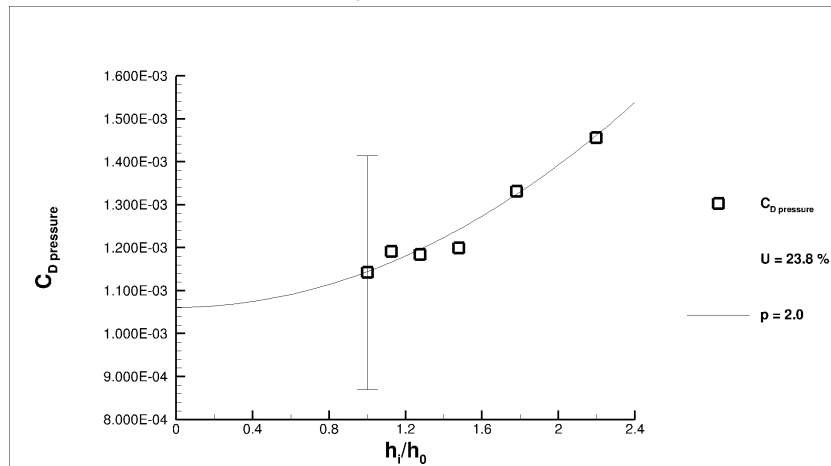
The trend of the friction coefficient over the refined grids looks converging (Figure 7.7a) and thus has a relatively low uncertainty of 1.6%. This is accordance with the trend the friction coefficient has in the previous cases double body and the flat plate).

For this case the pressure coefficients are in line with each other, but the differences between the grids is relatively large, see Figure 7.7b. This results in an uncertainty of 23.8%. The consequence of the large differences is that the pressure coefficient is under estimated, when the result of the method by Eça and Hoeksta is followed.

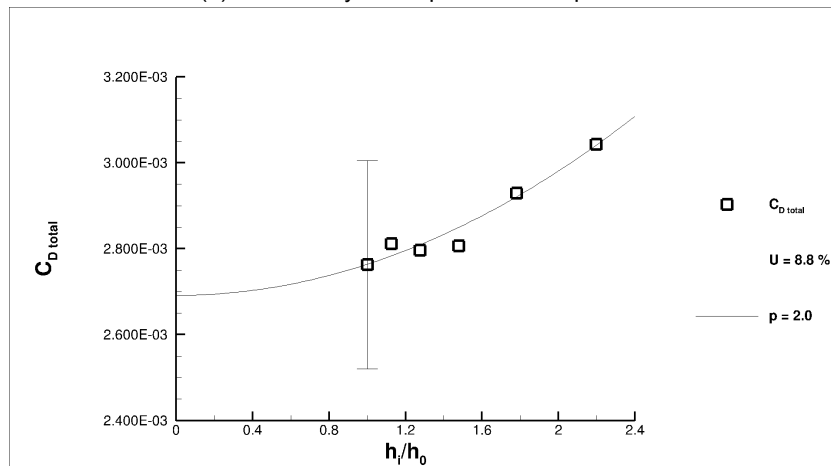
Continuing on the large differences for the pressure coefficient it can be seen that the total resistance coefficient also has a large difference between to grid refinements. The trend of the total resistance coefficient is given in Figure 7.7c and shows and uncertainty of 8.8%. Again, the predicted coefficient is under estimated significantly. Therefore it is recommended for this case to chose the resulting coefficient of the finest grid as final value.



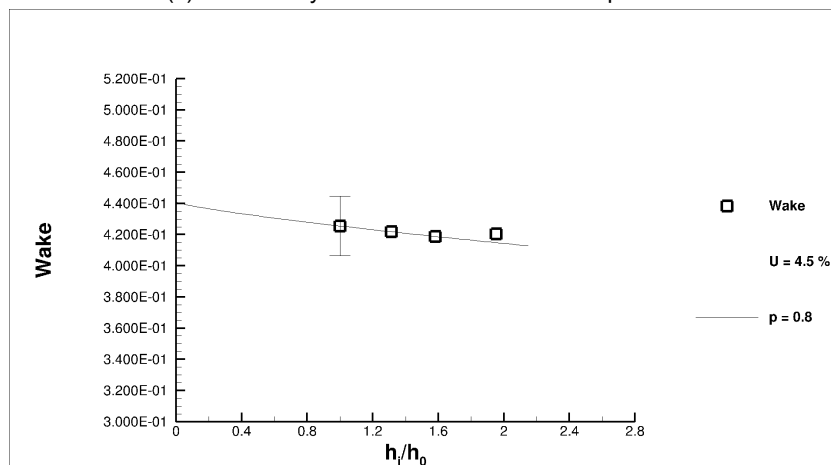
(a) Uncertainty of the friction component.



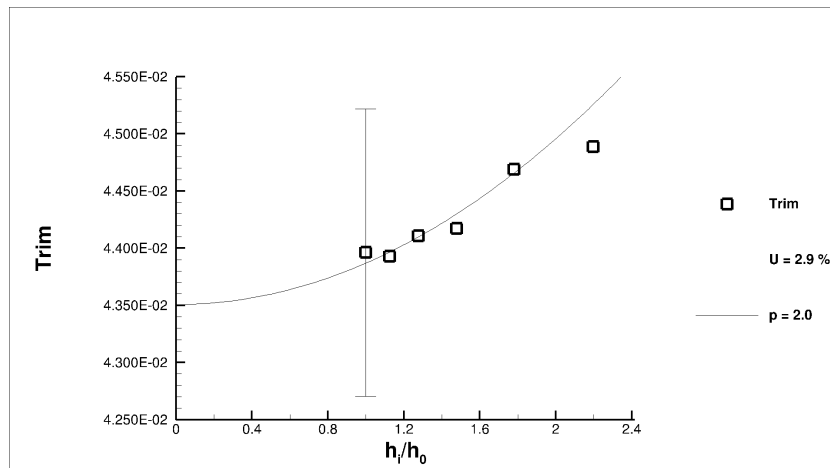
(b) Uncertainty of the pressure component.



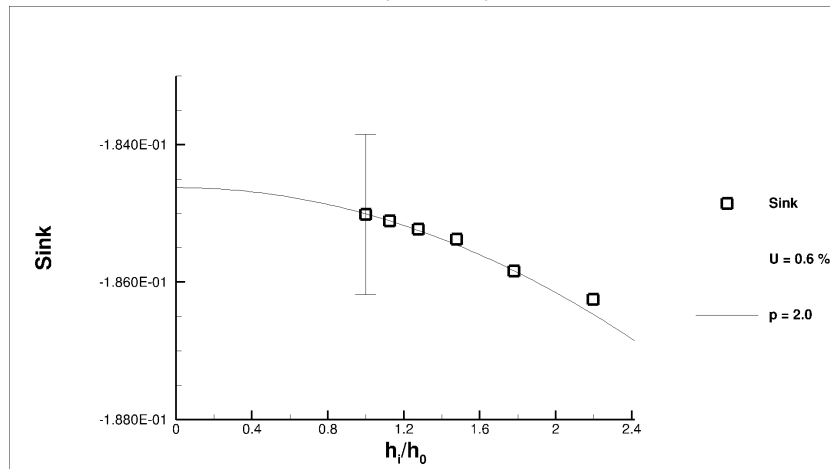
(c) Uncertainty of the total resistance component.



(d) Uncertainty of the wake factor.



(a) Uncertainty of the dynamic trim.



(b) Uncertainty of the dynamic sink.

Figure 7.8: The results of the grid refinement study by Eça and Hoekstra for the trim and sink.

The discretization uncertainty for the wake factor is estimated to be 4.5% (Figure 7.7d). The wakefield estimation is only based on 4 grids and the subgrid from which the value is interpolated is not on the same location relative to the ship. The dynamic trim and sink have an estimated discretization uncertainty of respectively 2.9 % and 0.6 %. The trend over the grid refinement study can be seen in Figures 7.8a and 7.8b

Discretization of the Free-Surface is more difficult to calculate, therefore the wave cuts for the grids 0, 1, 2 and 4 given in Figure 7.9. In the wake of the vessel the finest grid predicts the highest waves, however the simulation of the bow wave differs for the simulation and a less converging trend over the grids can be seen. This can be caused by the breaking bow wave, which creates unsteadiness in the calculation. The free surface result is taken for the same time step, but concluding from this image might be influenced on the combination time step and grid cell size.

Table 7.1: List of the estimated values and uncertainty by the method of Eça and Hoekstra.

	$\Phi_0[-]$	$U[\%]$	$\Delta_{max-min}[\%]$
$C_{friction}$	$1.664E-3$	1.6	1.94
$C_{pressure}$	$1.173E-3$	23.8	27.60
C_{total}	$2.837E-3$	8.8	10.30
<i>Wakefactor</i>	0.426	4.5	1.58
<i>Trim</i>	$4.296E-3$	2.9	2.18
<i>Sink</i>	$1.850E-1$	0.6	0.67

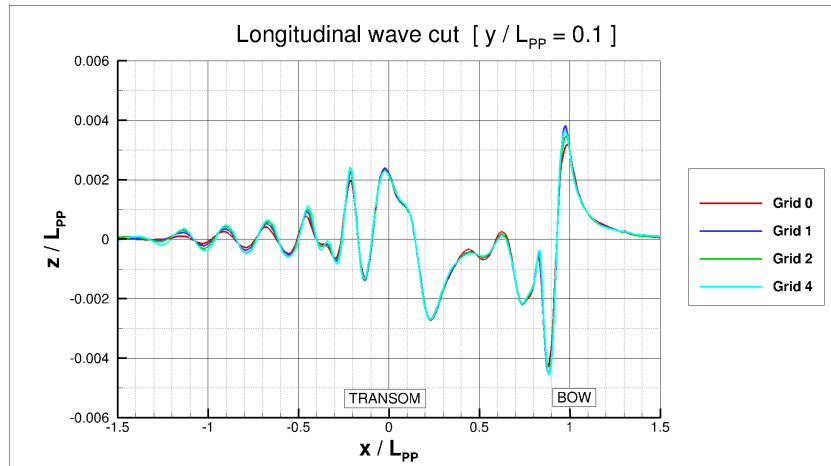


Figure 7.9: Wave cut presentation of the grids 0,1,2 and 4 in order to visualise the discretization error in the wave cut.

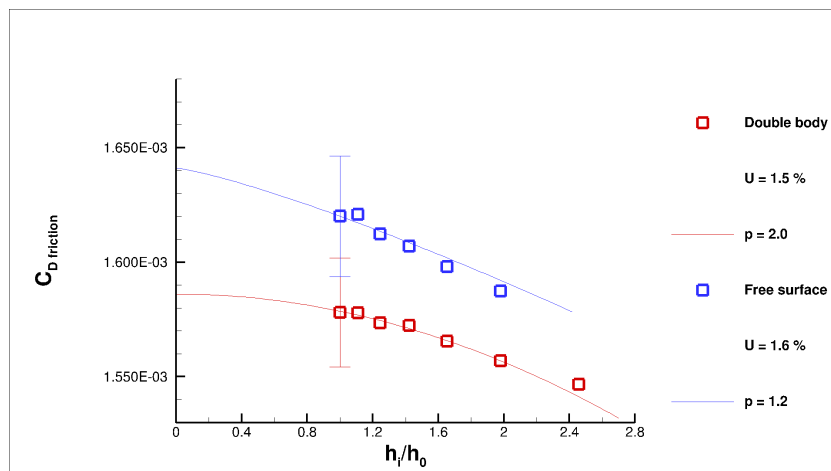


Figure 7.10: Grid refinement comparison for the double body (red) and the free surface (blue) simulations.

7.3. Comparison to Double body simulations

The uncertainties for the current prediction of the free surface are lower than the prediction for the double body. The main difference is the free surface which brings an extra pressure field in the domain.

7.3.1. Friction coefficients

The coefficients for the free surface simulation are adjusted for the added wetted surface. Therefore the differences in values are based on the shape of the vessel. Figure 7.10 both the grid refinement study for the double body (red) and the free surface (blue) are given. The values for the free surface simulation are shifted such that the grid refinement ratio (h_i/h_0) for the double body and the free surface calculation comply. The trend over the grid is the same for both grid series.

7.3.2. Pressure coefficients

An absolute comparison can not be made for the free surface and double body simulation. However for both simulations it can be seen that the largest residuals in the velocities are located close to the aft ship. From statistical analysis it is seen that the aftship, in both simulations, is a large contributor to the pressure coefficient. It is possible that the location of the residuals is therefore of large influence of the discretization uncertainty.

7.4. Comparison to Lloyd's case

For the validation with the data of Lloyd's case the results of the finest grid (Grid 5) are used. For this section the resistance components and a wave cut are compared to the results of the Lloyd's Register workshop.

7.4.1. Resistance coefficients

Starting with the friction components the value of grid 5 is plotted for validation in Figure 7.11. The friction coefficient ($c_F = 1.67 \cdot 10^{-3}$) is located well within the group, with uncertainty. As a reminder, the first three results from the Lloyd's case are calculated with surface roughness and are therefore have a higher value.

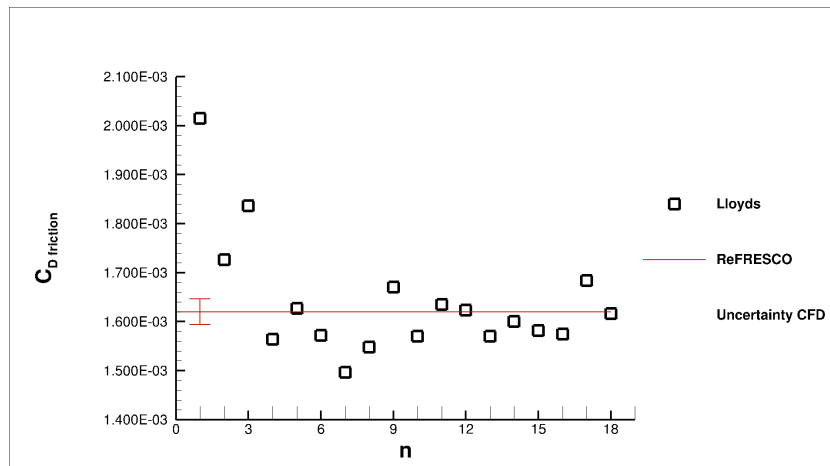


Figure 7.11: Comparison of the friction component with the Lloyd's register case for 14 knots.

The pressure coefficient is also well within boundaries of the group, but has a relatively small value. This is shown in Figure 7.12. The value of $c_F = 1.22 \cdot 10^{-3}$ is considered sufficiently well predicted.

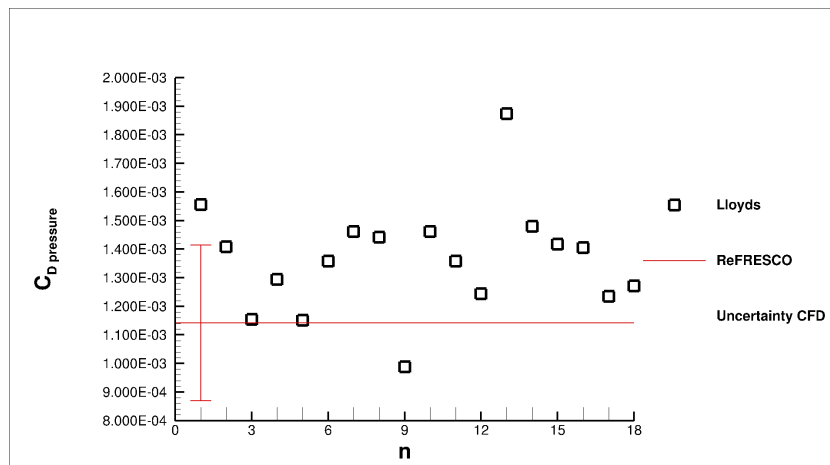


Figure 7.12: Comparison of the pressure component with the Lloyd's register case for 14 knots.

The total resistance coefficient of $c_t = 2.89 \cdot 10^{-3}$ is close to the average value of the numerical Lloyd's results. Figure 7.13 shows that, the majority of the results are closer together then for the friction or the pressure coefficient. Results by ReFRESCO are within the range of the mean and the standard deviation of 7.1 %, corresponding to the Lloyd's case.

7.4.2. Dynamic trim and sink

In the Lloyd's case the dynamic trim was around the 0.035 ± 0.01 degrees. The simulated trim for the finest grid resulted in 0.044 degrees. This is on the upper side of the range, but not outside of the range.

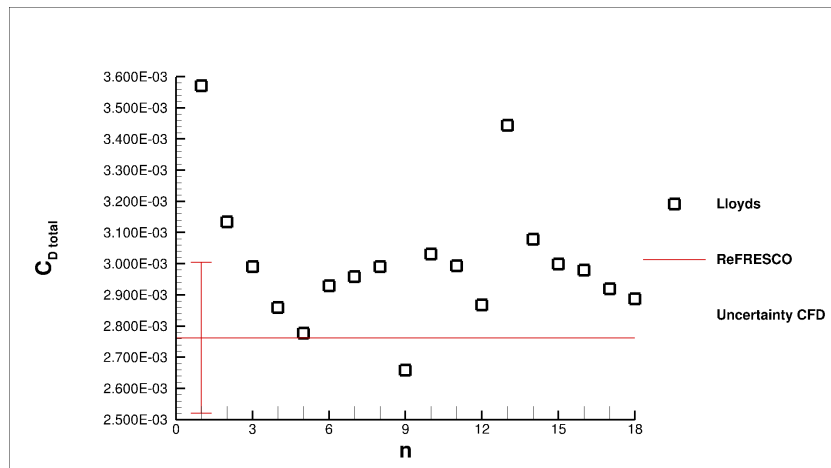


Figure 7.13: Comparison of the total resistance component with the Lloyd's register case for 14 knots.

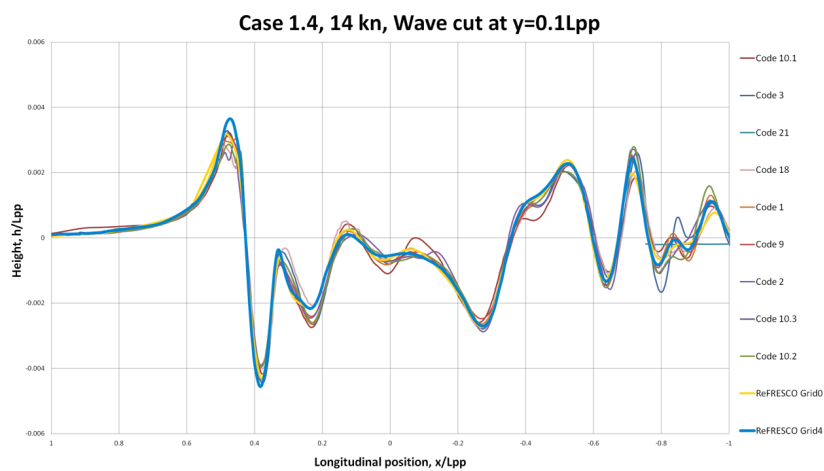


Figure 7.14: Wave cuts at $0.1L_{PP}$ for the coarsest (yellow) and the finest (blue) grid, plotted together with results of the Lloyd's workshop. The bow is located at 0.5 and the stern at -0.5 .

The predicted dynamic sink by the Lloyd's case was a sinkage of 0.2 meter. The numerical result of the calculations in this thesis is a sinkage of 0.19. This is on the lower side of the Lloyd's group, but within the 90 % standard deviation of the group. This gives confidence not only in the calculation, but also the range set for updating the values in the simulation.

7.4.3. Wave cuts

Wave cuts are taken out the free surface for the finest and the coarsest grids and plotted with a couple of the wave cuts from the Lloyd's case in Figure 7.14. The bow is located at the left and the stern at the right. Relatively large difference can be found in the bow wave, which is breaking and thus harder to solve.

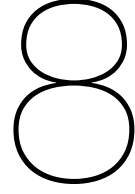
7.5. Conclusion

For the free surface simulation the following conclusions can be drawn:

Properties of the free surface flow - In the flow field similarities were seen with the double body calculation. The breaking wave in the simulation indicates unsteadiness in the results, which is solved by taking the values for the uncertainty study are all taken at the same time step.

Uncertainty estimation for resistance components and wake factors - The estimation for the discretization uncertainty is varying between the 0.6 and 23.8 percent. The pressure coefficient is the main contributor to the large discretization uncertainties and can be explained by the location of the residuals at the aftship of the vessel.

Comparison of the friction results with the double body calculations theoretical values and numerical results from the Lloyd's workshop - Although the discretization error differs for the parameters, all parameters satisfy the predictions by the numerical results of the Lloyd's case study and the theoretical friction lines.



Case 3: Open Water

An open water simulation is performed to gain more insight in the behaviour and efficiency of the propeller in full-scale conditions on a hybrid structured and unstructured grid. For a series of 5 grid refinements over a range from $J = 0.10$ up to $J = 0.65$ the propeller performance is calculated. The main objectives can be summed as:

- Presentation of the full-scale open water diagram
- Uncertainty estimation for thrust and torque coefficients
- Comparison with results from the Lloyd's workshop

In Section 8.1 the flow field is analysed, the grid quality determined and the open water diagram presented. Next, in section 8.2 the discretization uncertainty is analysed for the design point ($J = 0.5$) of the propeller, which is considered guiding in the analysis. To finalise this chapter the comparison is made with the numerical Lloyd's data in Section 8.3.

8.1. Evaluation of flow field characteristics

The flow field results are given for grid 3, which roughly contains 23.8 million cells in the whole domain. Grid 3 is chosen instead of the finest grid, because for grid 3 all the simulations converged and this is not the case for grid 4. Starting with the axial velocities presented in Figure 8.1, the acceleration in the normalised velocity field can be seen. On the left side the axial flow field for advance ratio (J) is 0.2 and on the right for $J=0.5$. For the low advance ratio the inflow velocity is low compared to the rotational speed of the propeller. For the flow around the design point ($J=0.5$) the relative acceleration is lower, but the absolute acceleration is higher.

Additional to the acceleration the wake behind the shaft is visualised in Figure 8.1. The corners on the shaft are slightly smoothed to avoid numerical problems in the wake.

The acceleration of the flow as described above is based on a pressure difference. The pressure field around 0.70 of the propeller radius is given in Figure 8.2b.

For all the grids these calculation have been performed on a range from $J = 0.1$ to 0.65 with steps of 0.05. From this an open water diagram (OWD) can be constructed, the formula's for this are given below. For the coarsest and finest grid this OWD can be found in Figure 8.3, The equations used in the OWD are listed below. This shows that the differences between the two grids are small.

$$Kt = \frac{T}{n^2 \cdot D^4 \cdot \rho} \quad (8.1)$$

$$KQ = \frac{Q}{n^2 \cdot D^5 \cdot \rho} \quad (8.2)$$

$$\eta_0 = \frac{J \cdot Kt}{2\pi \cdot KQ} \quad (8.3)$$

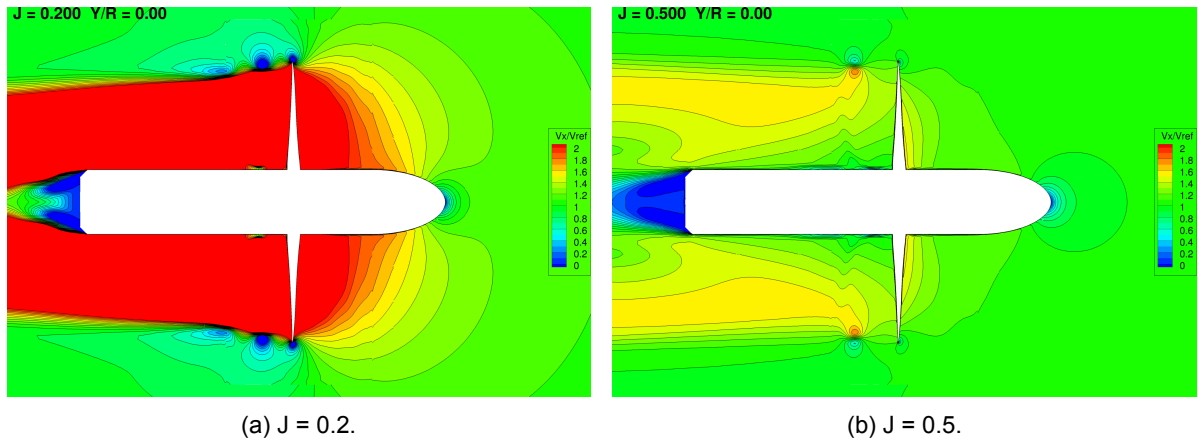


Figure 8.1: Axial velocities in the open water simulation for a low advance ratio and the advance ratio for the design point.

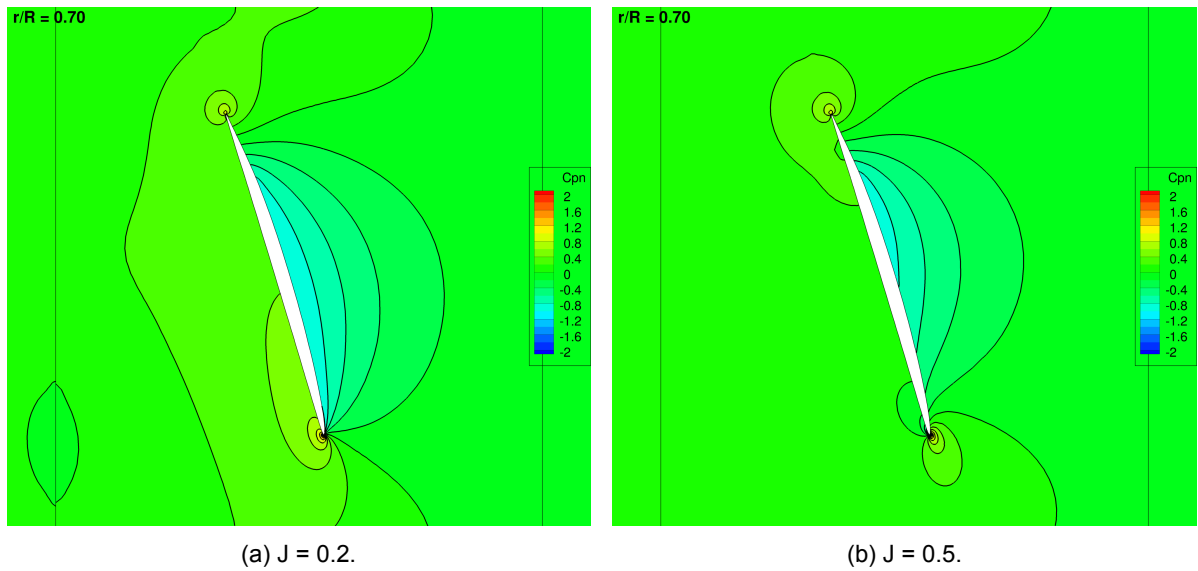


Figure 8.2: Pressure gradients on the propeller blade for a low advance ratio and the advance ratio for the design point at the location $r/R = 0.7$.

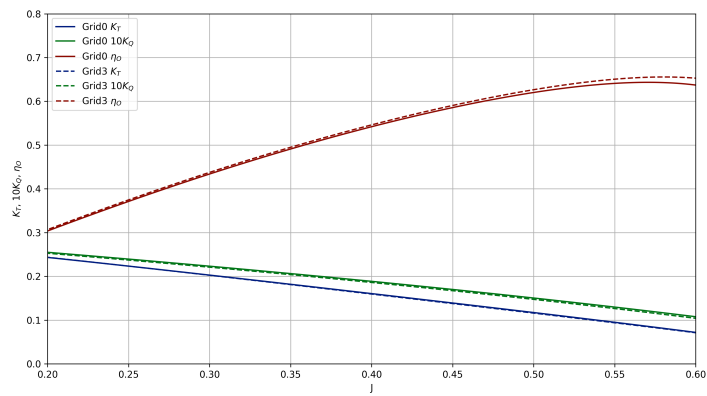


Figure 8.3: Comparison of the open water diagram for the coarsest (grid 0) and the finest grid (grid 3).

8.2. Uncertainty

The uncertainty analysis is based on the iterative error and the discretization error. However for the finest grid (grid 4) on the highest two advance ratios ($J=0.60$ and $J=0.65$) the simulation did not converge. Therefore, for these two situations the discretization uncertainty is taken without this calculation. For the method by Eça and Hoekstra to work a minimum of 4 grids is required.

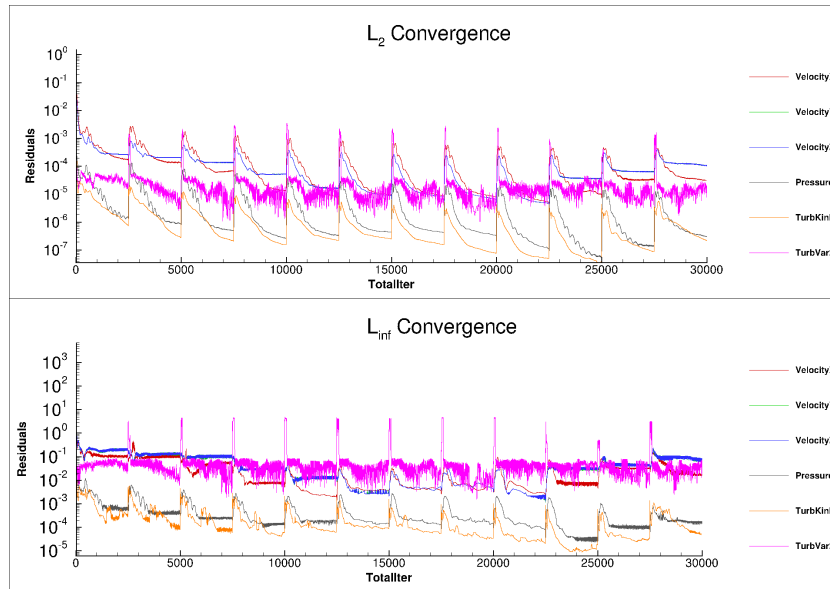


Figure 8.4: Iterative Error over the complete open water simulation on grid 3.

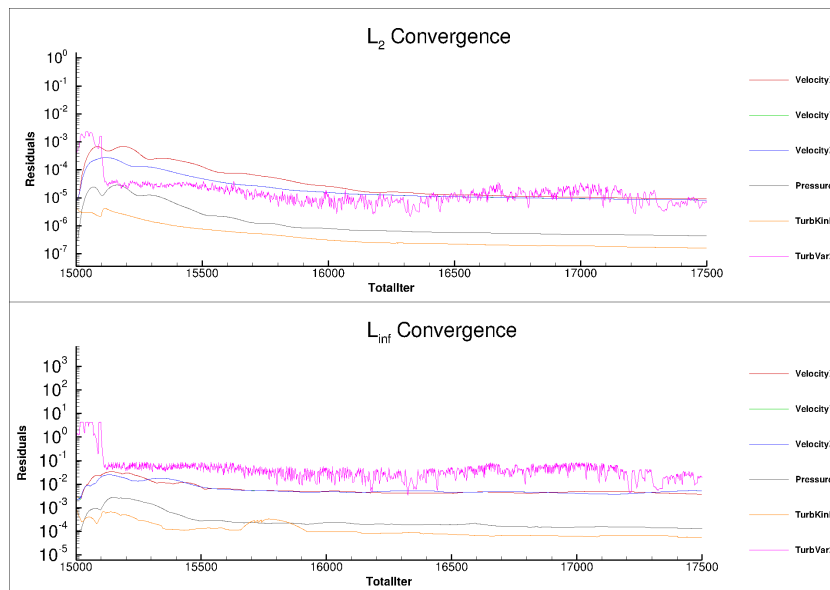
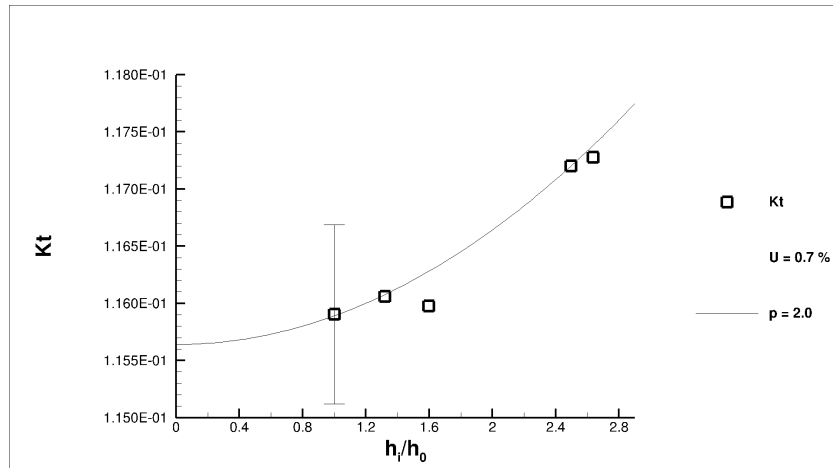


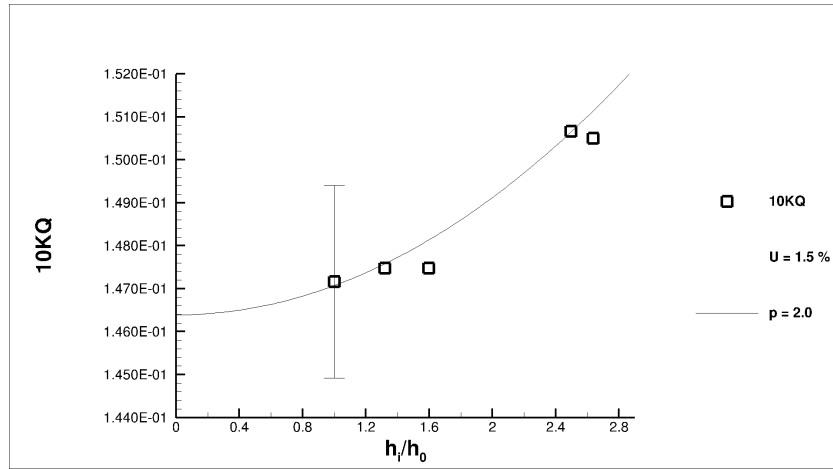
Figure 8.5: Iterative Error over the complete open water simulation on grid 3 zoomed in for $J = 0.5$.

8.2.1. Iterative error

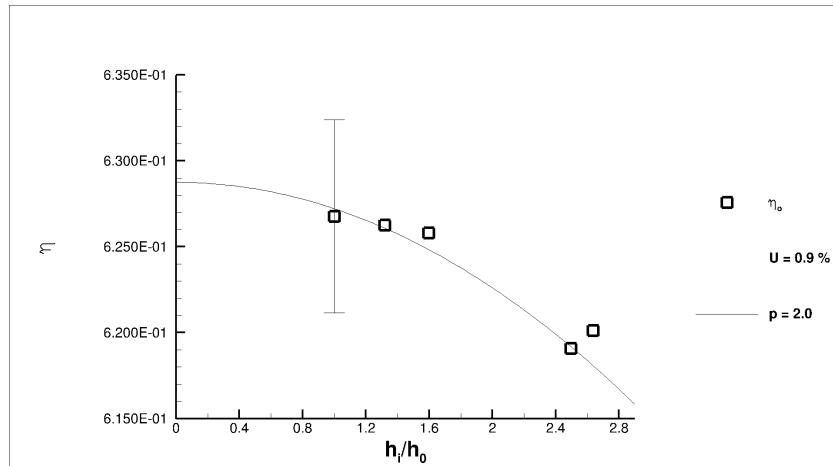
The convergence of the complete range of inflow velocities is given in Figure 8.4. The design point of the propeller is for advance ratio 0.5 which corresponds to the iterations 15000 to 17500 (see Figure 8.5). The iterative error is the lowest for the design point which is expected to have the least complex flow. For the higher and lower advance ratios the RaNS solver will have difficulty to capture flow separation or low pressures causing cavitation. The iterative error is in the same order of magnitude as the double body and free surface simulations, and considered to be sufficiently low.



(a) Thrust coefficient.



(b) Torque coefficient.



(c) Open water efficiency.

Figure 8.6: Discretization uncertainty for the torque, thrust and open water efficiency on the design point ($J = 0.5$).

8.2.2. Discretization uncertainty

The discretization uncertainty is discussed for the case around the design point ($J=0.5$) because it is considered to be guiding for the rest of the simulations. For reference the other grid refinement studies are presented in Appendix B. For all cases the uncertainty estimation is below 3.4 %, which is in line with the expectation of ow uncertainties for structured grid series. The resulting values of interest in

the open water simulation are the thrust (K_t) and torque coefficient (K_Q). For the case $J=0.5$ the final uncertainty values are listed in Table 8.1.

The grid refinement study results are given in Figure 8.6. While the results differ, the general trend through the results gives a relatively low uncertainty. A large cap between refinement 2.5 and 1.5 is caused by a mistake in the grid generation. Nevertheless the uncertainty estimations are low.

Compared to the double body simulations and the free surface simulations, which are performed on unstructured grids, the structured grid seem to have a better trend over the grid refinements. This should be taken into account for determination of the uncertainty.

Table 8.1: List of the estimated values and uncertainty by the method of Eça and Hoekstra for $J=0.5$.

	$\Phi_0[-]$	$U[\%]$	$\Delta_{max-min}[\%]$
K_t	0.116	1.5	3.60
$10K_Q$	0.147	0.7	2.27
η_0	0.626	0.9	1.06

8.3. Comparison to Lloyd's case

For validation the open water diagram from ReFRESCO grid 3 is compared to the Lloyd's study and for the situation $J=0.5$ the comparison for thrust coefficient and the torque coefficient is made.

Figure 8.7 shows the open water diagram for grid 3 and the averaged open water diagram from the Lloyd's results. Comparison these to diagrams to each other, the following remarks can be made. For the efficiency the least differences can be found in the middle of the advance ratio range. On the contrary the most similarities for the thrust and torque coefficients can be found for the higher advance ratio values.

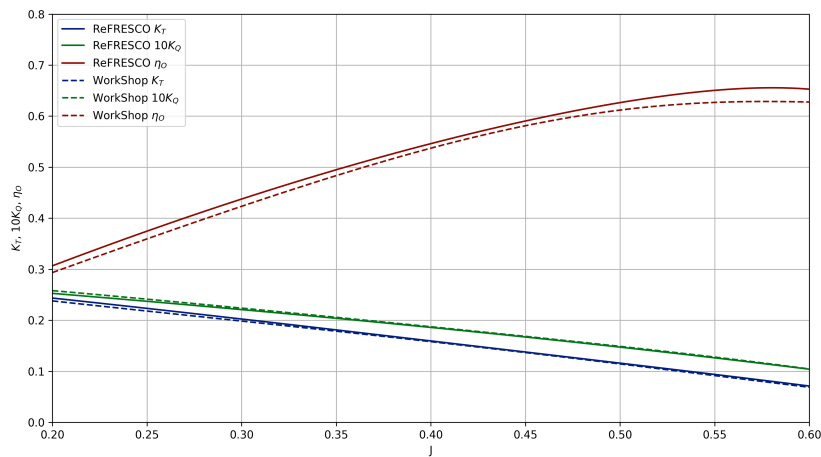
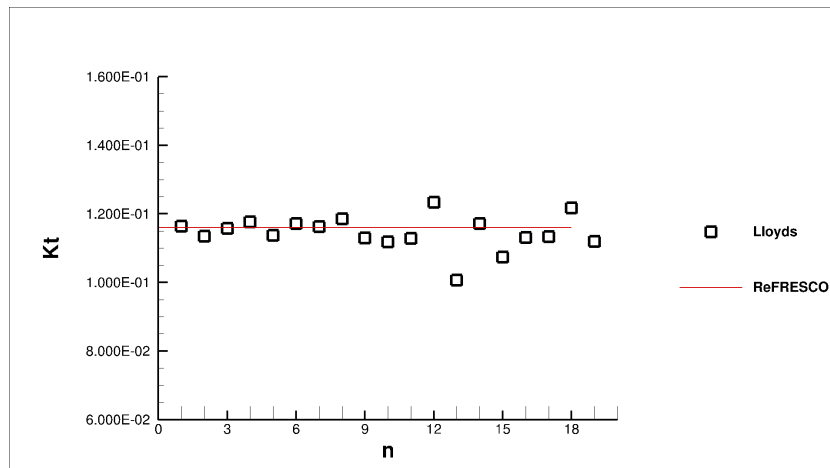
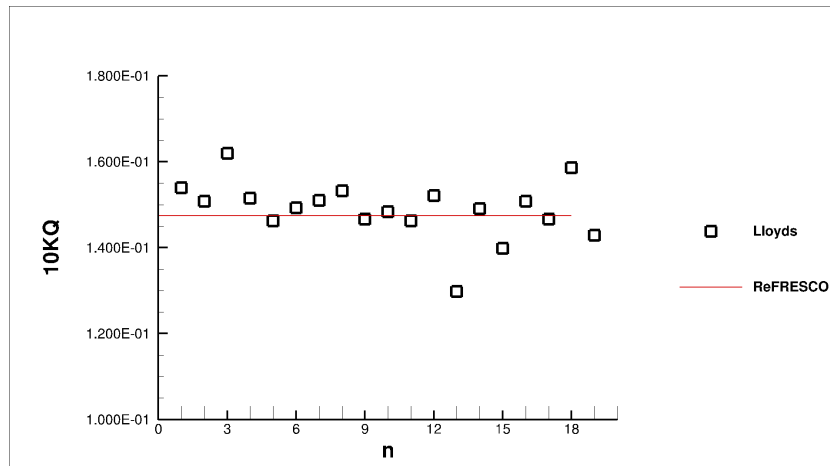


Figure 8.7: Comparison of the open water diagram for the finest grid (grid 3) and the resulting averaged OWD from the Lloyd's workshop.

In Figure 8.8 the results for $J=0.5$ are compared to the results from the Lloyd's participants. The results for both parameters fit within the range of the results. The results produced by this numerical setup is good compared to the 19 participants of the Lloyd's workshop. From this we can conclude that the results are reliable.

(a) Thrust coefficient (Kt).(b) Torque coefficient ($10KQ$).Figure 8.8: Comparison with Lloyd's results for Kt and $10KQ$ at $J = 0.5$.

8.4. Conclusions

The conclusions for the open water simulation are listed below.

Open water diagram - The transition between the grids was smooth enough to not show discrepancies in the flow at the interface of the grids. The simulation showed a good convergence around the design point of the propeller and lesser convergence for relative high and low advance ratios. These results give confidence in future full-scale propeller simulations.

Uncertainty estimation for thrust and torque coefficients - The uncertainties for all calculations were lower than 3.4 percent. The good trend over the grid series is probably caused by the structured grid. When comparing the coarsest and the finest grid of the series little differences in the trend of the open water diagram were found.

Comparison with results from the Lloyd's workshop - The comparison of the total open water diagram should show good agreement with the average numerical Lloyd's result. The example for the design point ($J=0.5$) showed little scatter in the Lloyd's results and no significant differences between the simulation and the numerical Lloyd's result. Combining this all together the full-scale propeller simulation is considered to be of sufficient quality for propulsion prediction.

9

Conclusions

Due to increased computational power, full-scale CFD calculations are becoming widely accessible. However, not much is known in terms of the uncertainty of the calculations. Therefore in this research the uncertainty of full-scale numerical prediction of the resistance and flow is accessed, by analysing the resistance coefficients, the wake factor and the propulsion coefficients. The accompanying research question is: **With what uncertainty can we currently numerically predict self-propulsion resistance and propeller power on full-scale Reynolds numbers?** The discretization uncertainty is determined with a grid refinement study as proposed by Eça and Hoekstra. The vessel that is used for this study is similar to the vessel used in a case study organised by Lloyd's, which also provided reference data for the simulations. Three case studies have been done and in order to answer the main question the following sub-questions will be answered per case.

- What is estimated uncertainty for the vessel?
- Does the data correspond to numerical results given in the Lloyd's workshop and theoretical estimations of the friction drag coefficient?

The main challenges for answering this research question is the geometrical similarity of the grid, since unstructured grids will be used to perform the simulation. A simulation for flow over a flat plate is performed at three Reynolds numbers; $Re = 10^4$, $Re = 10^7$ and $Re = 10^9$. At $Re = 10^7$ the trade off between a smooth transition from the Boundary layer grid to the Euler grid and the construction of a geometrical similar grid is made. This study concluded that the grid with the smooth transition had a lower uncertainty prediction for the friction, for which the result was also closer to the results from a structured grid. The grid refinement study gave a general good trend for the coarser grids, but for the finest grid the results were questionable. Because of the lower uncertainty, the construction of the grids with a smooth transition between the Euler grid and the boundary layer is selected to perform the grid refinement study for the vessel.

9.1. Double body

The double body simulations are performed at the design speed of the vessel ($V_s = 14kn$) which corresponds to a Reynolds number of $Re = 10^9$.

Uncertainty

The iterative error is determined by convergence of the calculations. The finest grids has the lowest quality and did not converge to machine accuracy, which is required for the grid refinement study, but to order of magnitude 10^{-4} for the highest residuals. The average residuals were one to two orders of magnitude lower. This is considered to be of sufficient accuracy for full-scale calculations.

The discretization error is determined for the resistance components on the hull and the wake factor. The friction coefficient showed a similar behaviour as for the flat plate simulation and resulted

in an uncertainty of $U_f = 1.5\%$. The grid refinement study for the pressure coefficient resulted in less converging trend over the grid series with an uncertainty of $U_p = 140.2\%$. This resulted in an overprediction of the pressure coefficient. This effect was also visible for the total resistance coefficient, which resulted in an uncertainty of $U_t = 20.2\%$ and an overprediction of the resistance coefficient. The estimated uncertainty of the wake factor was 24.5% .

The method used showed high uncertainty estimations, and thus it can be concluded that further investigation in the estimation of the uncertainty in combination with unstructured grids should be considered. For now it is of importance to not use the predicted value by the method, but the result from the finest grid calculations.

Comparison to Lloyd's data

Next to the comparison with the Lloyd's result, the friction coefficient was compared with friction lines of ITTC, Grigson and Katsui. The resulting friction coefficient was close the friction line value for this Reynolds number. Comparison with values from the Lloyd's case showed that the friction coefficient determined in this case study was close to the average from the Lloyd's workshop. However, it must be noted that the values from the workshop are calculations with a free surface. In general the results from the double body calculation provide a reliable basis with significant confidence for further application.

9.2. Free surface

In the free surface calculation additional grid refinements are added and optimised to correctly model the free surface and the ship wave system. Extra refinements are placed at the wave system around the ship. From the results it seems that a breaking bow wave is present at the design speed of the vessel. This makes a final steady solution harder to reach.

Uncertainty

The residuals in the field especially for the turbulence model did not converge well. After analysing the location of the residuals it was noticed that the highest residuals were mainly located at the sharp corner between the hull and the deck. The average in the flow field had a lower order of magnitude.

The uncertainties for the friction, pressure and total resistance coefficients are respectively $U_f = 1.3\%$, $U_p = 23.8\%$ and $U_t = 13.1\%$. The convergence over the grid for the friction coefficient had the same behaviour as the double body calculations. However, the pressure and total resistance coefficients had a more linear decreasing trend, which resulted in a large underestimation of the coefficients. Regarding the grid refinement method the free surface simulation confirms the statements that the results of the finest grid will give a better prediction than the grid refinement method.

Analysis of the contribution of the of the various hull parts (bow, aft, midship, hub and rudder) concluded that the aftship is the main contributor. However, the aftship is also the location of the highest residuals for the pressure coefficient, which seem to be source of the high discretization uncertainty.

Comparison to Lloyd's data

The analysis on the differences between the double body and the free surface simulation showed a clear influence of the free surface. The absolute result for the friction coefficient is higher for the free surface simulation, which is mostly likely due to the added friction by the waves.

Regarding the validation with the Lloyd's case, it can be seen that the friction coefficient is relatively large. On the contrary the pressure coefficient is on the lower side of the group, which together resulted in an average total resistance coefficient.

9.3. Open water

The open water simulations have been performed for 5 grids on a wide spectrum of advance ratios ($J = 0.5-6.5$). The propeller is modelled with a structured grid and the outer domain has an unstructured grid. The linking of the two grids is done by matching the nearest gradients over the interface. The flow though the interface is relatively smooth over the grids, which confirms the quality of the coupling of the grids.

Uncertainty

The discretization uncertainty for the analysed thrust and torque coefficients show good results in the range of $U = 0.6 - 3.4\%$. The cases considered, thus give results with a low discretization uncertainty.

The low values on the structured grid of the full-scale propeller simulation implies that the high uncertainties predicted for the double body and free surface simulations are caused by the unstructured grid. Two main differences are pointed out to be source of this discretization error, namely the hanging nodes and the non-similarity of the cell shapes.

Comparison to Lloyd's data

Comparison with the Lloyd's register CFD data show good similarities in the results for the thrust and torque coefficients. The variation in the Lloyd's results is low and the computed results are located close to the mean. This results in a good validation with the Lloyd's results.

10

Recommendations

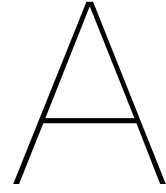
In this chapter future research recommendations are written. Number one to three are recommendations for improvement of the uncertainty estimation. The next two points discuss additional cases which could be performed. The last two recommendations involve experiments that would increase validation on full-scale calculations.

1. The current research can be expended into a more fundamental research by also modelling the viscous layer variation for the remaining two Reynolds numbers ($Re = 10^4$ and $Re = 10^9$) for the full-scale flat plate study. Although the absolute differences are already low in these current cases, this could improve the understanding of the trend over the grids for an unstructured grid study.
2. The convergence around the aft ship causes the main difficulty of determining the discretization error, especially for the pressure. A next research proposal should elaborate this research with a parameter sensitivity study on more parameters then the grid refinement study. An interesting subject would be the influence of the turbulence model on the free surface calculation.
3. A more detailed research on the influence of the time step is proposed for the free surface simulation. Because a breaking bow wave is present in the free surface simulation, a study on the time step and steadiness of the wave is proposed.
4. The current cases (double body, free surface and open water) can be extended with a self-propulsion case. For a final version a full ship included rotating propeller can be validated with measurements, from for example the Lloyd's case study. Intermediate calculations could include a actuator disk simulation and a RaNS-BEM coupled calculation finishing.
5. This research can be extended by also performing these calculations also on model-scale. This could be combined with experimental work and provide a validation. Additionally, scale effects in numerical calculations can be assessed and the influence of scale on the uncertainty estimation for unstructured grids can be explored.
6. For validation purposes the open water diagram of the propeller can be created by model test in a basin. Combined with model simulations the data for the full-scale propeller can be validated.
7. Full-scale validation on flow is more difficult then validation of shaft forces. In order to validate more details in the flow of the simulation, flow visualisation on full-scale should be researched. Methods like Particle Image Velocimetry (PIV) can be used to visualize fow in the wakefield and create validation data.

Bibliography

- [1] *Proceedings of the 8th ITTC, Madrid*, 1957.
- [2] *Proceedings: 2016 Workshop on ship hydrodynamics Computer simulation*, 2016.
- [3] H. Abreu, L. Eça, and G. Vaz. On the calculation of the flow around 2-d square cylinder with rounded corners. 2015.
- [4] A. Bakker. Computational Fluid Dynamics Lectures [Powerpoint slides], 2012. URL <https://www.bakker.org>.
- [5] T. Bugalski and P. Hoffmann. Numerical simulation of the self-propulsion model tests. 2011.
- [6] A. M. Castro, Pablo M. Carrica, and Frederick Stern. Full scale self-propulsion computations using discretized propeller for the kriso container ship kcs. *Computers & Fluids*, 51:35 – 47, 2011.
- [7] P. Crepier and A.R. Starke. Ship resistance calculation with the RANS solver ReFRESCO and Hexpress grids, 2017.
- [8] H. Deconinck. Introduction to computational fluid dynamics, 2018.
- [9] Robert Eymard, Thierry Gallouët, and Raphaële Herbin. *Finite volume methods*, volume 7 of *Handbook of Numerical Analysis*. Elsevier, 2000.
- [10] L. Eça and M. Hoekstra. Evaluation of numerical error estimation based on grid refinement studies with the method of manufactured solutions. 38:1580–1591, 2009.
- [11] L. Eça and M. Hoekstra. A procedure for estimation of the numerical uncertainty of CFD calculations based on grid refinement studies. 262:104–130, 2014.
- [12] L. Eça, G. Vaz, and M. Hoekstra. Code verification of refresco with a statistically periodic manufactured solution. page 1:11, 2014.
- [13] L. Eça, C.M. Klaij, G. Vaz, M. Hoekstra, and F.S. Pereira. On code verification of rans solvers. *Journal of Computational Physics*, 310:418 – 439, 2016. ISSN 0021-9991.
- [14] L. Eça, R. Lopes, G. Vaz, J. Baltazar, and D. Rijpkema. Validation exercises of mathematical models for the prediction of transitional flows, 2016.
- [15] C.W.B. Grigson. A planar friction algorithm and its use in analysing hull resistance, 1999.
- [16] K. Hochkirch and Mallol. On the Importance of Full-Scale CFD Simulations for Ships, 2013.
- [17] Satu Hänninen and Tommi Mikkola. Computation of ship-hull flows at model-and full-scale reynolds numbers. 2018. URL www.researchgate.net.
- [18] T. Katsui, H. Asai, Y. Himeno, and Y. Tahara. The proposal of a new friction line, 2005.
- [19] P.K. Kundu and D.R. Cohen, I.M. Dowling. *Fluid Mechanics*. Academic Press, sixth edition edition, 2016.
- [20] L. Larson and H.C. Raven. *The principles of naval architecture series: Ship Resistance and Flow*. Jersey City, 2010.
- [21] Numeca. User manual hexpress™.
- [22] F.S. Pereira, L. Eça, and G. Vaz. Verification and Validation exercise for the flow around the KVLCC2 tanker at model and full-scale Reynolds numbers. 129:133–148, 2017.

-
- [23] ReFRESHCO. Refresco, November 2017. URL <http://www.refresco.org>.
 - [24] G. Vaz, F. Jouen, and M. Hoekstra. Free-surface viscous flow computations. validation of urans code fresco, 2009.
 - [25] B. Vink. A Verification and validation study of CFD Simulations for the flow around the RSD tug 2513, 2017.



Flat plate grid quality study

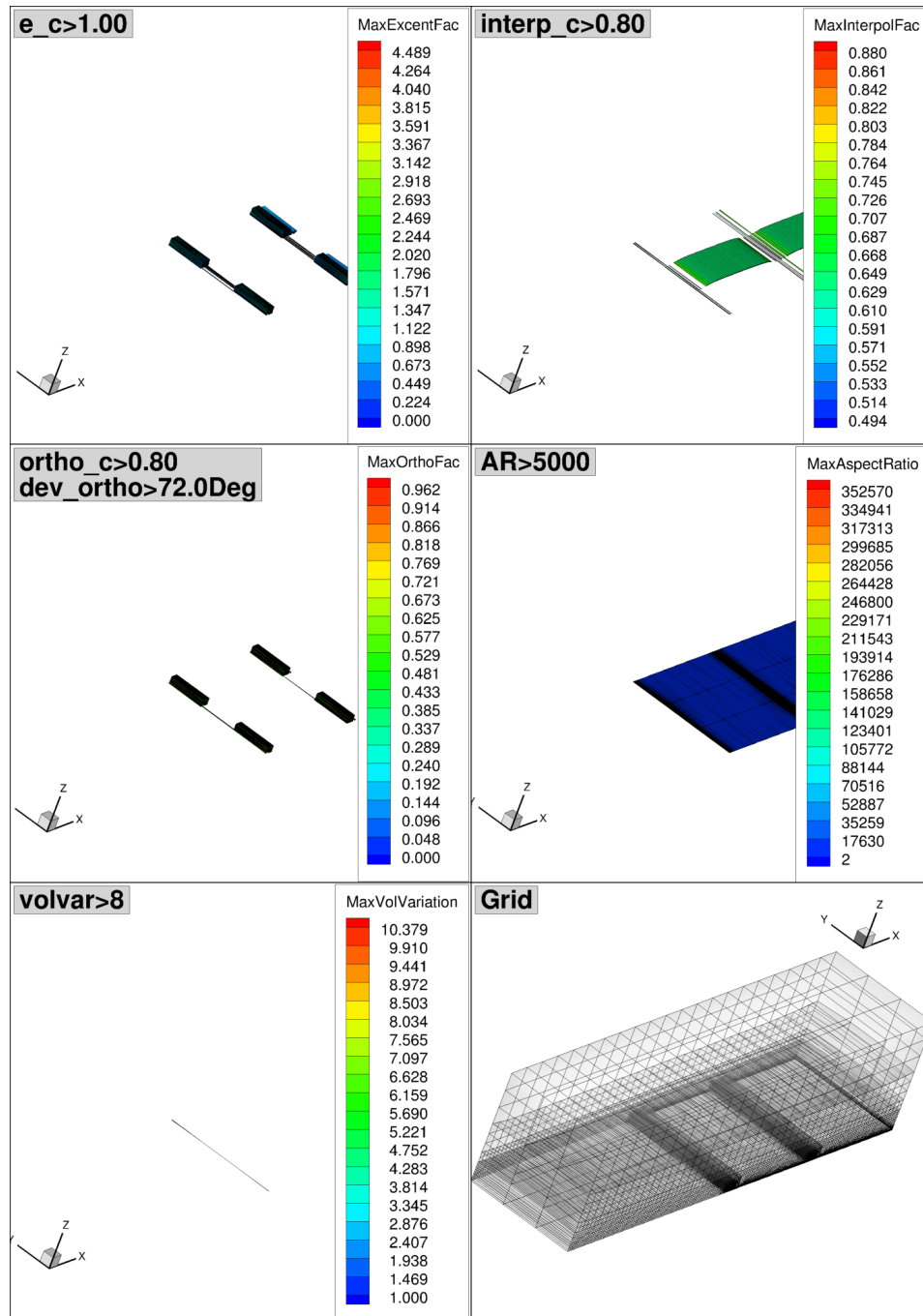
In order to define the grid quality the properties (such as orthogonality, aspect ratio and skewness) in the grid are listed together with the grid quality parameter($Quality_c$). This, together with the assessment for the location of the residuals, will show the quality of the grid and the quality of the convergence. The images are shown for both the *Hexpress-Default* and the *Geometric similar* grid.

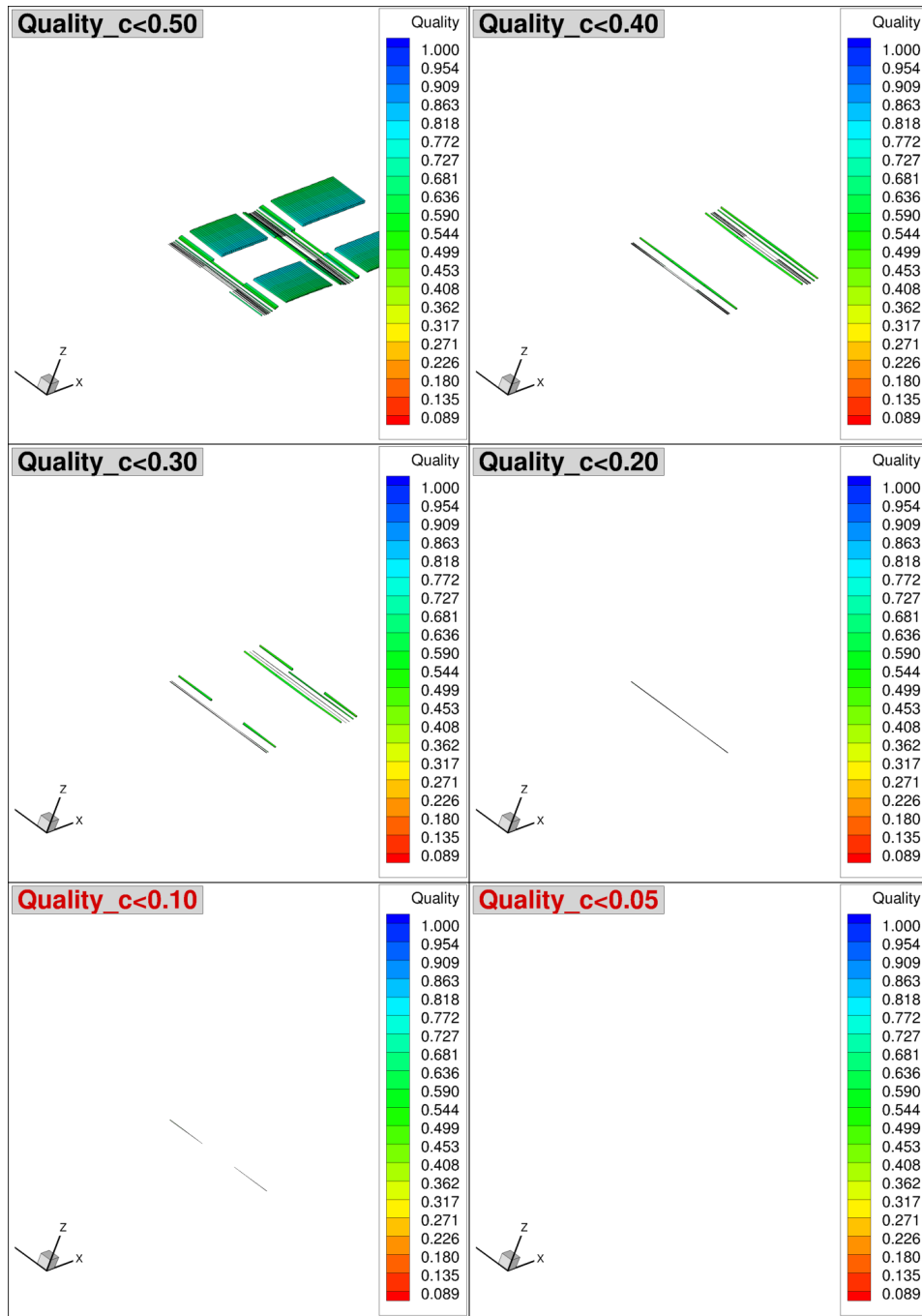
A.1. Hexpress-Default

Figure A.1 and A.2 show the grid properties and the grid quality for the *Hexpress-Default* grid. The grid quality improves for finer grids, so to take into account the minimum grid quality the quality images of the coarsest grid is shown. In Figure A.3 and A.4 the location of the residuals, which are basically already at machine accuracy) are shown. It is clear that the cells with the lowest quality are also the cells with the highest residuals. In the finer grids the residuals are at the same location, but the parameter with the highest residuals is now the turbulence parameter ω .

A.2. Geometrical Similar

For the *Geometrical Similar* grid the same trend can be seen. The locations with the lowest grid quality also have the highest residuals. Also the same trend on which variable has the highest residuals (Velocity X for the coarsest grid and ω for the finest grid) can be seen. When comparing the grid quality of the *Hexpress-Default* grid and the *Geometrical Similar* grid a small difference can be seen in the amount of cells with a low quality. It can be seen that more cells with a lesser quality can be found in the *Geometric Similar* grid.

Figure A.1: Grid Properties of the coarsest *Hexpress-Default* grid.

Figure A.2: Grid Quality of the coarsest *Hexpress-Default* grid.

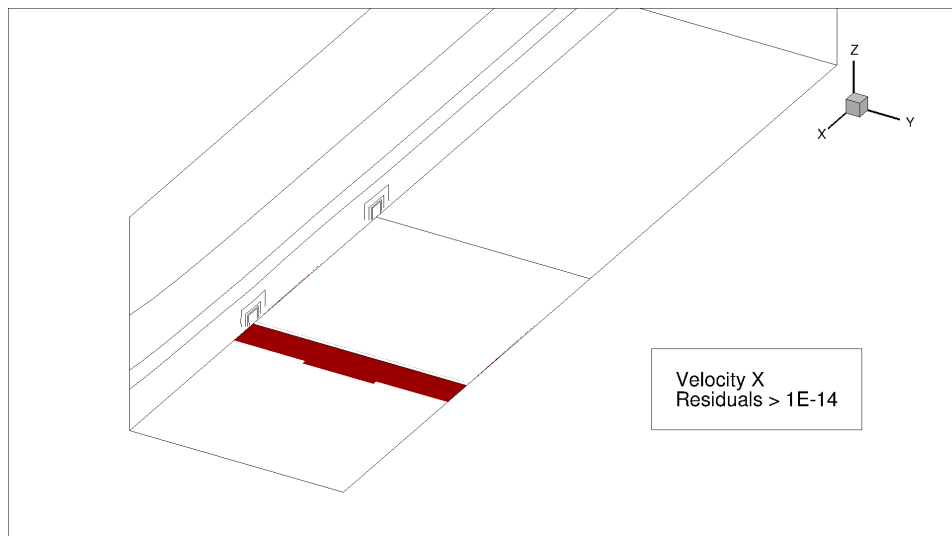


Figure A.3: Residuals on the coarsest grid: Velocity X.

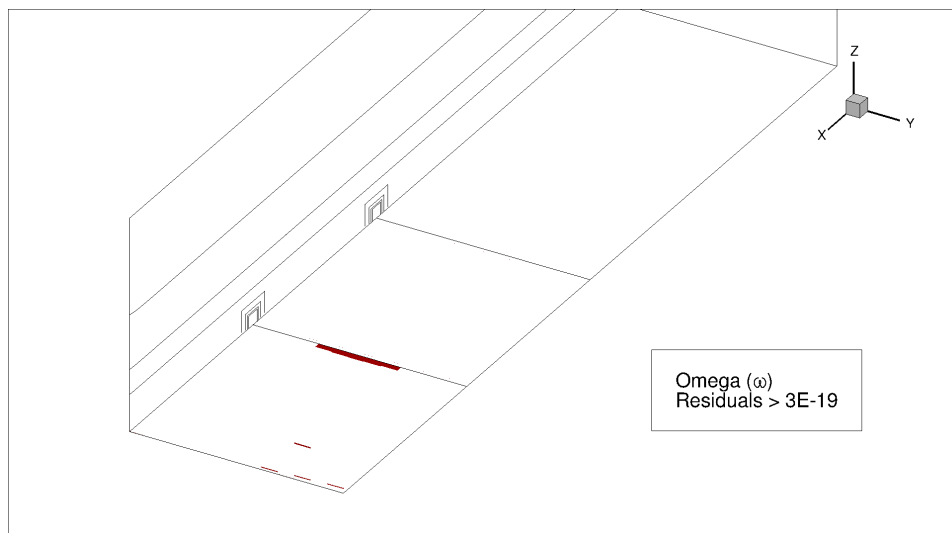
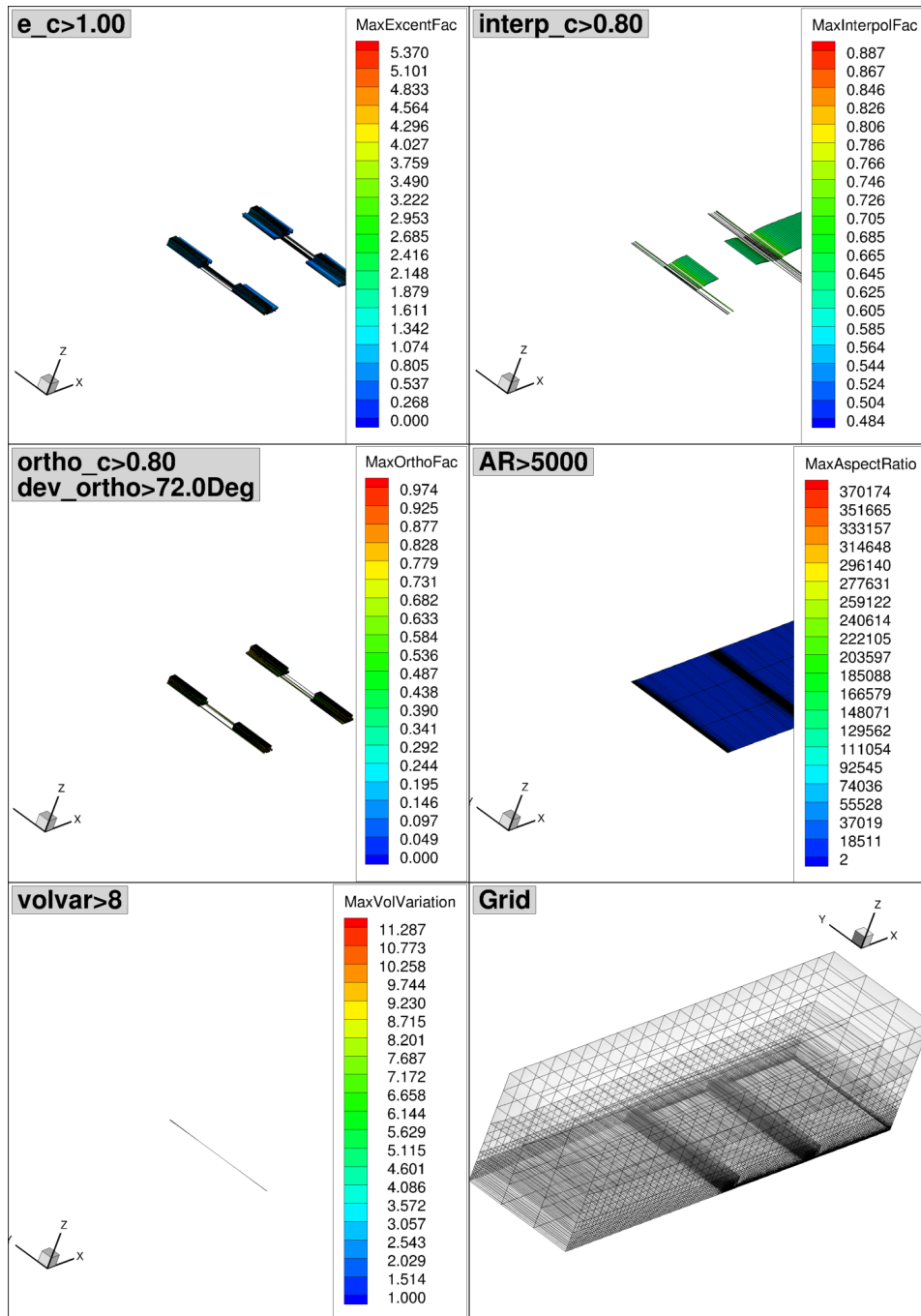
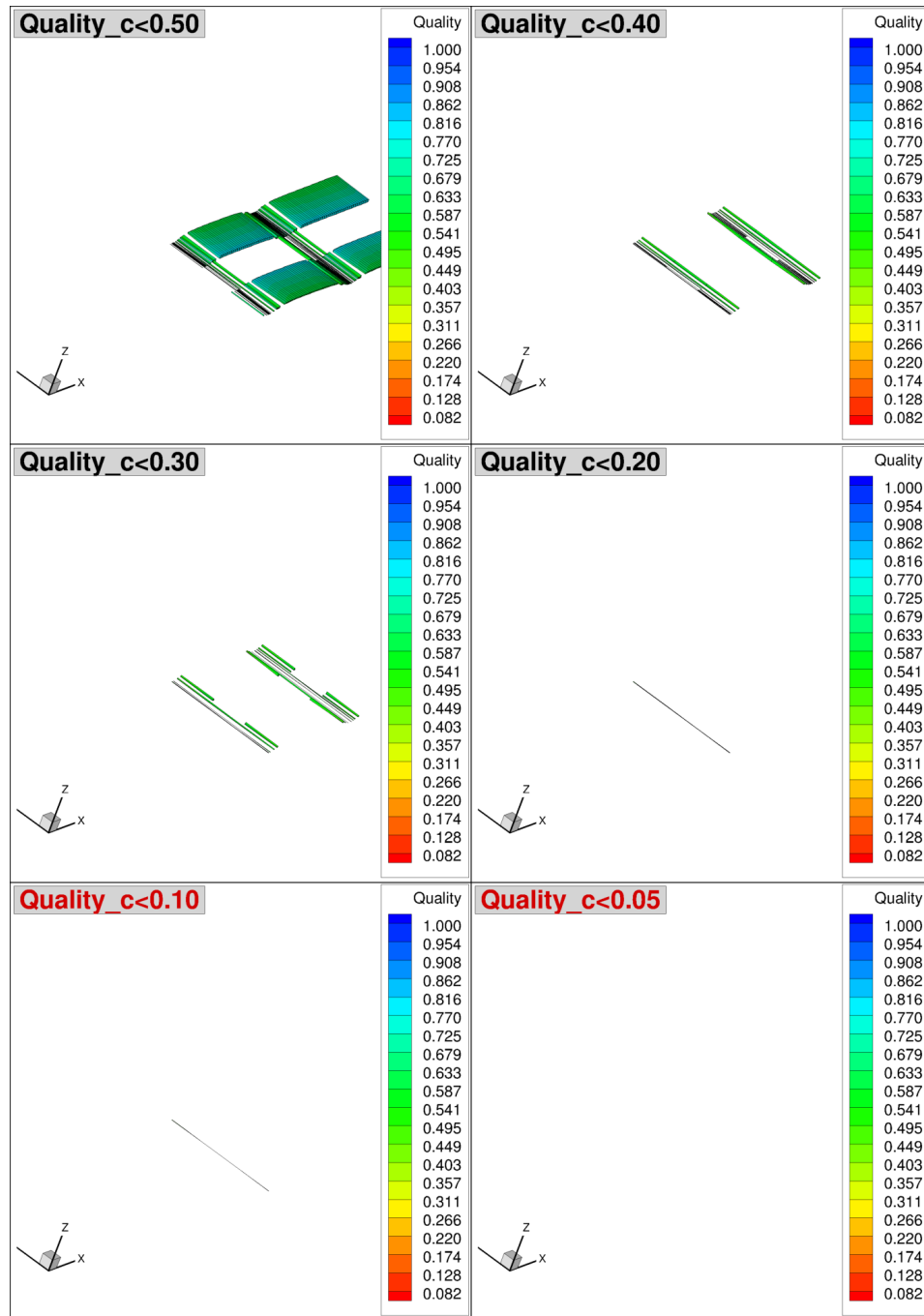


Figure A.4: Residuals on the finest grid: Omega (ω).

Figure A.5: Grid Properties of the coarsest *Geometric Similar* grid.

Figure A.6: Grid Quality of the coarsest *Geometrical Similar* grid.

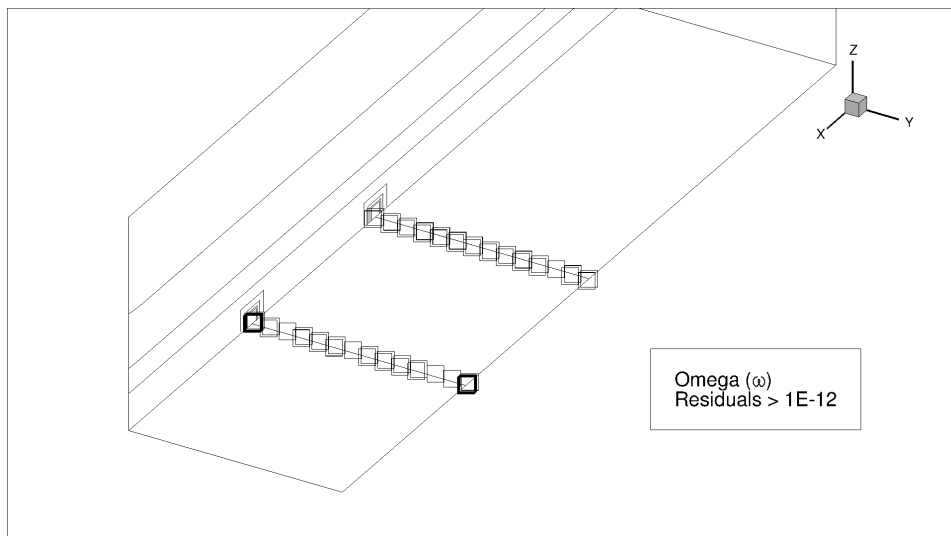


Figure A.7: Residuals on the finest grid: Omega (ω).

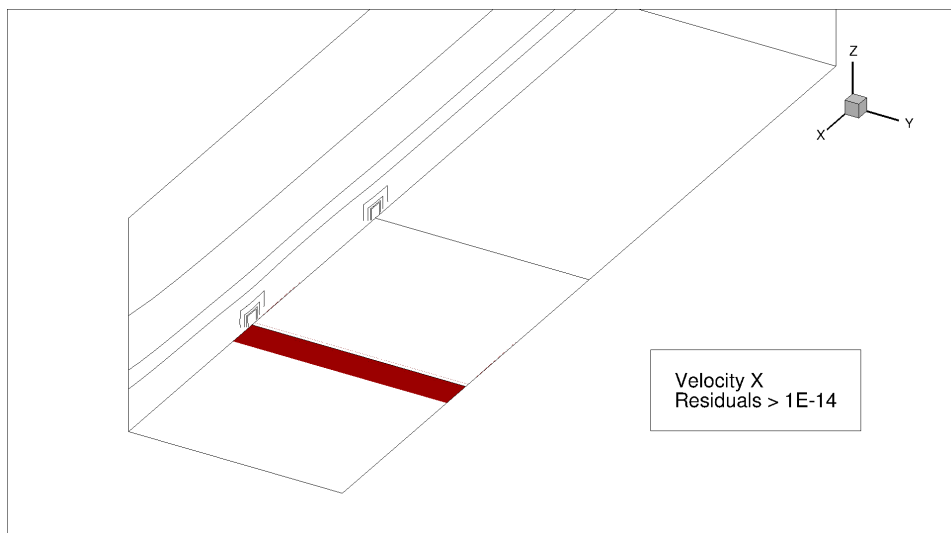
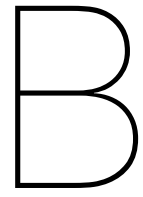


Figure A.8: Residuals on the coarsest grid: Velocity X.



Grid refinement study for propeller parameters

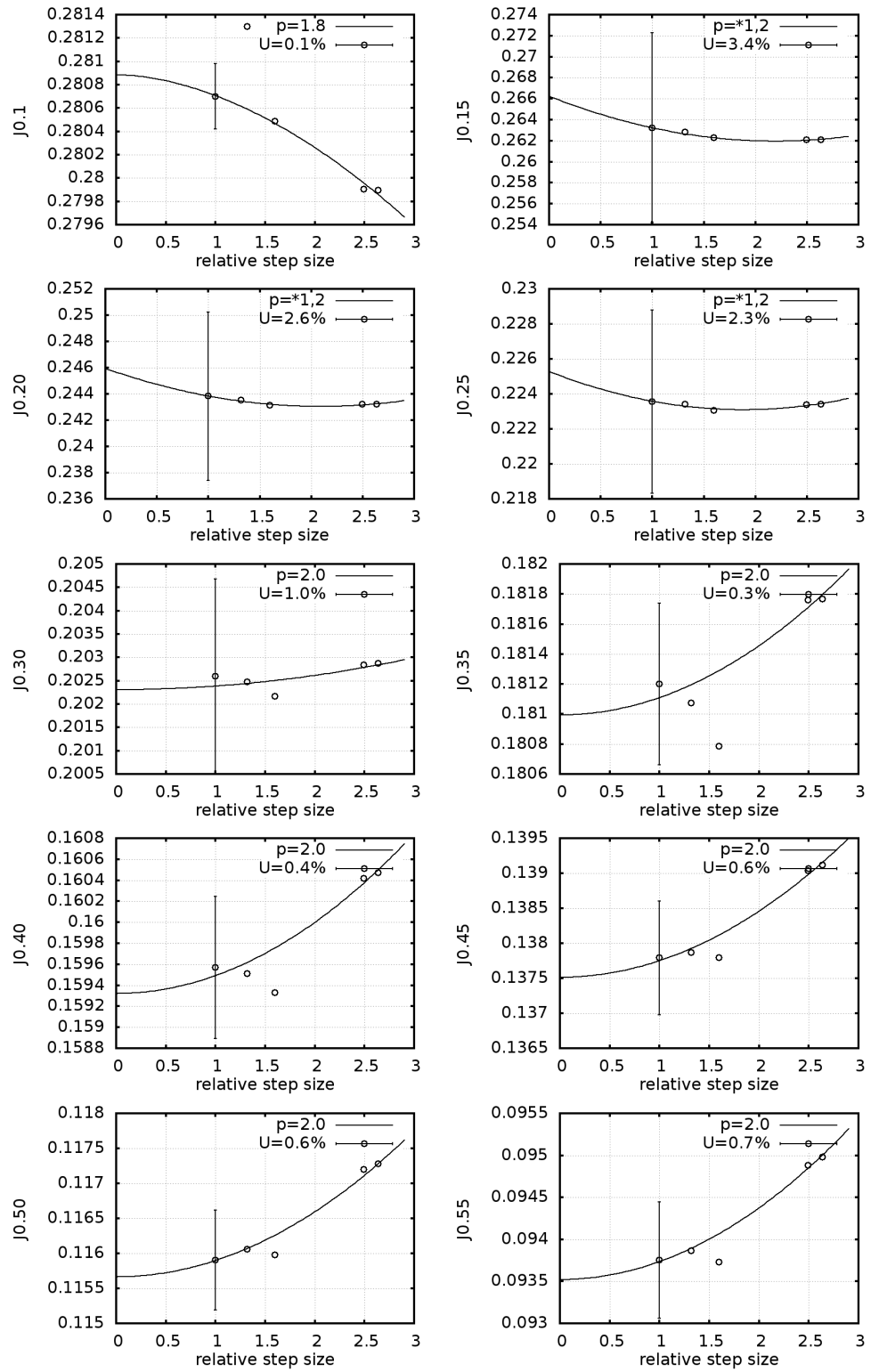


Figure B.1: Thrust coefficients for the total range of advance ratio's.

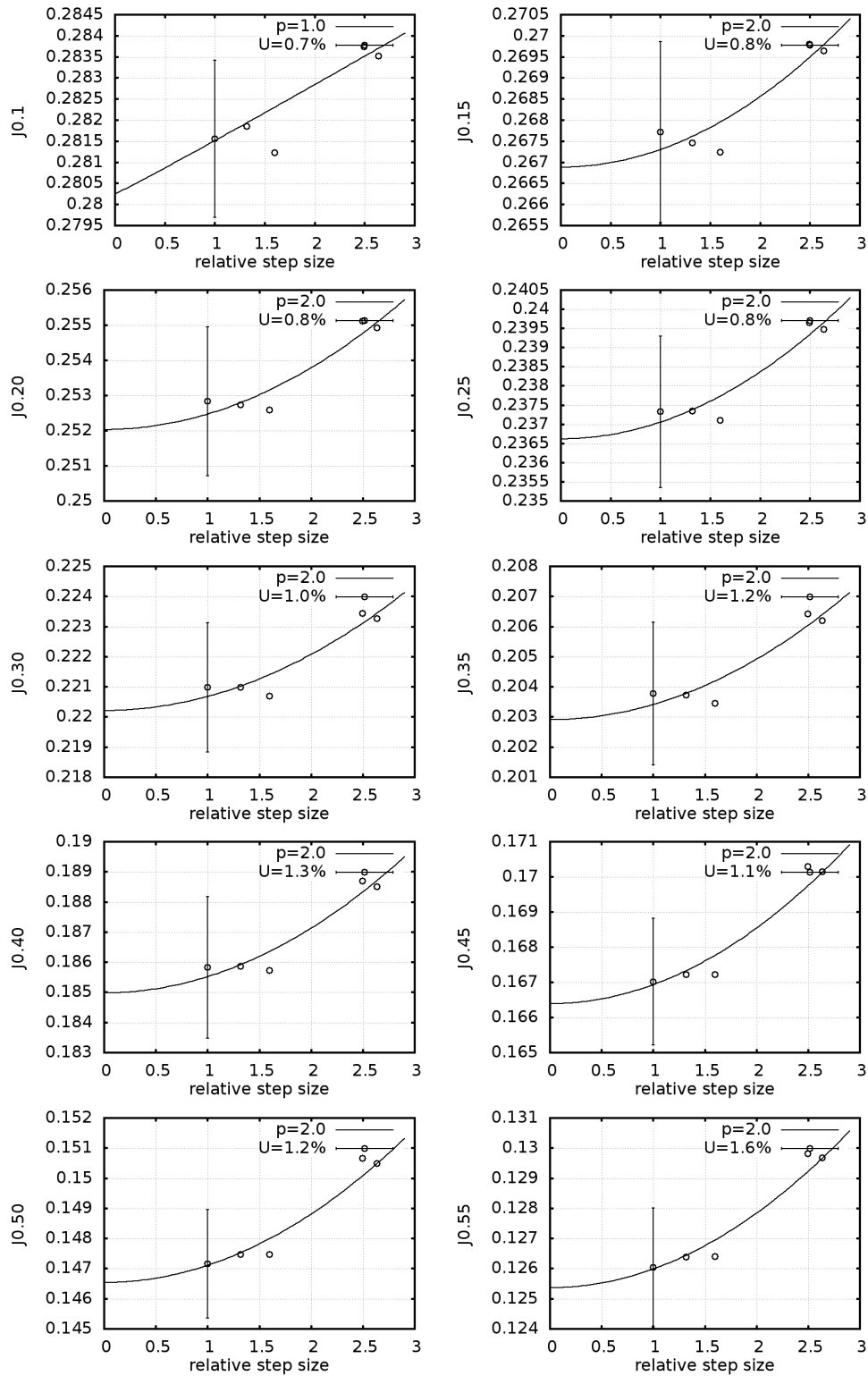
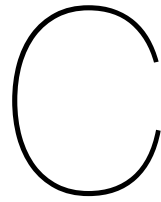


Figure B.2: Torque coefficients for the total range of advance ratio's.



ReFresco input

C.1. Flat plate

```
<?xml version="1.0"?>
<controls>

<!--

-->

  <general>
    <codeVersion>2.4</codeVersion>
    <name>Viscous_Loss_Analysis_Flat - Plate</name>
    <description>Grid0</description>
    <caseid>Grid0</caseid>
    <material>WATER</material>
    <referenceLength>1.0</referenceLength>
    <referenceVelocity>10</referenceVelocity>
    <referenceMaterial>WATER</referenceMaterial>
    <referencePressure>0.0</referencePressure>
    <gridFileName>Grid0</gridFileName>
    <gridFilePath>../ ../ Grids/Grid0</gridFilePath>
    <outFileName>output</outFileName>
    <outFilePath>./ data</outFilePath>
    <nsave>50</nsave>
    <suppressOutput>>false</suppressOutput>
  </general>

<!--

-->

  <userCode>

    <EnergyAnalysis>
      <analysisMode>general</analysisMode>
      <energySubGrid>Interior</energySubGrid>
      <writeEnergyFile>true</writeEnergyFile>
    </EnergyAnalysis>
  </userCode>
</controls>
```



```
-->

<restart>
  <restart>false</restart>
  <resetCounter>false</resetCounter>
  <restartFileName></restartFileName>
  <restartFilePath>.</restartFilePath>
</restart>

<! --

-->

<timeLoop>
  <unsteady>false</unsteady>
  <solutionScheme>IMPLICIT THREE TIME LEVEL</solutionScheme>
  <maxTimesteps>100</maxTimesteps>
  <timeDelta>1.0</timeDelta>
</timeLoop>

<! --

-->

<outerLoop>
  <maxIteration>20000</maxIteration>
  <convergenceTolerance>1e-12</convergenceTolerance>
  <residualNorm>INFINITY</residualNorm>
  <divergenceTolerance>1e+10</divergenceTolerance>
</outerLoop>

<! --

-->

<accelerationOfGravity>
  <apply>false</apply>
  <gravityVector>0. 0. 0.</gravityVector>
</accelerationOfGravity>

<! --

-->

<bodyForces>
  <apply>false</apply>
  <userDefined>false</userDefined>
  <toSave>true</toSave>
```



```
<!--
    <solver>FRESKO</solver>
    <approxInvMomMat>ABROWSUM</approxInvMomMat>
    </segregated>
    </massMomentumSolverType>
</massMomentumSolver>

<!--
    <math>\frac{\partial}{\partial t}(\rho \mathbf{U}) + \nabla \cdot (\rho \mathbf{U} \mathbf{U}) = -\nabla p + \nabla \cdot \boldsymbol{\tau}</math>
-->

<equations>

<!--
    <math>\frac{\partial}{\partial t}(\rho) + \nabla \cdot (\rho \mathbf{U}) = 0</math>
-->

    <equation name="Momentum Equation">
        <EQMomentum>
            <solve_x>>true</solve_x>
            <solve_y>>true</solve_y>
            <solve_z>>true</solve_z>
            <solver>
                <PETSCK>
                    <solver>GMRES</solver>
                    <preconditioner>JACOBI</preconditioner>
                </PETSCK>
            </solver>
            <convergenceTolerance>0.01</convergenceTolerance>
            <maxIteration>400</maxIteration>
            <relaxationProcedure>
                <IMPLICIT_EXPLICIT>
                    <imp_relax_min>0.9</imp_relax_min>
                    <imp_relax_max>0.9</imp_relax_max>
                    <imp_relax_fac>1</imp_relax_fac>
                    <exp_relax>0.5</exp_relax>
                </IMPLICIT_EXPLICIT>
            </relaxationProcedure>
            <convectiveFluxDiscretisation>
                <KAPPA_SCHEME>
                    <schemeName>QUICK</schemeName>
                </KAPPA_SCHEME>
            </convectiveFluxDiscretisation>
            <gradientCalculation>
                <GAUSS />
            </gradientCalculation>
            <applyEccentricityCorrection>true</applyEccentricityCorrection>
            <userSource>>false</userSource>
            <residualNormalisation>PARNASSOS_LIKE</residualNormalisation>
            <toSave>true</toSave>
            <saveResidual>true</saveResidual>
            <saveGradLimiter>>false</saveGradLimiter>
            <saveFluxLimiter>true</saveFluxLimiter>
            <saveYplus>true</saveYplus>
            <saveShearStress>true</saveShearStress>
            <initialization>
                <FAMILY_BASED>
                    <familyName>Inflow</familyName>
                </FAMILY_BASED>
            </initialization>
        </EQMomentum>
    </equation>

<!--
```

```

<!--
<equation name="Pressure Equation">
  <EQPressure>
    <solver>
      <PETSC>
        <solver>CG</solver>
        <preconditioner>BJACOBI</preconditioner>
      </PETSC>
    </solver>
    <convergenceTolerance>0.01</convergenceTolerance>
    <maxIteration>500</maxIteration>
    <relaxationProcedure>
      <EXPLICIT>
        <exp_relax>0.25</exp_relax>
      </EXPLICIT>
    </relaxationProcedure>
    <gradientCalculation>
      <GAUSS />
    </gradientCalculation>
    <applyEccentricityCorrection>true</applyEccentricityCorrection>
    <pressureReference>0.0</pressureReference>
    <userSource>>false</userSource>
    <residualNormalisation>PARNASSOS_LIKE</residualNormalisation>
    <toSave>true</toSave>
    <saveResidual>true</saveResidual>
    <saveGradients>>false</saveGradients>
    <saveChanges>>false</saveChanges>
    <initialPressure userCode="false">0.0</initialPressure>
  </EQPressure>
</equation>

<!--
<equation name="Turbulence Equation">
  <EQTurbulence>
    <turbulenceModel>
      <K_OMEGA>
        <K_OMEGA_TYPE>SST_2003</K_OMEGA_TYPE>
      </K_OMEGA>
    </turbulenceModel>
    <solver>
      <PETSC>
        <solver>GMRES</solver>
        <preconditioner>BJACOBI</preconditioner>
      </PETSC>
    </solver>
    <convergenceTolerance>0.01</convergenceTolerance>
    <maxIteration>200</maxIteration>
    <relaxationProcedure>
      <IMPLICIT_EXPLICIT>
        <imp_relax_min>0.9</imp_relax_min>
        <imp_relax_max>0.9</imp_relax_max>
        <imp_relax_fac>1</imp_relax_fac>
        <exp_relax>0.5</exp_relax>
      </IMPLICIT_EXPLICIT>
    </relaxationProcedure>
    <relaxEddyViscosity>1.0</relaxEddyViscosity>
  </EQTurbulence>
</equation>
-->

```

```
<stagnationRegionCorrection>  
  <REALIZABILITY>  
    <realizabilityLimiter>10.0</realizabilityLimiter>  
  </REALIZABILITY>  
</stagnationRegionCorrection>  
<daclesMarianiCorrection>0.0</daclesMarianiCorrection>  
<convectiveFluxDiscretisation>  
  <FOU_CDS_BLEND>  
    <blendingFactor>0.0</blendingFactor>  
  </FOU_CDS_BLEND>  
</convectiveFluxDiscretisation>  
<gradientCalculation>  
  <GAUSS />  
</gradientCalculation>  
<toSave>>true</toSave>  
<toSaveEddyVisc>true</toSaveEddyVisc>  
<userSource>>false</userSource>  
<saveChanges>>false</saveChanges>  
<saveResidual>true</saveResidual>  
<residualNormalisation>PARNASSOS_LIKE</residualNormalisation>  
<applyEccentricityCorrection>true</applyEccentricityCorrection>  
<initial>  
  <eddyVisc>  
    <eddyVisc userCode="false">1.e-2</eddyVisc>  
  </eddyVisc>  
</initial>  
</EQTurbulence>  
</equation>  
  
<!--  
  
-->  
  
<materials>  
  <material name="WATER" >  
    <fluid>  
      <viscosityMolecular>1.00202e-3</viscosityMolecular>  
      <density>998.2104045</density>  
      <referenceTemperature>286.</referenceTemperature>  
    </fluid>  
  </material>  
</materials>  
  
<!--  
  
-->  
  
<extraQuantities>  
  <saveVorticity>true</saveVorticity>  
  <saveHelicity>true</saveHelicity>  
  <saveQ>true</saveQ>  
</extraQuantities>  
  
<!--  

```

```

-->

    <monitors>

<!-- Propeller Monitors -->

    <monitor name="Forces_FlatPlate" >
        <MO_Force>
            <fileName>Forces_FlatPlate_tec</fileName>
            <saveFrequency>1</saveFrequency>
            <label></label>
            <families>Wall</families>
            <forTecplot>true</forTecplot>
        </MO_Force>
    </monitor>

    <monitor name="Yplus">
        <MO_Yplus>
            <fileName>yplus</fileName>
            <saveFrequency>1</saveFrequency>
            <label></label>
            <families>Wall</families>
            <forTecplot>true</forTecplot>
        </MO_Yplus>
    </monitor>

</monitors>

<!--

-->

    <developer>
        <outputDebugInfo>true</outputDebugInfo>
        <outputLinSolverInfo>true</outputLinSolverInfo>
        <faceInterpolationScheme>FACEPOINT</faceInterpolationScheme>
        <massFluxApplyEccentricityCorrection>true</massFluxApplyEccentricityCorrection>
        <faceInterpolation_nonOrthogonalityCorrection>1000000000.0</faceInterpolation_nonOrthogonalityCorrection>
    </developer>
</controls>

```

C.2. Case1: Double Body

```

<?xml version="1.0"?>
<controls>

<!--

-->

    <general>
        <codeVersion>2.4</codeVersion>
        <name>DoubleBody_Full</name>
        <description>Grid0</description>
        <caseid>Grid0</caseid>
        <material>WATER</material>
        <referenceLength>138.0</referenceLength>
        <referenceVelocity>7.202222</referenceVelocity>
    </general>

```

```

    <referenceMaterial>WATER</referenceMaterial>
    <referencePressure>0.0</referencePressure>
    <gridFileName>Grid0_v13</gridFileName>
    <gridFilePath>../../Grids/Grid0_v13</gridFilePath>
    <outFileName>output</outFileName>
    <outFilePath>./data</outFilePath>
    <nsave>50</nsave>
    <suppressOutput>>false</suppressOutput>
</general>

<!--

-->

<userCode>

  <EnergyAnalysis>
    <analysisMode>general</analysisMode>
    <energySubGrid>Interior</energySubGrid>
    <writeEnergyFile>true</writeEnergyFile>
    <energyFileName>EnergyResults</energyFileName>
    <saveFrequency>1</saveFrequency>

    <general>
      <domainBoxCoordinate1>1 0 0</domainBoxCoordinate1>
      <domainBoxCoordinate2>-2 1 1</domainBoxCoordinate2>
      <stepSize>0.01</stepSize>
      <refMonitor>Forces_FlatPlate</refMonitor>
    </general>

    <ship>
      <domainBoxCoordinate1>-1 0 0</domainBoxCoordinate1>
      <domainBoxCoordinate2>-2 1 1</domainBoxCoordinate2>
      <stepSize>0.01</stepSize>
      <refMonitor>Forces_FlatPlate</refMonitor>
    </ship>

    <propeller>
      <energyFamilies></energyFamilies>
      <propellerMonitor>Moments_Propeller</propellerMonitor>
    </propeller>
  </EnergyAnalysis>

  <readControlFile>

    <DynamicControlFile>
      <DynamicControlFileName>dynamic_controls</DynamicControlFileName>
      <NumberOfTimeStepsControlChange>50</NumberOfTimeStepsControlChange>
      <nread>4200</nread>
    </DynamicControlFile>
  </readControlFile>

</userCode>

<!--

-->

```

```
-->

<subGrids>

  <subGrids name="Interior" >
    <subGrid>
      <moveGridApply>false</moveGridApply>
      <moveGridMethod>MVG</moveGridMethod>
      <moveGridUserDefined>false</moveGridUserDefined>
      <rotationAxis>0.0 0.0 0.0</rotationAxis>
      <rotationOrigin>0.0 0.0 0.0</rotationOrigin>
      <rotationRate>0.0</rotationRate>
    </subGrids>
  </subGrids>

<!--

<deformGrid />
<adaptiveGrid />
<imposedMotion />
<adaptLoop />

<!--

<restart>
  <restart>true</restart>
  <resetCounter>true</resetCounter>
  <restartFileName>output</restartFileName>
  <restartFilePath>./restart</restartFilePath>
</restart>

<!--

<timeLoop>
  <unsteady>false</unsteady>
  <solutionScheme>IMPLICIT_THREE_TIME_LEVEL</solutionScheme>
  <maxTimesteps>100</maxTimesteps>
  <timeDelta>1.0</timeDelta>
</timeLoop>


<!--

-->
```




```


<outerLoop>
  <maxIteration>200000</maxIteration>
  <convergenceTolerance>1e-12</convergenceTolerance>
  <residualNorm>INFINITY</residualNorm>
  <divergenceTolerance>1e+10</divergenceTolerance>
</outerLoop>

<!--

-->

  <accelerationOfGravity>
    <apply>false</apply>
    <gravityVector>0. 0. 0.</gravityVector>
  </accelerationOfGravity>

<!--

-->

  <bodyForces>
    <apply>false</apply>
    <userDefined>false</userDefined>
    <toSave>true</toSave>
    <bodyforceTreatment>EXPLICIT_SOURCE</bodyforceTreatment>
    <bodyForce>0.0 0.0 0.0</bodyForce>
  </bodyForces>

<!--

-->

  <boundaries>
    <family name="Inflow">
      <BCInflow>
        <velocity userCode="false">-7.202222 0.0 0.0</velocity>
        <turbulence>
          <turbIntensity_eddyVisc>
            <turbIntensity>0.1</turbIntensity>
            <eddyVisc userCode="false">10</eddyVisc>
          </turbIntensity_eddyVisc>
        </turbulence>
      </BCInflow>
    </family>

    <family name="Outflow">
      <BCOutflow />
    </family>

    <family name="LeftExterior">
      <BCSymmetryPlane />
    </family>

    <family name="Symmplane">
      <BCSymmetryPlane />
    </family>
  </boundaries>

```

```

    </family>

    <family name="FreeSurface">
    <BCSymmetryPlane />
    </family>

    <family name="Bow">
    <BCWall />
    </family>

    <family name="MidShip">
    <BCWall />
    </family>

    <family name="AftShip">
    <BCWall />
    </family>

    <family name="Hub">
    <BCWall />
    </family>

    <family name="Rudder">
    <BCWall />
    </family>

    <family name="BottomExterior">
    <BCPressure />
    </family>

</boundaries>

<!--

-->

    <massMomentumSolver>
    <massMomentumSolverType name="SEGREGATED">
    <segregated>
    <solver>FRESCO</solver>
    <approxInvMomMat>ABSORWSUM</approxInvMomMat>
    </segregated>
    </massMomentumSolverType>
    </massMomentumSolver>

<!--

-->

    <equations>

<!--

-->

    <equation name="Momentum Equation">

```

```

<EQMomentum>
  <solve_x>true</solve_x>
  <solve_y>true</solve_y>
  <solve_z>true</solve_z>
  <solver>
    <PETSC>
      <solver>GMRES</solver>
      <preconditioner>JACOBI</preconditioner>
    </PETSC>
  </solver>
  <convergenceTolerance>0.001</convergenceTolerance>
  <maxIteration>500</maxIteration>
  <relaxationProcedure>
    <IMPLICIT_EXPLICIT>
      <imp_relax_min>0.3</imp_relax_min>
    <imp_relax_max>0.9</imp_relax_max>
    <imp_relax_fac>60</imp_relax_fac>
    <exp_relax>0.2</exp_relax>
    </IMPLICIT_EXPLICIT>
  </relaxationProcedure>
  <convectiveFluxDiscretisation>
<TVD_SCHEME>
  <schemeName>LIMITED_QUICK</schemeName>
</TVD_SCHEME>
    </convectiveFluxDiscretisation>
    <gradientCalculation>
      <GAUSS />
    </gradientCalculation>
    <applyEccentricityCorrection>true</applyEccentricityCorrection>
    <userSource>false</userSource>
    <residualNormalisation>PARNASSOS_LIKE</residualNormalisation>
    <toSave>true</toSave>
    <saveResidual>true</saveResidual>
    <saveGradLimiter>false</saveGradLimiter>
    <saveFluxLimiter>true</saveFluxLimiter>
    <saveYplus>true</saveYplus>
    <saveShearStress>true</saveShearStress>
    <initialization>
      <FAMILY_BASED> <familyName>Inflow</familyName> </FAMILY_BASED>
    </initialization>
  </EQMomentum>
</equation>

<!--

-->

<equation name="Pressure Equation">
  <EQPressure>
    <solver>
      <PETSC>
        <solver>CG</solver>
        <preconditioner>BJACOBI</preconditioner>
      </PETSC>
    </solver>
    <convergenceTolerance>0.001</convergenceTolerance>
    <maxIteration>500</maxIteration>
    <relaxationProcedure>
      <EXPLICIT>
    <exp_relax>0.1</exp_relax>
    </EXPLICIT>
  </relaxationProcedure>
  <gradientCalculation>
    <GAUSS />
  </gradientCalculation>
  <applyEccentricityCorrection>true</applyEccentricityCorrection>

```

```

        <pressureReference>0.0</pressureReference>
        <userSource>>false</userSource>
        <residualNormalisation>PARNASSOS_LIKE</residualNormalisation>
        <toSave>true</toSave>
        <saveResidual>true</saveResidual>
        <saveGradients>>false</saveGradients>
        <saveChanges>>false</saveChanges>
        <initialPressure userCode="false">0.0</initialPressure>
    </EQPressure>
</equation>

<!--

-->

<equation name="Turbulence Equation">
    <EQTurbulence>
        <turbulenceModel>
            <K_OMEGA>
                <K_OMEGA_TYPE>SST_2003</K_OMEGA_TYPE>
            </K_OMEGA>
        </turbulenceModel>
        <solver>
            <PETSC>
                <solver>GMRES</solver>
                <preconditioner>BJACOBK</preconditioner>
            </PETSC>
        </solver>
        <convergenceTolerance>0.001</convergenceTolerance>
        <maxIteration>500</maxIteration>
        <relaxationProcedure>
            <IMPLICIT_EXPLICIT>
                <imp_relax_min>0.3</imp_relax_min>
                <imp_relax_max>0.9</imp_relax_max>
                <imp_relax_fac>60</imp_relax_fac>
                <exp_relax>0.2</exp_relax>
            </IMPLICIT_EXPLICIT>
        </relaxationProcedure>
        <relaxEddyViscosity>0.9</relaxEddyViscosity>
        <stagnationRegionCorrection>
            <REALIZABILITY>
                <realizabilityLimiter>10.0</realizabilityLimiter>
            </REALIZABILITY>
        </stagnationRegionCorrection>
        <daclesMarianiCorrection>0.0</daclesMarianiCorrection>
        <convectiveFluxDiscretisation>
            <FOU_CDS_BLEND>
                <blendingFactor>0.0</blendingFactor>
            </FOU_CDS_BLEND>
        </convectiveFluxDiscretisation>
        <gradientCalculation>
            <GAUSS />
        </gradientCalculation>
        <toSave>true</toSave>
        <toSaveEddyVisc>true</toSaveEddyVisc>
        <userSource>>false</userSource>
        <saveChanges>>false</saveChanges>
        <saveResidual>true</saveResidual>
        <residualNormalisation>PARNASSOS_LIKE</residualNormalisation>
        <applyEccentricityCorrection>true</applyEccentricityCorrection>
        <initial>
            <turbIntensity_eddyVisc>
                <turbIntensity>0.1</turbIntensity>
                <eddyVisc userCode="false">10</eddyVisc>
            </turbIntensity_eddyVisc>
        </initial>
    </EQTurbulence>
</equation>

```

```

        </EQTurbulence>
    </equation>
<!--

-->

    <materials>
    <material name="WATER" >
        <fluid>
            <viscosityMolecular>8.92770e-4</viscosityMolecular>
            <density>1010</density>
            <referenceTemperature>299.65</referenceTemperature>
        </fluid>
    </material>

    </materials>

<!--

-->

    <extraQuantities>
        <saveVorticity>true</saveVorticity>
        <saveHelicity>true</saveHelicity>
        <saveQ>true</saveQ>
    </extraQuantities>

<!--

-->

    <monitors>

<!-- Force Monitors -->

    <monitor name="Force_Bow" >
        <MO_Force>
            <fileName>Force_Bow_tec</fileName>
            <saveFrequency>1</saveFrequency>
            <label></label>
            <families>Bow</families>
            <forTecplot>true</forTecplot>
        </MO_Force>
    </monitor>

    <monitor name="Force_AftShip" >
        <MO_Force>
            <fileName>Force_AftShip_tec</fileName>
            <saveFrequency>1</saveFrequency>
            <label></label>
            <families>AftShip</families>
            <forTecplot>true</forTecplot>
        </MO_Force>
    </monitor>

    <monitor name="Force_Hub" >

```

```

    <MO_Force>
      <fileName>Force_Hub_tec</fileName>
      <saveFrequency>1</saveFrequency>
      <label></label>
      <families>Hub</families>
      <forTecplot>true</forTecplot>
    </MO_Force>
  </monitor>

  <monitor name="Force_MidShip" >
    <MO_Force>
      <fileName>Force_MidShip_tec</fileName>
      <saveFrequency>1</saveFrequency>
      <label></label>
      <families>MidShip</families>
      <forTecplot>true</forTecplot>
    </MO_Force>
  </monitor>

  <monitor name="Force_Rudder" >
    <MO_Force>
      <fileName>Force_Rudder_tec</fileName>
      <saveFrequency>1</saveFrequency>
      <label></label>
      <families>Rudder</families>
      <forTecplot>true</forTecplot>
    </MO_Force>
  </monitor>

  <monitor name="Force_Ship" >
    <MO_Force>
      <fileName>Force_Ship_tec</fileName>
      <saveFrequency>1</saveFrequency>
      <label></label>
      <families>AftShip MidShip Hub Bow Rudder</families>
      <forTecplot>true</forTecplot>
    </MO_Force>
  </monitor>

<!-- Yplus Monitors -->

  <monitor name="Yplus">
    <MO_Yplus>
      <fileName>yplus</fileName>
      <saveFrequency>1</saveFrequency>
      <label></label>
      <families>AftShip MidShip Hub Bow Rudder</families>
      <forTecplot>true</forTecplot>
    </MO_Yplus>
  </monitor>

<!-- Propellor Monitors -->

  <monitor name="plane_xR=0.0eff_tec">
    <MO_Disc>
      <fileName>wake_0eff_tec</fileName>
      <saveFrequency>-1</saveFrequency>
      <label></label>
      <fields>Velocity</fields>
      <planeCentre>2.787126 0.0 2.814335</planeCentre>
      <planeNormal>0.9999872 0.0 0.0050562</planeNormal>
      <planeOuterRadius>3.12</planeOuterRadius>
      <planeInnerRadius>0.26</planeInnerRadius>
      <numberPointsRadial>23</numberPointsRadial>
      <numberPointsTangential>73</numberPointsTangential>
      <outputFormat>TEC</outputFormat>
      <interpolation>
        <NEAREST_CELL_GRADIENT/>
      </interpolation>
    </MO_Disc>
  </monitor>
  <includeBoundaryData>false</includeBoundaryData>

```



```

<shipWavePattern>

  <acceleration>
    <applyAccelerationFunction>true</applyAccelerationFunction>
    <initialVelocity>0.0 0.0 0.0</initialVelocity>
    <terminalVelocity>-7.20222 0.0 0.0</terminalVelocity>
    <accelerationTime>60.0</accelerationTime>
  </acceleration>

  <initialDamping>
    <initialDampingType>ACCELERATION</initialDampingType>
    <initialDampingGain>1.0</initialDampingGain>
    <initialDampingForceThickness>5.0</initialDampingForceThickness>
    <decayDamping>
      <dampingOrigin>0.0 0.0 0.0</dampingOrigin>
      <decayTime>2.5</decayTime>
    </decayDamping>
  </initialDamping>

  <farFieldDamping>
    <applyFarFieldDamping>true</applyFarFieldDamping>
    <dampingOrigin>69.0 0.0</dampingOrigin>
    <dampingLength>207.0</dampingLength>
    <dampingWidth>138.0</dampingWidth>
    <dampingGain>1.0</dampingGain>
    <dampingForceThickness>5.0</dampingForceThickness>
  </farFieldDamping>

  <startUpRelaxation>
    <applyFirstTimeStepRelaxation>true</applyFirstTimeStepRelaxation>
    <firstTimeStepRelaxationReductionFactor>0.2</firstTimeStepRelaxationReductionFactor>
    <firstTimeStepRelaxationNumberOfOuterIterations>50</firstTimeStepRelaxationNumberOfOuterIterations>
    <numberOfOuterIterationsFirstTimeStep>150</numberOfOuterIterationsFirstTimeStep>
  </startUpRelaxation>

  <dynamicControlFile>
    <dynamicControlFileName>controls2</dynamicControlFileName>
    <numberOfTimeStepsControlChange>1</numberOfTimeStepsControlChange>
    <nread>4000</nread>
  </dynamicControlFile>

  <dynamicTrimAndSinkage>
    <general>
      <applyDynamicTrimAndSinkage>true</applyDynamicTrimAndSinkage>
      <bodyFamilies>Bow MidShip AftShip Hub Rudder Deck Stern</bodyFamilies>
      <interfaceFamilies/>
      <halfDomain>true</halfDomain>
      <zeroOnRestart>>false</zeroOnRestart>
    </general>

    <procedure>
      <dynamicTrimAndSinkageMode>AUTOMATIC</dynamicTrimAndSinkageMode>
      <trimSinkageChangeMode>MAXCHANGE</trimSinkageChangeMode>
      <timeStepChangeTrim>0.01</timeStepChangeTrim>
      <timeStepChangeSinkage>0.01</timeStepChangeSinkage>
      <maxNumberOfTimeSteps>50</maxNumberOfTimeSteps>
    </procedure>

    <dynamicTrim>
      <dynamicTrimAngle>0.0</dynamicTrimAngle>
      <dynamicTrimRotationOrigin>69.0 0.0 0.0</dynamicTrimRotationOrigin>
      <dynamicTrimRotationAxis>0.0 1.0 0.0</dynamicTrimRotationAxis>
    </dynamicTrim>

    <dynamicSinkage>
      <initialDynamicSinkage>MOVEGRID</initialDynamicSinkage>
      <dynamicSinkage>0.0 0.0 0.0</dynamicSinkage>
    </dynamicSinkage>

    <automatic>
      <forceOscillationMethod>MINMAX</forceOscillationMethod>

```



```

    <forceOscillationTolerance>1E-4</forceOscillationTolerance>
    <numberOfTimeStepsForceCheck>75</numberOfTimeStepsForceCheck>
    <convergenceTolerance>0.0001</convergenceTolerance>
  </automatic>

  <hydroStatics>
    <lengthBetweenPerpendiculars>138.000</lengthBetweenPerpendiculars>
    <waterPlaneArea>2601.070</waterPlaneArea>
    <displacement>12790.921</displacement>
    <centreOfBuoyancy>66.687</centreOfBuoyancy>
    <centreOfFlotation>66.784</centreOfFlotation>
    <Iyy>2.925E6</Iyy>
  </hydroStatics>
</dynamicTrimAndSinkage>

  <writeResultsFile>true</writeResultsFile>
  <resultsFileOutputFormat>TECPLOT</resultsFileOutputFormat>

</shipWavePattern>

</userCode>

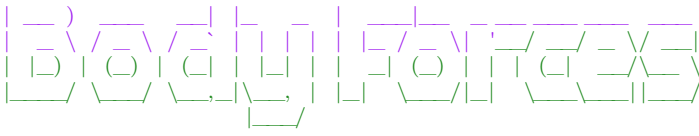
<!--
<subGrids>
  <subGrids name="Interior" >
    <subGrid>
      <moveGridApply>false</moveGridApply>
      <moveGridMethod>MVG</moveGridMethod>
      <moveGridUserDefined>false</moveGridUserDefined>
      <rotationAxis>0.0 0.0 0.0</rotationAxis>
      <rotationOrigin>0.0 0.0 0.0</rotationOrigin>
      <rotationRate>0.0</rotationRate>
    </subGrid>
  </subGrids>
</subGrids>

<!--
<deformGrid>
  <deformGridSetup name="general">
    <general>
      <deformGridApply>true</deformGridApply>
      <deformGridUserDefined>true</deformGridUserDefined>
    </general>
  </deformGridSetup>
  <deformGridSetup name="method">
    <deformMethod_RBF>
      <supportRadius>138.0</supportRadius>
      <convergenceTolerance>1.0e-4</convergenceTolerance>
      <greedyTolerance>1.0e-2</greedyTolerance>
      <solver>GMRES</solver>
    </deformMethod_RBF>
  </deformGridSetup>
</deformGrid>
-->

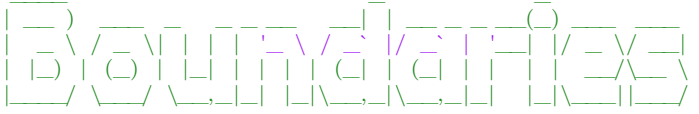
```



```

<!--

-->

<bodyForces>
  <apply>true</apply>
  <userDefined>true</userDefined>
  <toSave>true</toSave>
  <bodyforceTreatment>EXPLICIT_SOURCE</bodyforceTreatment>
  <bodyForce>0.0 0.0 0.0</bodyForce>
</bodyForces>

<!--

-->

<boundaries>

  <family name="Inflow">
    <BCInflow>
      <velocity userCode="true">0.0 0.0 0.0</velocity>
      <checkFlux>false</checkFlux>
      <turbulence>
        <eddyVisc>
          <eddyVisc userCode="false">10.0</eddyVisc>
        </eddyVisc>
      </turbulence>
    </BCInflow>
  </family>

  <family name="Outflow">
    <BCPressure />
  </family>

  <family name="LeftExterior">
    <BCSymmetryPlane />
  </family>

  <family name="Symmplane">
    <BCSymmetryPlane />
  </family>

  <family name="FreeSurface">
    <BCPressure />
  </family>

  <family name="Bow">
    <BCWall />
  </family>

  <family name="MidShip">
    <BCWall />
  </family>

  <family name="AftShip">
    <BCWall />
  </family>

  <family name="Hub">
    <BCWall />
  </family>

```

```

    <family name="Rudder">
      <BCWall />
    </family>

    <family name="Deck">
      <BCSlipWall />
    </family>

    <family name="Stern">
      <BCSlipWall />
    </family>

    <family name="BottomExterior">
      <BCPressure />
    </family>

  </boundaries>

<!--

-->

  <massMomentumSolver>
    <massMomentumSolverType name="SEGREGATED">
      <segregated>
        <solver>FRESCO</solver>
        <approxInvMomMat>DIAG</approxInvMomMat>
      </segregated>
    </massMomentumSolverType>
  </massMomentumSolver>

<!--

-->

  <equations>

<!--

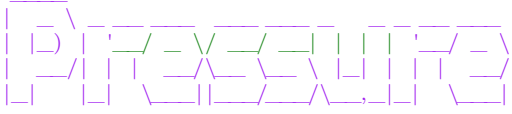
-->

    <equation name="Momentum Equation">
      <EQMomentum>
        <solve_x>true</solve_x>
        <solve_y>true</solve_y>
        <solve_z>true</solve_z>
        <solver>
          <PETSC>
            <solver>GMRES</solver>
            <preconditioner>JACOBI</preconditioner>
          </PETSC>
        </solver>
        <convergenceTolerance>0.001</convergenceTolerance>
        <maxIteration>500</maxIteration>
        <relaxationProcedure>

```

```

        <IMPLICIT_EXPLICIT>
            <imp_relax_min>0.5</imp_relax_min>
            <imp_relax_max>0.9</imp_relax_max>
            <imp_relax_fac>50</imp_relax_fac>
            <exp_relax>0.3</exp_relax>
        </IMPLICIT_EXPLICIT>
    </relaxationProcedure>
    <convectiveFluxDiscretisation>
        <TVD_SCHEME>
            <schemeName>HARMONIC</schemeName>
        </TVD_SCHEME>
    </convectiveFluxDiscretisation>
    <gradientCalculation>
        <GAUSS />
    </gradientCalculation>
    <applyEccentricityCorrection>true</applyEccentricityCorrection>
    <userSource>>false</userSource>
    <residualNormalisation>PARNASSOS_LIKE</residualNormalisation>
    <toSave>true</toSave>
    <saveResidual>true</saveResidual>
    <saveGradLimiter>>false</saveGradLimiter>
    <saveFluxLimiter>true</saveFluxLimiter>
    <saveYplus>true</saveYplus>
    <saveShearStress>true</saveShearStress>
    <initialization>
        <USER_DEFINED>
            <initialVelocity userCode="true">0.0 0.0 0.0</initialVelocity>
            <referenceSystem>EARTH_FIXED</referenceSystem>
        </USER_DEFINED>
    </initialization>
</EQMomentum>
</equation>

<!--

-->

    <equation name="Pressure Equation">
        <EQPressure>
            <solver>
                <PETSC>
                    <solver>CG</solver>
                    <preconditioner>BJACOBI</preconditioner>
                </PETSC>
            </solver>
            <convergenceTolerance>0.001</convergenceTolerance>
            <maxIteration>5000</maxIteration>
            <relaxationProcedure>
                <EXPLICIT>
                    <exp_relax>0.15</exp_relax>
                </EXPLICIT>
            </relaxationProcedure>
            <gradientCalculation>
                <GAUSS />
            </gradientCalculation>
            <applyEccentricityCorrection>true</applyEccentricityCorrection>
            <pressureReference>0.0</pressureReference>
            <userSource>>false</userSource>
            <residualNormalisation>PARNASSOS_LIKE</residualNormalisation>
            <toSave>true</toSave>
            <saveResidual>true</saveResidual>
            <saveGradients>>false</saveGradients>
            <saveChanges>>false</saveChanges>
            <initialPressure userCode="false">0.0</initialPressure>
        </EQPressure>
    </equation>

```



```

-->
    <equation name="Free Surface Equation">
        <EQFreeSurface>
            <solver>
                <PETSC>
                    <solver>GMRES</solver>
                    <preconditioner>BJACOBI</preconditioner>
                </PETSC>
            </solver>
            <convergenceTolerance>0.001</convergenceTolerance>
            <maxIteration>500</maxIteration>
            <relaxationProcedure>
                <IMPLICIT_EXPLICIT>
                    <imp_relax_min>0.9</imp_relax_min>
                    <imp_relax_max>0.9</imp_relax_max>
                    <imp_relax_fac>50</imp_relax_fac>
                    <exp_relax>0.3</exp_relax>
                </IMPLICIT_EXPLICIT>
            </relaxationProcedure>
            <convectiveFluxDiscretisation>
                <REFRICS/>
            </convectiveFluxDiscretisation>
            <material>AIR</material>
            <gradientCalculation>
                <GAUSS/>
            </gradientCalculation>
            <toSave>true</toSave>
            <residualNormalisation>PARNASSOS_LIKE</residualNormalisation>
            <applyEccentricityCorrection>false</applyEccentricityCorrection>
            <saveResidual>true</saveResidual>
            <contactLineCorrection>
                <apply>true</apply>
                <distance>5.0E-5</distance>
                <toSave>false</toSave>
            </contactLineCorrection>
            <initialWaterLevel>5.2480</initialWaterLevel>
        </EQFreeSurface>
    </equation>
</equations>

<!--
<math display="block">\frac{\partial}{\partial t} \left( \int_V \rho \mathbf{u} \cdot \mathbf{n} \, dV \right) + \int_V \rho \mathbf{u} \cdot \mathbf{n} \, dV = 0
-->

<materials>
    <material name="WATER" >
        <fluid>
            <viscosityMolecular>8.92770e-4</viscosityMolecular>
            <density>1010</density>
            <referenceTemperature>299.65</referenceTemperature>
        </fluid>
    </material>
    <material name="AIR">
        <fluid>
            <viscosityMolecular>1.87e-5</viscosityMolecular>
            <density>1.1649e0</density>
            <referenceTemperature>286.</referenceTemperature>
        </fluid>
    </material>
</materials>

<!--
<math display="block">\frac{\partial}{\partial t} \left( \int_V \rho \mathbf{u} \cdot \mathbf{n} \, dV \right) + \int_V \rho \mathbf{u} \cdot \mathbf{n} \, dV = 0

```



```

    <families>Rudder</families>
    <forTecplot>true</forTecplot>
  </MO_Force>
</monitor>

<monitor name="Force_Deck" >
  <MO_Force>
    <fileName>Force_Deck_tec</fileName>
    <saveFrequency>1</saveFrequency>
    <label></label>
    <families>Deck</families>
    <forTecplot>true</forTecplot>
  </MO_Force>
</monitor>

<monitor name="Force_Stern" >
  <MO_Force>
    <fileName>Force_Deck_tec</fileName>
    <saveFrequency>1</saveFrequency>
    <label></label>
    <families>Deck</families>
    <forTecplot>true</forTecplot>
  </MO_Force>
</monitor>

<monitor name="Force_Ship" >
  <MO_Force>
    <fileName>Force_Ship_tec</fileName>
    <saveFrequency>1</saveFrequency>
    <label></label>
    <families>AftShip MidShip Hub Bow Rudder Deck Stern</families>
    <forTecplot>true</forTecplot>
  </MO_Force>
</monitor>

<!-- Yplus Monitors -->

<monitor name="Yplus">
  <MO_Yplus>
    <fileName>yplus</fileName>
    <saveFrequency>1</saveFrequency>
    <label></label>
    <families>AftShip MidShip Hub Bow Rudder</families>
    <forTecplot>true</forTecplot>
  </MO_Yplus>
</monitor>

<!-- Propellor Monitors -->
<monitor name="plane_xR=0.0eff_tec">
  <MO_Disc>
    <fileName>wake_0eff_tecplot</fileName>
    <saveFrequency>-1</saveFrequency>
    <label></label>
    <fields>Velocity</fields>
    <planeCentre>2.787126 0.0 2.814335</planeCentre>
    <planeNormal>0.9999872 0.0 0.0050562</planeNormal>
    <planeOuterRadius>3.12</planeOuterRadius>
    <planeInnerRadius>0.26</planeInnerRadius>
    <numberPointsRadial>23</numberPointsRadial>
    <numberPointsTangential>73</numberPointsTangential>
    <outputFormat>TECPLOT</outputFormat>
    <interpolation>
      <NEAREST_CELL_GRADIENT />
    </interpolation>
  </MO_Disc>
</monitor>

<monitor name="plane_xR=0.0eff">
  <MO_Disc>
    <fileName>wake_0eff</fileName>
    <saveFrequency>-1</saveFrequency>
    <includeBoundaryData>false</includeBoundaryData>
  </MO_Disc>
</monitor>

```

```

        <label></label>
        <fields>Velocity</fields>
        <planeCentre>2.787126 0.0 2.814335</planeCentre>
        <planeNormal>0.9999872 0.0 0.0050562</planeNormal>
        <planeOuterRadius>3.12</planeOuterRadius>
        <planeInnerRadius>0.26</planeInnerRadius>
        <numberPointsRadial>23</numberPointsRadial>
        <numberPointsTangential>73</numberPointsTangential>
        <outputFormat>MARIN</outputFormat>
        <interpolation>
            <NEAREST_CELL_GRADIENT />
        </interpolation>
    </MO_Disc>
</monitor>

</monitors>

<!--
<!--
-->

    <dynamicControls>
        <dynamicMode>NONE</dynamicMode>
    </dynamicControls>

    <acoustics>
    </acoustics>

    <freeMotion>
    </freeMotion>

    <fsi>
    </fsi>

<!--
-->

    <developer>
        <outputDebugInfo>false</outputDebugInfo>
        <outputLinSolverInfo>true</outputLinSolverInfo>
        <faceInterpolationScheme>FACEPOINT</faceInterpolationScheme>
        <cellCenterScheme>AreaAvCenter2</cellCenterScheme>
        <approxInvMomMat_noDt>false</approxInvMomMat_noDt>
        <gradLimiter>BARTH_JESPERSEN</gradLimiter>
    </developer>
</controls>

```

C.4. Case3: Propeller

```

<?xml version="1.0"?>
<controls>

```

```

<!--

```

```

<!--

```



```

    <relaxIterJ>100</relaxIterJ>
    <monitorNameForces>Forces_Propeller</monitorNameForces>
    <monitorNameMoments>Moments_Propeller</monitorNameMoments>
    <writeIntermediateData>true</writeIntermediateData>
    <scaleAxialVelocities>true</scaleAxialVelocities>
    <scalePressure>false</scalePressure>
    <scaleKineticEnergy>true</scaleKineticEnergy>
    <adaptRelaxation>true</adaptRelaxation>
  </openWater>

</userCode>

<!--

-->

  <subGrids>
    <subGrids name="Interior_1">
      <subGrid>
        <moveGridApply>true</moveGridApply>
        <moveGridMethod>AFM</moveGridMethod>
        <moveGridUserDefined>false</moveGridUserDefined>
        <rotationAxis>1.0 0.0 0.0</rotationAxis>
        <rotationOrigin>0.0 0.0 0.0</rotationOrigin>
        <rotationRate>7.50002886167003</rotationRate>
      </subGrid>
    </subGrids>

    <subGrids name="Interior_2">
      <subGrid>
        <moveGridApply>false</moveGridApply>
        <moveGridMethod>AFM</moveGridMethod>
        <moveGridUserDefined>false</moveGridUserDefined>
        <rotationAxis>1.0 0.0 0.0</rotationAxis>
        <rotationOrigin>0.0 0.0 0.0</rotationOrigin>
        <rotationRate>7.50002886167003</rotationRate>
      </subGrid>
    </subGrids>

  </subGrids>

<!--

-->

  <deformGrid />
  <adaptiveGrid />
  <imposedMotion />
  <adaptLoop />

<!--

-->

  <restart>
    <restart>false</restart>

```

[illegible]


```

<family name="Farfield_2">
  <BCPressure>
    <pressure>0.0</pressure>
    <extrapolationOrder>0</extrapolationOrder>
  </BCPressure>
</family>

<!-- InnerDomain -->

<family name="BCWall_1"> <!-- Hub -->
  <BCWall>
    <velocity userCode="false">0 0 0</velocity>
    <referenceSystem>BODY_FIXED</referenceSystem>
    <extrapolationOrder>0</extrapolationOrder>
    <useWallFunction>AUTOMATIC</useWallFunction>
  </BCWall>
</family>

<family name="BCWallInviscid_1"> <!-- Blade 1 -->
  <BCWall>
    <velocity userCode="false">0 0 0</velocity>
    <referenceSystem>BODY_FIXED</referenceSystem>
    <extrapolationOrder>0</extrapolationOrder>
    <useWallFunction>AUTOMATIC</useWallFunction>
  </BCWall>
</family>

<family name="BCWallViscous_1"> <!-- Blade 2 -->
  <BCWall>
    <velocity userCode="false">0 0 0</velocity>
    <referenceSystem>BODY_FIXED</referenceSystem>
    <extrapolationOrder>0</extrapolationOrder>
    <useWallFunction>AUTOMATIC</useWallFunction>
  </BCWall>
</family>

<family name="BCWallViscousHeatFlux_1"> <!-- Blade 3 -->
  <BCWall>
    <velocity userCode="false">0 0 0</velocity>
    <referenceSystem>BODY_FIXED</referenceSystem>
    <extrapolationOrder>0</extrapolationOrder>
    <useWallFunction>AUTOMATIC</useWallFunction>
  </BCWall>
</family>

<family name="BCWallViscousIsothermal_1"> <!-- Blade 4 -->
  <BCWall>
    <velocity userCode="false">0 0 0</velocity>
    <referenceSystem>BODY_FIXED</referenceSystem>
    <extrapolationOrder>0</extrapolationOrder>
    <useWallFunction>AUTOMATIC</useWallFunction>
  </BCWall>
</family>

<!-- INTERFACE BOUNDARY CONDITIONS -->

<family name="InnerInlet_2" >
  <BCInterface>
    <partnerName>BCInflow_1</partnerName>
    <interfaceType>STATIC</interfaceType>
    <haloType>HALO_1</haloType>
    <interpolation>
      <NEAREST_CELL/>
    </interpolation>
    <deformGridSetting>DEFORM_FIXED</deformGridSetting>
  </BCInterface>
</family>

<family name="BCInflow_1" >

```

```

    <BCInterface>
      <partnerName>InnerInlet_2</partnerName>
      <interfaceType>STATIC</interfaceType>
      <haloType>HALO_1</haloType>
      <interpolation>
        <NEAREST_CELL/>
      </interpolation>
      <deformGridSetting>DEFORM_FIXED</deformGridSetting>
    </BCInterface>
  </family>

  <family name="InnerOutlet_2" >
    <BCInterface>
      <partnerName>BCOutflow_1</partnerName>
      <interfaceType>STATIC</interfaceType>
      <haloType>HALO_1</haloType>
      <interpolation>
        <NEAREST_CELL/>
      </interpolation>
      <deformGridSetting>DEFORM_FIXED</deformGridSetting>
    </BCInterface>
  </family>

  <family name="BCOutflow_1" >
    <BCInterface>
      <partnerName>InnerOutlet_2</partnerName>
      <interfaceType>STATIC</interfaceType>
      <haloType>HALO_1</haloType>
      <interpolation>
        <NEAREST_CELL/>
      </interpolation>
      <deformGridSetting>DEFORM_FIXED</deformGridSetting>
    </BCInterface>
  </family>

  <family name="InnerCylinder_2" >
    <BCInterface>
      <partnerName>BCFarfield_1</partnerName>
      <interfaceType>STATIC</interfaceType>
      <haloType>HALO_1</haloType>
      <interpolation>
        <NEAREST_CELL/>
      </interpolation>
      <deformGridSetting>DEFORM_FIXED</deformGridSetting>
    </BCInterface>
  </family>

  <family name="BCFarfield_1" >
    <BCInterface>
      <partnerName>InnerCylinder_2</partnerName>
      <interfaceType>STATIC</interfaceType>
      <haloType>HALO_1</haloType>
      <interpolation>
        <NEAREST_CELL/>
      </interpolation>
      <deformGridSetting>DEFORM_FIXED</deformGridSetting>
    </BCInterface>
  </family>

</boundaries>

<!--

-->

```



```

        </USER_DEFINED>
    </initialization>
</EQMomentum>
</equation>

<!--

-->

    <equation name="Pressure Equation">
        <EQPressure>
            <solver>
                <PETSC>
                    <solver>CG</solver>
                    <preconditioner>BJACOBI</preconditioner>
                </PETSC>
            </solver>
            <convergenceTolerance>0.001</convergenceTolerance>
            <maxIteration>5000</maxIteration>
            <relaxationProcedure>
                <EXPLICIT>
                    <exp_relax>0.075</exp_relax>
                </EXPLICIT>
            </relaxationProcedure>
            <gradientCalculation>
                <GAUSS />
            </gradientCalculation>
            <applyEccentricityCorrection>true</applyEccentricityCorrection>
            <pressureReference>0.0</pressureReference>
            <userSource>>false</userSource>
            <residualNormalisation>PARNASSOS_LIKE</residualNormalisation>
            <toSave>true</toSave>
            <saveResidual>true</saveResidual>
            <saveGradients>>false</saveGradients>
            <saveChanges>>false</saveChanges>
            <initialPressure userCode="false">0.0</initialPressure>
        </EQPressure>
    </equation>

    <!--

-->

    <equation name="Turbulence Equation">
        <EQTurbulence>
            <turbulenceModel>
                <K_OMEGA>
                    <K_OMEGA_TYPE>SST_2003</K_OMEGA_TYPE>
                </K_OMEGA>
            </turbulenceModel>
            <solver>
                <PETSC>
                    <solver>GMRES</solver>
                    <preconditioner>BJACOBI</preconditioner>
                </PETSC>
            </solver>
            <convergenceTolerance>0.001</convergenceTolerance>
            <maxIteration>500</maxIteration>
            <relaxationProcedure>
                <IMPLICIT_EXPLICIT>
                    <imp_relax_min>0.9</imp_relax_min>
                </IMPLICIT_EXPLICIT>
            </relaxationProcedure>
        </EQTurbulence>
    </equation>

```

```

        <imp_relax_max>0.9</imp_relax_max>
        <imp_relax_fac>500</imp_relax_fac>
        <exp_relax>0.15</exp_relax>
        </IMPLICIT_EXPLICIT>
    </relaxationProcedure>
        <relaxEddyViscosity>0.75</relaxEddyViscosity>
    <stagnationRegionCorrection>
        <REALIZABILITY>
            <realizabilityLimiter>10.0</realizabilityLimiter>
        </REALIZABILITY>
    </stagnationRegionCorrection>
    <daclesMarianiCorrection>0.0</daclesMarianiCorrection>
    <convectiveFluxDiscretisation>
        <FOU_CDS_BLEND>
            <blendingFactor>0.0</blendingFactor>
        </FOU_CDS_BLEND>
    </convectiveFluxDiscretisation>
    <gradientCalculation>
        <GAUSS />
    </gradientCalculation>
    <toSave>true</toSave>
    <toSaveEddyVisc>true</toSaveEddyVisc>
    <userSource>false</userSource>
    <saveChanges>false</saveChanges>
    <saveResidual>true</saveResidual>
    <residualNormalisation>PARNASSOS_LIKE</residualNormalisation>
    <applyEccentricityCorrection>true</applyEccentricityCorrection>
    <initial>
        <turbIntensity_eddyVisc>
            <turbIntensity>0.1</turbIntensity>
            <eddyVisc userCode="false">10</eddyVisc>
        </turbIntensity_eddyVisc>
    </initial>
</EQTurbulence>
</equation>

</equations>

<!--
<math display="block">\frac{\partial}{\partial t} \left( \rho \frac{d\mathbf{x}}{dt} \right) = \mathbf{F} + \mathbf{G}
-->

<materials>

    <material name="WATER" >
        <fluid>
            <viscosityMolecular>8.92770e-4</viscosityMolecular>
            <density>1010</density>
            <referenceTemperature>299.65</referenceTemperature>
        </fluid>
    </material>

</materials>

<!--
<math display="block">\frac{\partial}{\partial t} \left( \rho \frac{d\mathbf{x}}{dt} \right) = \mathbf{F} + \mathbf{G}
-->

    <extraQuantities>
        <saveVorticity>true</saveVorticity>
        <saveHelicity>true</saveHelicity>
    </extraQuantities>

```

```

    <saveQ>true</saveQ>
  </extraQuantities>

<!--

-->

<monitors>

  <!-- Forces Propeller -->

  <monitor name="TotalForces" >
    <MO_TotalForce>
      <fileName>forcestotal</fileName>
      <saveFrequency>1</saveFrequency>
      <label></label>
      <excludeFamilies></excludeFamilies>
      <forTecplot>true</forTecplot>
    </MO_TotalForce>
  </monitor>

  <monitor name="Forces_Blade1" >
    <MO_Force>
      <fileName>Forces_Blade1_tec</fileName>
      <saveFrequency>1</saveFrequency>
      <label></label>
      <families>BCWallInviscid_1</families>
      <forTecplot>true</forTecplot>
    </MO_Force>
  </monitor>

  <monitor name="Forces_Blade2" >
    <MO_Force>
      <fileName>Forces_Blade2_tec</fileName>
      <saveFrequency>1</saveFrequency>
      <label></label>
      <families>BCWallViscous_1</families>
      <forTecplot>true</forTecplot>
    </MO_Force>
  </monitor>

  <monitor name="Forces_Blade3" >
    <MO_Force>
      <fileName>Forces_Blade3_tec</fileName>
      <saveFrequency>1</saveFrequency>
      <label></label>
      <families>BCWallViscousHeatFlux_1</families>
      <forTecplot>true</forTecplot>
    </MO_Force>
  </monitor>

  <monitor name="Forces_Blade4" >
    <MO_Force>
      <fileName>Forces_Blade4_tec</fileName>
      <saveFrequency>1</saveFrequency>
      <label></label>
      <families>BCWallViscousIsothermal_1</families>
      <forTecplot>true</forTecplot>
    </MO_Force>
  </monitor>

  <monitor name="Forces_Hub" >
    <MO_Force>
      <fileName>Forces_Hub_tec</fileName>
      <saveFrequency>1</saveFrequency>
      <label></label>

```

```

    <families>BCWall_1</families>
    <forTecplot>true</forTecplot>
  </MO_Force>
</monitor>

<monitor name='Forces_Blades '>
  <MO_Force>
    <fileName>Forces_Blades_tec</fileName>
    <saveFrequency>1</saveFrequency>
    <label></label>
    <families>BCWallInviscid_1 BCWallViscous_1 BCWallViscousHeatFlux_1 BCWallViscousIsothermal_1</families>
    <forTecplot>true</forTecplot>
  </MO_Force>
</monitor>

<monitor name='Forces_Propeller '>
  <MO_Force>
    <fileName>Forces_Propeller</fileName>
    <saveFrequency>1</saveFrequency>
    <label></label>
    <families>BCWallInviscid_1 BCWallViscous_1 BCWallViscousHeatFlux_1 BCWallViscousIsothermal_1 BCWall_1</families>
    <forTecplot>true</forTecplot>
  </MO_Force>
</monitor>

<monitor name="Forces_StreamCap" >
  <MO_Force>
    <fileName>Forces_StreamCap_tec</fileName>
    <saveFrequency>1</saveFrequency>
    <label></label>
    <families>StreamCap_2</families>
    <forTecplot>true</forTecplot>
  </MO_Force>
</monitor>

<monitor name="Forces_Shaft1" >
  <MO_Force>
    <fileName>Forces_Shaft1_tec</fileName>
    <saveFrequency>1</saveFrequency>
    <label></label>
    <families>Shaft1_2</families>
    <forTecplot>true</forTecplot>
  </MO_Force>
</monitor>

<monitor name="Forces_Shaft2" >
  <MO_Force>
    <fileName>Forces_Shaft2_tec</fileName>
    <saveFrequency>1</saveFrequency>
    <label></label>
    <families>Shaft2_2</families>
    <forTecplot>true</forTecplot>
  </MO_Force>
</monitor>

<monitor name="Forces_Shaft3" >
  <MO_Force>
    <fileName>Forces_Shaft3_tec</fileName>
    <saveFrequency>1</saveFrequency>
    <label></label>
    <families>Shaft3_2</families>
    <forTecplot>true</forTecplot>
  </MO_Force>
</monitor>

<monitor name='Moments_Blade1 '>
  <MO_Moment>
    <fileName>Moments_Blade1_tec</fileName>
    <saveFrequency>1</saveFrequency>
    <label></label>
    <families>BCWallInviscid_1</families>

```

```

    <referencePoint>0 0 0</referencePoint>
    <forTecplot>true</forTecplot>
  </MO_Moment>
</monitor>

<monitor name='Moments_Blade2'>
  <MO_Moment>
    <fileName>Moments_Blade2_tec</fileName>
    <saveFrequency>1</saveFrequency>
    <label></label>
    <families>BCWallViscous_1</families>
    <referencePoint>0 0 0</referencePoint>
    <forTecplot>true</forTecplot>
  </MO_Moment>
</monitor>

<monitor name='Moments_Blade3'>
  <MO_Moment>
    <fileName>Moments_Blade3_tec</fileName>
    <saveFrequency>1</saveFrequency>
    <label></label>
    <families>BCWallViscousHeatFlux_1</families>
    <referencePoint>0 0 0</referencePoint>
    <forTecplot>true</forTecplot>
  </MO_Moment>
</monitor>

<monitor name='Moments_Blade4'>
  <MO_Moment>
    <fileName>Moments_Blade4_tec</fileName>
    <saveFrequency>1</saveFrequency>
    <label></label>
    <families>BCWallViscousIsothermal_1</families>
    <referencePoint>0 0 0</referencePoint>
    <forTecplot>true</forTecplot>
  </MO_Moment>
</monitor>

<monitor name='Moments_Hub'>
  <MO_Moment>
    <fileName>Moments_Hub_tec</fileName>
    <saveFrequency>1</saveFrequency>
    <label></label>
    <families>BCWall_1</families>
    <referencePoint>0 0 0</referencePoint>
    <forTecplot>true</forTecplot>
  </MO_Moment>
</monitor>

<monitor name="Moments_Blades" >
  <MO_Moment>
    <fileName>Moments_Blades_tec</fileName>
    <saveFrequency>1</saveFrequency>
    <label></label>
    <families>BCWallInviscid_1 BCWallViscous_1 BCWallViscousHeatFlux_1 BCWallViscousIsothermal_1</families>
    <referencePoint>0.0 0.0 0.0</referencePoint>
    <forTecplot>true</forTecplot>
  </MO_Moment>
</monitor>

<monitor name="Moments_Propeller" >
  <MO_Moment>
    <fileName>Moments_Propeller_tec</fileName>
    <saveFrequency>1</saveFrequency>
    <label></label>
    <families>BCWallInviscid_1 BCWallViscous_1 BCWallViscousHeatFlux_1 BCWallViscousIsothermal_1 BCWallViscousHeatFlux_1</families>
    <referencePoint>0.0 0.0 0.0</referencePoint>
    <forTecplot>true</forTecplot>
  </MO_Moment>
</monitor>

```

```

    <monitor name="Yplus Propeller">
      <MO_Yplus>
        <fileName>yplus_propeller</fileName>
        <saveFrequency>1</saveFrequency>
        <label></label>
        <families>BCWallInviscid_1 BCWallViscous_1 BCWallViscousHeatFlux_1 BCWallViscousIsothermal_1 BCWall_
        <forTecplot>true</forTecplot>
      </MO_Yplus>
    </monitor>

  </monitors>

<!--

-->

  <dynamicControls />
  <acoustics />
  <freeMotion />
  <fsi />

<!--

-->

  <developer>

  </developer>
</controls>

```